(2)

主論文

Studies on the Structures and the Electronic States of Ternary Copper Chalcogenides A-Cu-X (A=Na, K, Rb and Cs; X=S and Se)

三元系銅カルコゲナイド　A－Cu－X　（A＝Na，K，Rb，Cs；X＝S，Se）　の構造と電子状態に関する研究

京都大学理学研究科化学専攻　（分光化学）

佐　藤　博　彦

CONTENTS

Chapter 1. General Introduction

Low-dimensionality and mixed valence are important concepts to develop new interesting electron systems. For example, many studies on the high-T_c superconducting copper oxides have revealed that the mixed valence state in the two-dimensional CuO_2 layers relates to the high-T_c superconductivity.[1)]

A number of ternary copper chalcogenides A-Cu-X (A=Na, K, Rb, Cs; X=S, Se) have various kinds of low-dimensional structures, and some of them have compositional ratios suggesting the existence of mixed valence states. In the following, we review the aspects of their structures and their valence states.

§ 1-1 Structures of ternary alkali copper chalcogenides.

A. Binary CuS (covellite)

The features of the local structures of ternary alkali copper chalcogenides are seen in binary CuS (covellite). As shown in Fig. 1-1[2)], there are two kinds of copper sites in CuS: triangular Cu(1) site and tetrahedral Cu(2) site. The Cu(1) atoms are included in the CuS sheet which is obtained when Cu and S are put at the vertices

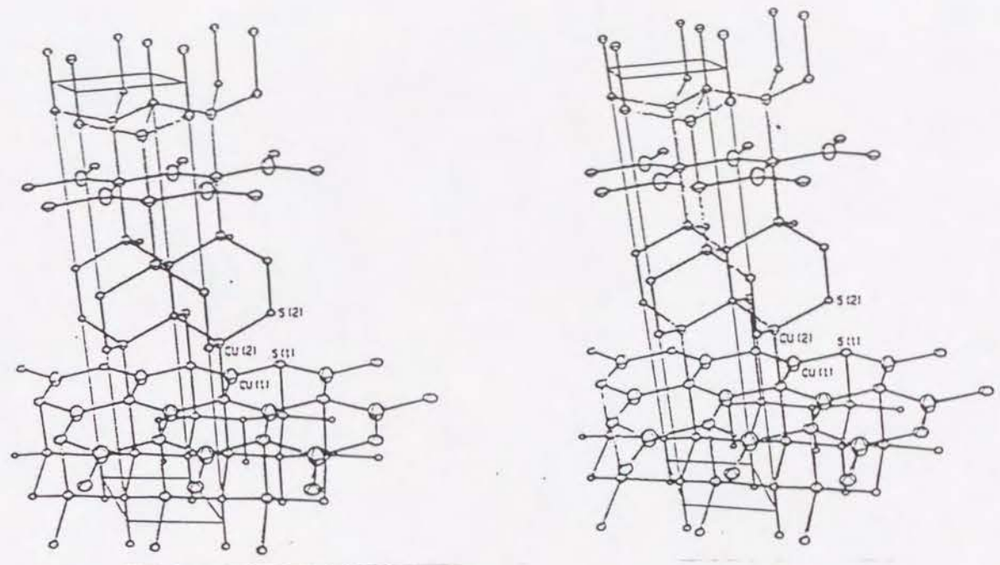

Fig. 1-1 The crystal structure of CuS (covellite).[2)]

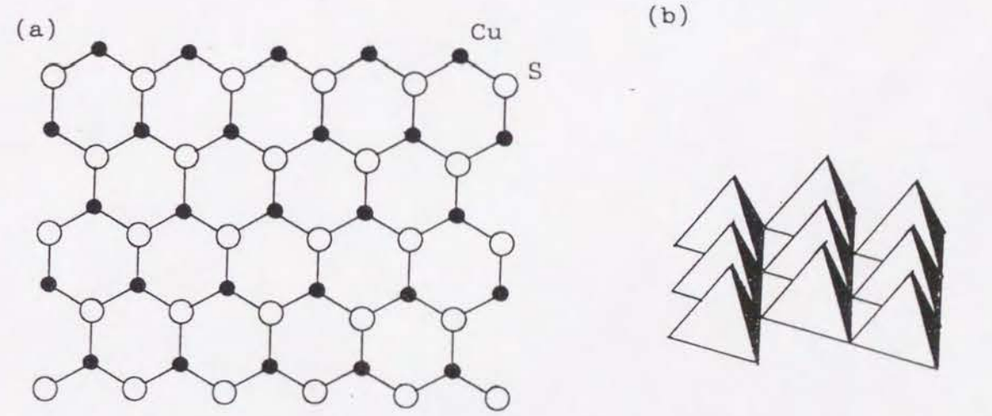

Fig. 1-2 (a) The honeycomb CuS sheet structures, and (b) the trigonal sheet of edge-shared CuS_4 tetrahedrons.

of the honeycomb lattice alternately like Fig. 1-2(a). On the other hand, the Cu(2) atoms are included in the edge-shared CuS_4 tetrahedrons (Fig. 1-2(b)) forming layered structure having trigonal symmetry.

Like CuS, in the case of ternary alkali copper chalcogenides, the copper atoms are usually located at tetrahedral sites or triangular sites. However, the manners of the formation of the crystal structure are different from that in CuS as shown below.

B. Tetrahedrally coordinated structures

$TlCu_2Se_2$[3,4] is a prototype for considering the structure of ternary alkali copper chalcogenides.* $TlCu_2Se_2$ has only tetrahedral copper sites. Its structure is classified into the $ThCr_2Si_2$-type[5] structure. the $CuSe_4$ tetrahedrons form the Cu_2Se_2 sheet with tetragonal symmetry, by sharing their edges. The Cu_2Se_2 sheets are separated each other by thallium atoms. The crystal structure of $TlCu_2Se_2$ is schematically shown in Fig. 1-3(a).

---

* Although Tl is not alkali metal, a number of thallium copper chalcogenides have common structures to that of alkali copper chalcogenides. Therefore, we include the thallium compounds here for the convenience of discussion.

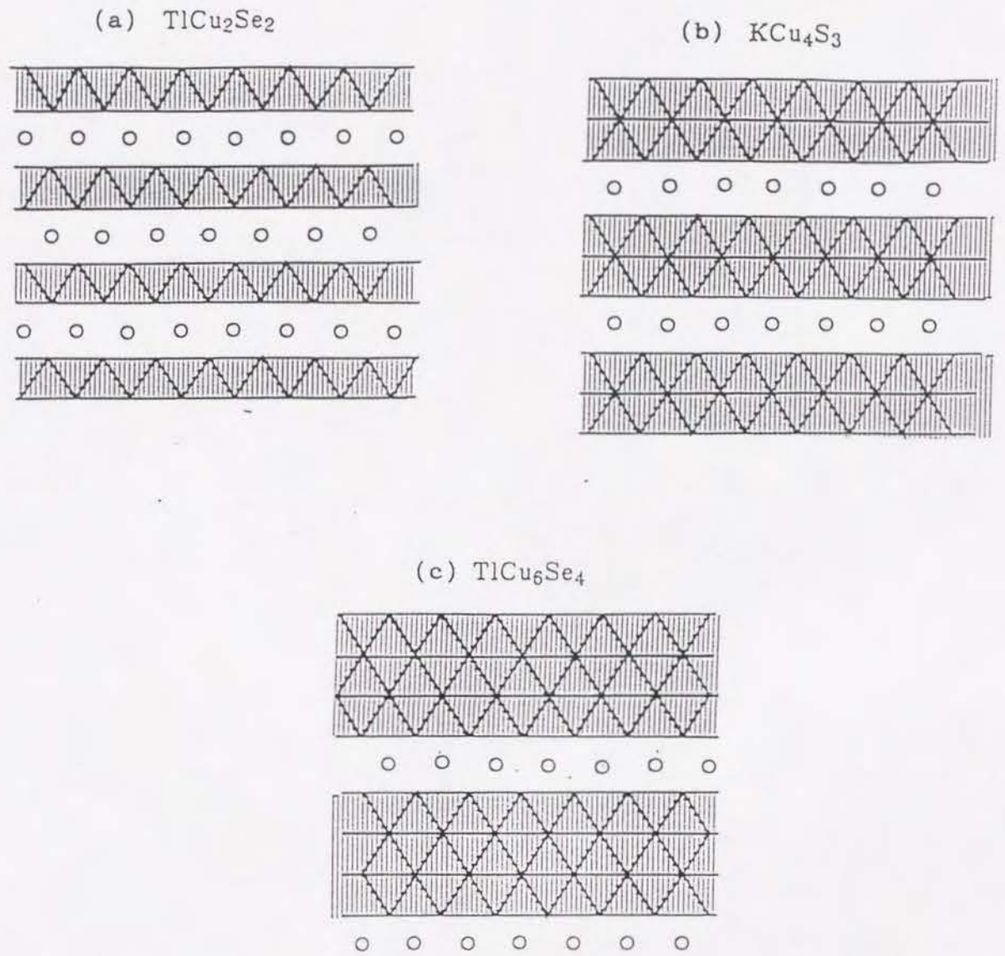

Fig. 1-3 The schematic view of the crystal structures of (a) $TlCu_2Se_2$, (b) $TlCu_4Se_3$ (or KCu_4S_3), and (c) $TlCu_6Se_4$.

In all the schematic figures in this chapter, the shaded regions express the copper-chalcogen networks, and the open circles express the alkali ions (or thallium ions). The triangles in the schematic figures mean the tetrahedral columns of edge-shared CuS_4 (or $CuSe_4$) like Fig. 1-4.

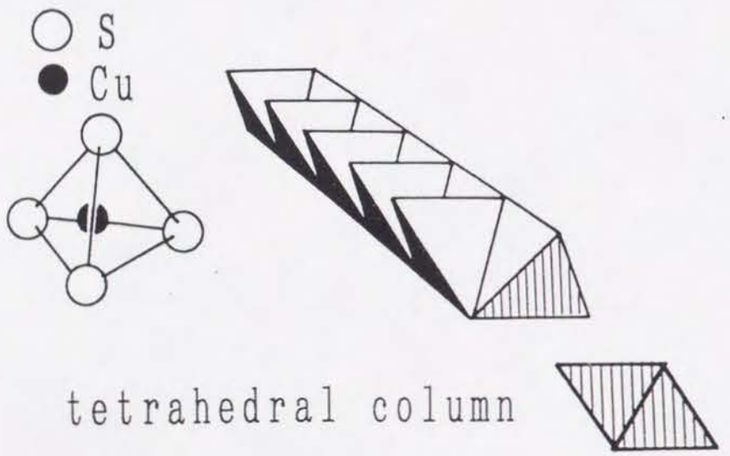

Fig. 1-4 The column of the edge-shared CuS_4 (or $CuSe_4$) tetrahedrons.

$TlCu_2S_2$[6] and $BaCu_2S_2$[7,8] also have the $TlCu_2Se_2$ structure. However, no alkali-metal copper chalcogenides have been reported to have this structure at present.

As shown in Fig. 1-3(b), in $TlCu_4Se_3$[9], the edge-shared $CuSe_4$ tetrahedrons form the tetragonal Cu_4Se_3 "double" layer, which are almost two times thicker than the Cu_2Se_2 sheet in $TlCu_2Se_2$. The Cu_4Se_3 layers are separated by thallium ions. Alkali copper chalcogenides ACu_4X_3, (A=K, Rb, Cs; X=S, Se) also have structure of this type.

As shown in Fig. 1-3(c), $TlCu_6Se_4$[10] has the Cu_6Se_4 "triple" layer about three times thicker than the Cu_2Se_2 sheet in $TlCu_2Se_2$.

C. Triangularly coordinated Cu_4S_4 chain structure

The compounds shown above include only tetrahedrally coordinated copper atoms. On the other hand, $Na_3Cu_4S_4$ contains only the copper atoms coordinated by sulfur atoms almost triangularly. Figure 1-5 shows the schematic crystal

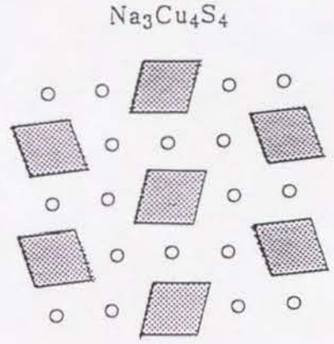

Fig. 1-5 The schematic view of the crystal structure of $Na_3Cu_4S_4$.

structure[11] of $Na_3Cu_4S_4$. The shaded tetragons are the Cu_4S_4 chains included commonly in several ternary copper sulfides and also ternary silver sulfides. Figure 1-6 shows the Cu_4S_4 structure. It can be obtained by wrapping around the ribbon of the honeycomb Cu-S sheet included in CuS (Fig. 1-2(a)).

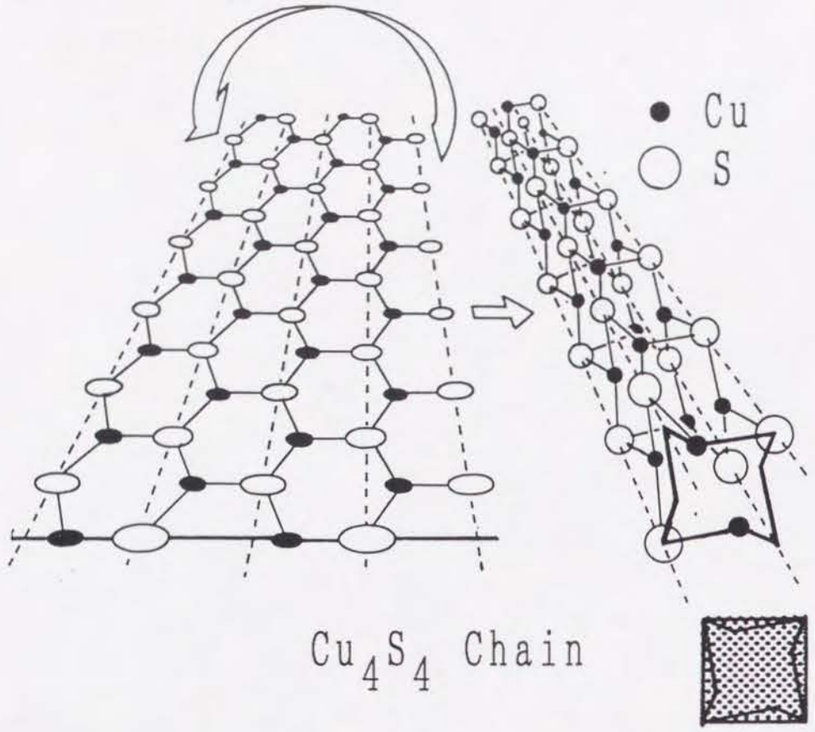

Fig. 1-6 The Cu_4S_4 chain structure (right hand side). This structure can be obtained by wrapping around the honeycomb Cu-S sheet (left hand side).

In this structure, the copper atoms are coordinated almost triangularly.

D. Compounds including both tetrahedrally and triangularly coordinated coppers

Several phases of alkali copper chalcogenides contain both the columns of the edge-shared CuS_4 (or $CuSe_4$) tetrahedrons (Fig. 1-4) and Cu_4S_4 (or Cu_4Se_4) chains (Fig. 1-6). As shown in Fig. 1-7(a), KCu_3S_2[12] has layered

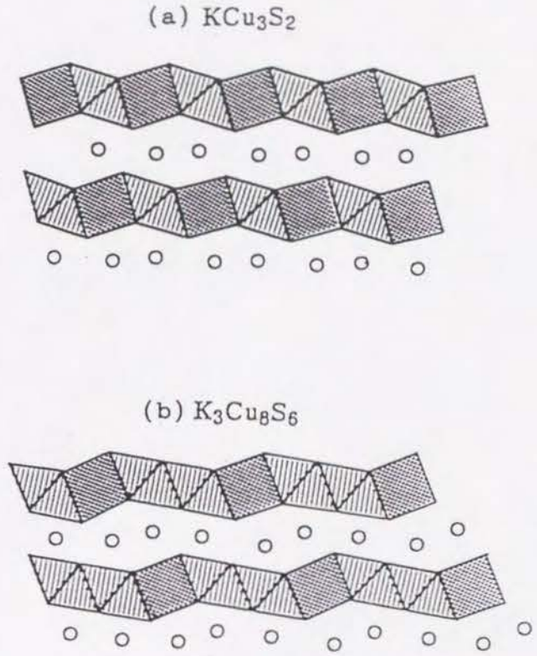

Fig. 1-7 The schematic view of the crystal structures of (a) KCu_3S_2, (b) $K_3Cu_8S_6$, and (c) $Tl_5Cu_{14}Se_{10}$.

structure. The Cu_3S_2 sheet is composed of the Cu_4S_4 chains bridged by the edge-shared CuS_4 tetrahedral columns.

The structure of $K_3Cu_8S_6$[13], shown in Fig. 1-7(b), resembles that of KCu_3S_2, but the bridging CuS_4 tetrahedral columns are two times wider than those in KCu_3S_2. $Rb_3Cu_8S_6$[14], $Rb_3Cu_8Se_6$ and $Cs_3Cu_8Se_6$ also have the $K_3Cu_8S_6$-type structure.

Interestingly, $Tl_5Cu_{14}Se_{10}$[15] has a structure just intermediate between that of KCu_3S_2 and that of $K_3Cu_8S_6$ as shown in Fig. 1-7(c).

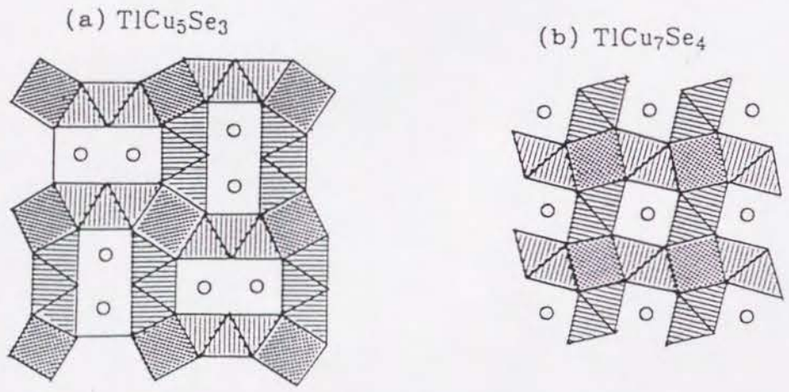

Fig. 1-8 The schematic view of the crystal structures of (a) $TlCu_5Se_3$ and (b) $TlCu_7Se_4$

$TlCu_5Se_3$[16] and $TlCu_7Se_4$[17] are also composed of columns of the $CuSe_4$ tetrahedrons and the Cu_4Se_4 chains. However, their structures are not layered-type. As shown in Fig. 1-8(a), in $TlCu_5Se_3$, the Cu_4Se_4 chains are bridged by the tetrahedral columns each other forming three-dimensional network of copper and selenium, leaving the channel of thallium ions.

The structure of $TlCu_7Se_4$ resembles that of $TlCu_5Se_3$ as shown in Fig. 1-8(b). In this structure, however, the occupancy of the copper atoms at the tetrahedral sites is 3/4. $NH_4Cu_7S_4$[18], $TlCu_7S_4$[19], and KCu_7S_4[20] also have the structure of this type.

$Cs_2Cu_5Se_4$[21] has a corrugated sheet structure composed of the columns of edge-shared $CuSe_4$ tetrahedrons (Fig. 1-9). The columns are bound each other sharing the face of the $CuSe_4$ tetrahedrons. On such faces, there are triangularly coordinated copper atoms in addition to the tetrahedrally coordinated copper atoms in the columns.

E. Linearly coordinated structures

$KCuS$[22] and $CsCu_3S_2$[23] have completely different crystal structures from other ternary copper chalcogenides. In both compounds, all the copper atoms are linearly coordinated by two sulfur atoms as shown in Fig. 1-10.

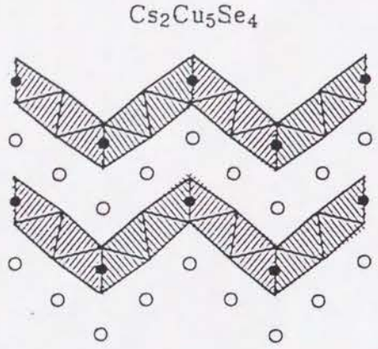

Fig. 1-9 The schematic view of the crystal structure of $Cs_2Cu_5Se_4$. The closed circles indicate the copper atoms on the center of the faces of the $CuSe_4$ tetrahedrons.

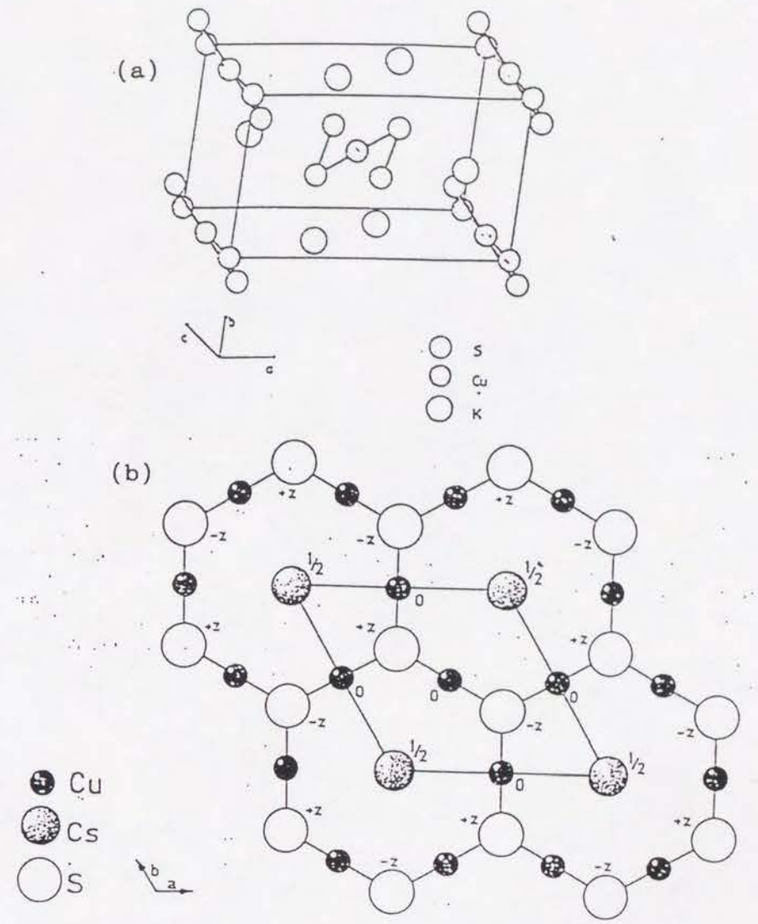

Fig. 1-10 The crystal structures of (a) $KCuS$[22] and (b) $CsCu_3S_2$[23].

§ 1-2 Electronic states of ternary alkali copper chalcogenides.

Among ternary alkali transition-metal chalcogenides, many copper chalcogenides show metallic behaviors.[24,25] What is the origin of this?

In order to explain the highly conducting property of KCu_4S_3, Robin and Day[26] remarked its mixed valence state. Clearly, it is impossible to explain the compositional ratio of KCu_4S_3 if we assume the unique integral oxidation number for each element. They attributed the "strange" compositional ratio of KCu_4S_3 to the mixed valence state in copper as $K^+Cu^{2+}Cu^+{}_3S^{2-}{}_3$. Since all the copper sites are equivalent in KCu_4S_3, the Cu^{2+} sites and the Cu^+ sites may rapidly exchange each other. On this point of view, the metallic property of KCu_4S_3 was discussed by Brown et al.[27]

On the other hand, however, the systematic studies by means of x-ray photoemission spectroscopy (XPS) by Folmer et al.[28] revealed that the copper is always monovalent in binary and multinary sulfides and selenides even though their compositional ratios suggest the existence of divalent copper.

Generally, the XPS core signals of 3d transition metal compounds show complicated satellite structures because of the electron transfer from the ligands to the 3d metals

which occurs simultaneously with the photoemission process.

Fig. 1-11 shows the XPS 2p core signals of copper

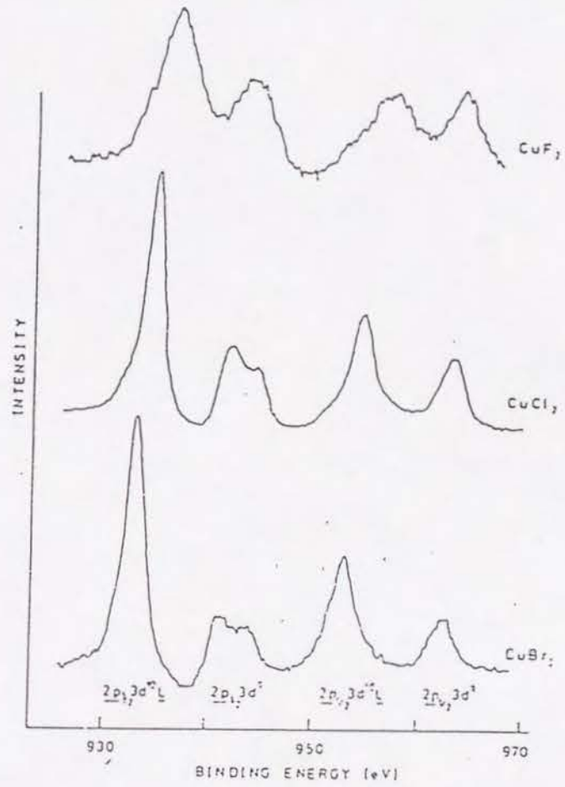

Fig. 1-11 The Cu 2p XPS signals of copper dihalides.[29]

dihalides[29]. In the Cu^{2+} compounds, the initial state is expressed as $c3d^9L$, where c, 3d and L mean the core orbital, the 3d orbitals of Cu, and the outer orbital in the ligand, respectively. Since the XPS process removes the core

electron, a hole is generated in the core orbital in the final states.

Laan et al. have successfully made an assignment of the observed core signal of copper dihalides. The main peaks and the satellites correspond to the photoemission with the final state $\underline{c}3d^{10}\underline{L}$ and $\underline{c}3d^{9}L$, respectively, where the underlines indicate the existence of a hole in the corresponding orbitals. The final $\underline{c}3d^{10}\underline{L}$ state results from the electron transfer from the ligand to the 3d orbital in order to screen the strong Coulomb interaction between the core hole and the 3d hole.

On the other hand, the initial state of Cu^{+} compounds is $c3d^{10}L$. Since the 3d orbital of Cu is completely filled, no electron transfer from the ligand to the 3d orbital of Cu is expected. Thus, in the case of Cu^{+} compounds, the final state is only $\underline{c}3d^{10}L$ and there are no satellite structures. Therefore, XPS is a very useful tool to distinguish Cu^{2+} from Cu^{+}.[30]

Figure 1-12 shows the Cu 2p 3/2 spectra of CuO and Cu_2O.[31] The existence of a satellite in the signal of CuO indicates that the copper is divalent, while the absence of a satellite in the signal of Cu_2O shows that the copper is monovalent. This is what is expected from their formula expressed as $Cu^{2+}O^{2-}$ and $Cu^{+}{}_2O^{2-}$, respectively.

On the other hand, both the Cu 2p XPS core signals of

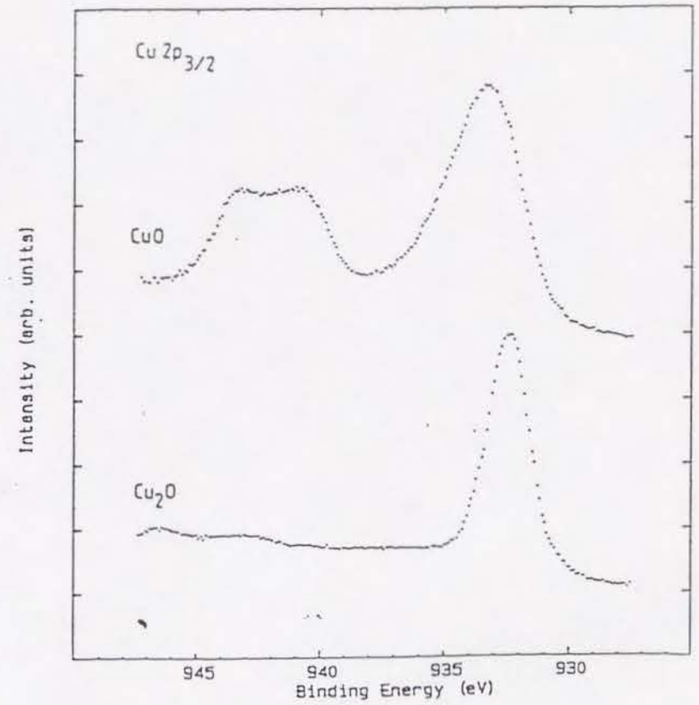

Fig. 1-12 The Cu 2p 3/2 XPS signals of CuO and Cu_2O.[31]

Cu_2S and of CuS have no satellite structures as shown in Fig. 1-13. Furthermore, Folmer et al. revealed that the satellite structure is almost absent in the XPS core signals of many binary and ternary copper chalcogenides they studied. This shows that copper is monovalent in the chalcogenides even in the case of the chalcogenides like CuS whose compositional ratio suggests the existence of divalent copper.

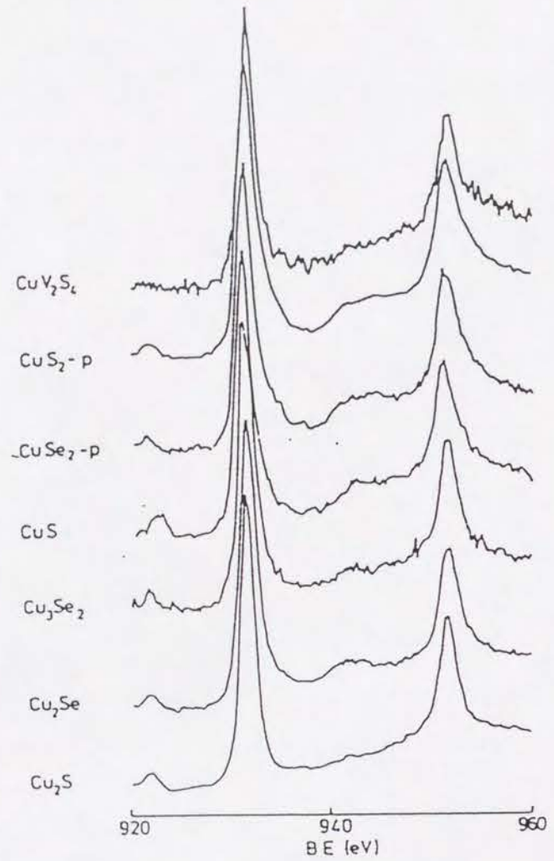

Fig. 1-13 The Cu 2p XPS signal of copper sulfides.[28)]

The absence of the divalent copper in sulfides and selenides is because the electronegativities of sulfur and

of selenium are not large enough to oxidize the copper into Cu^{2+}.[25)]

Therefore, the valence state of KCu_4S_3 should be expressed as $K^+Cu^+_4S^{(2-x)-}_3$, where x=1/3. Similarly, the valence state of $TlCu_2Se_2$ is expressed as $Tl^+Cu^+_2Se^{(2-x)-}_2$, where x=1/2. Consequently, if simple band structures are assumed, these compounds are metals with hole-like (p-type) carriers because the tops of the 3p bands of S are vacant. In fact, positive Hall coefficients and positive thermoelectric powers (TEPs) are observed in KCu_4S_3[28)] and $TlCu_2S_2$[7)].

§ 1-3 Scope of this thesis

It is natural to consider that the bondings between alkali atoms and chalcogen atoms are ionic in alkali copper chalcogenides. On the other hand, slight covalent character is expected in the bonding between copper and chalcogen because the 3d level of copper and the p level of chalcogen (3p for sulfur and 4p for selenium) are not so separated. Therefore, the 3d orbitals of copper and the p orbitals of chalcogen hybridize each other forming the wave functions delocalized in the copper-chalcogen networks.

Especially in the case of "mixed valence" alkali copper

chalcogenides, metallic electronic states are expected because the bands composed of mainly p orbitals of chalcogen are not completely filled. Furthermore, it is expected that the electronic states reflect a variety of the low-dimensional copper-chalcogen networks.

Recently, ter Haar et al.[32] and Fleming et al.[33] discovered that $K_3Cu_8S_6$ undergoes charge-density wave (CDW) transitions. Charge-density wave transition[34] is the phase transition, characteristic of low-dimensional metals, caused by the interaction between conduction electrons and a lattice distortion. When a metallic system undergoes a CDW transition, the electric conductivity decreases because a part of (or all) the conduction electrons condense into a CDW state, which does not contribute to the electric conduction under low electric field. Since a CDW is accompanied by a periodic lattice distortion, a superstructure which is detectable by x-ray scattering, for example, appears.

The discovery of CDW transitions in $K_3Cu_8S_6$ stimulated us to search other interesting low-dimensional electron systems in ternary copper chalcogenides.

In Chapter 2, we report the systematic studies on the electronic properties of several ternary copper chalcogenides by means of the measurements of the resistivities and the thermoelectric powers (TEPs).

In order to investigate the details of the CDW transitions of $K_3Cu_8S_6$, we have synthesized the mixed crystals $(K_{1-x}Rb_x)_3Cu_8S_6$, $(Rb_{1-x}Cs_x)_3Cu_8S_6$, $K_3Cu_8(S_{1-x}Se_x)_6$ and $Rb_3Cu_8(S_{1-x}Se_x)_6$. In Chapter 3, we report their transport properties and pressure effects.

In order to obtain information about the superstructures caused by the CDW transitions, we have carried out x-ray diffuse scattering studies on $(K_{1-x}Rb_x)_3Cu_8S_6$. Their results are reported in Chapter 4.

Chapter 2. Electronic Properties of Alkali Copper Chalcogenides: resistivities and thermoelectric powers.

§ 2-1 Introduction

Table 2-1 and 2-2 summarize the reported phases of alkali copper chalcogenides. Many alkali copper chalcogenides show metallic properties.

As discussed in the previous chapter, this is explained by the existence of holes in the bands predominantly made of p orbitals of chalcogen. However, it is only KCu_4S_3 that the existence of p-type (hole-like) carriers is experimentally confirmed[28], and it is unknown whether other mixed valence alkali copper chalcogenides such as $Na_3Cu_4S_4$ and $K_3Cu_8S_6$ have p-type carriers or not.

As shown in the previous chapter, most of alkali copper chalcogenides have crystal structures which suggest low-dimensional electron states. However, it is only $K_3Cu_8S_6$ that has been reported to have the physical property characteristic of low-dimensional electronic systems, CDW transitions.

In order to investigate the electronic states of the alkali copper chalcogenides, we carried out the measurements of the resistivities and the thermoelectric powers (TEPs) down to liquid helium temperature.

Another purpose of the present study is to find new superconductors. The report that CuS becomes superconducting below 1.35K[35] stimulated us to investigate the electronic properties of alkali copper chalcogenides at low temperature.

§ 2-2 Experimental

A. Syntheses

All the samples were prepared by fusion reactions of alkali carbonate, copper, and sulfur (or selenium). The mixture of starting materials was put in an alumina crucible with a graphite cap. Then it was kept at 800-900℃ for about a few hours under an Ar or N_2 gas flow. The apparatus for the syntheses is shown in Fig. 2-1. The products were washed with pure water in order to remove the polysulfides surrounding the crystals. They were further washed with ethanol and ether, then the crystals were dried under vacuum. The synthetic conditions are summarized in table 2-3. The obtained phases are characterized by x-ray powder patterns.

Table 2-1 : alkali copper sulfides and selenides (x-y-z represents the composions)

	Na	K	Rb	Cs
S	3-4-4	1-4-3 1-7-4 3-8-6	1-4-3 3-8-6	1-4-3 1-3-2 (hexagonal)
	?-?-? (hexagonal)	1-3-2 (monoclinic) 1-1-1		
Se		1-4-3	1-4-3 3-8-6	1-4-3 2-5-4 3-8-6

Table 2-2 : Lattice constants and Electronic Properties

	Symmetry and Lattice Constants	Electronic Properties
$Na_3Cu_4S_4$	orthorhombic[11], a=14.624, b=7.163, c=3.771	metallic[43] <present study>
KCu_4S_3	tetragonal[27,48], a=3.899, c=9.262	metallic[27,28,48] p-type carriers <present study>
KCu_7S_4	tetragonal[20], a=10.176, c=3.849	(semi)metallic[20] phase transitions
$K_3Cu_8S_6$	monoclinic[13], a=17.332, b=3.830, c=9.889, β =104.12	metallic[13] CDW transitions
		<present study>
KCu_3S_2	monoclinic[12], a=14.773, b=3.946, c=8.182, β =113.5	<present study>
KCuS	orthorhombic[22], a=10.66, b=6.20, c=5.32,	----------
$RbCu_4S_3$	tetragonal[9], a=3.920, c=9.41	metallic[40] <present study>
$Rb_3Cu_8S_6$	monoclinic[13], a=17.840, b=3.865, c=10.011, β =104.91	metallic[51] <present study>
$CsCu_4S_3$	tetragonal[23], a=3.975, c=9.689	metallic[40]
$CsCu_3S_2$	hexagonal[23], a=5.469, c=6.354	<present study>
KCu_4Se_3	tetragonal[9], a=3.963, c=9.81	----------
$RbCu_4Se_3$	tetragonal[9], a=3.964, c=9.67	----------
$Rb_3Cu_8Se_6$	monoclinic[14], a=18.458, b=4.010, c=10.212, β =104.44	<present study>
$CsCu_4Se_3$	tetragonal[9], a=4.091, c=10.08	----------
$Cs_2Cu_5Se_4$	orthorhombic[21], a=3.992, b=19.417, c=13.219	<present study>
$Cs_3Cu_8Se_6$	monoclinic*), a=19.076, b=4.078, c=10.449, β =106.04	----------

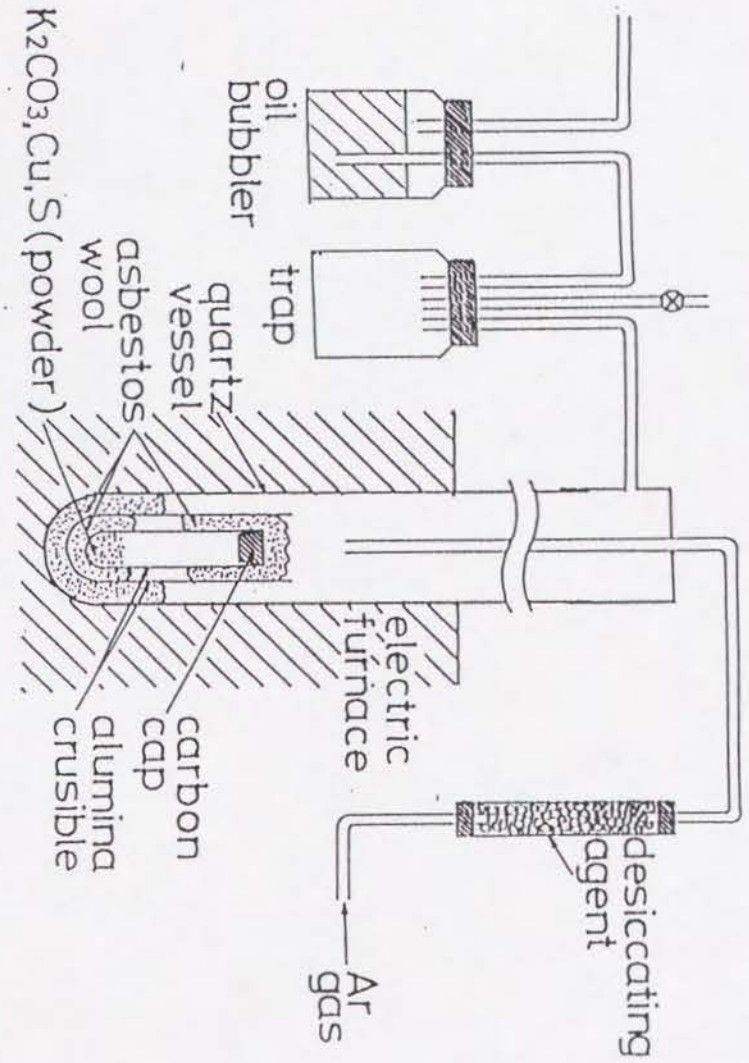

Fig. 2-1 The apparatus for syntheses of ternary alkali copper chalcogenides.

Table 2-3 : the purities of the reagent and the synthetic conditions of the alkali copper chalcogenides.

Sample	purities A_2CO_3	Cu	S (or Se)	molar ratios A_2CO_3 : Cu : S(Se)	reaction temperatures(℃)	reaction periods (hour)
$Na_3Cu_4S_4$	99.97%	99.999%	99.999%	2.8 : 1 : 12	800	2
Hexagonal Na-Cu-S	99.97%	99.999%	99.999%	2.8 : 1 : 12	700	2
KCu_4S_3	99.5% 99.99%	99.9% 99.999%	99.9% 99.999%	2.8 : 1 : 12	800	2
$K_3Cu_8S_6$	99.5% 99.99%	99.9% 99.999%	99.9% 99.999%	2.8 : 1 : 12	875	2
KCu_3S_2	99.5%	99.9%	99.9%	2.8 : 1 : 12	900	4
$RbCu_4S_3$	99% 99.9%	99.9% 99.999%	99.9% 99.999%	2.8 : 1 : 12	815	2
$Rb_3Cu_8S_6$	99% 99.9%	99.9% 99.999%	99.9% 99.999%	2.8 : 1 : 12	900	5
$CsCu_3S_2$	99.99%	99.999%	99.999%	2.8 : 1 : 12	900	4
$Rb_3Cu_8Se_6$	99.9%	99.999%	99.999%	0.6 : 1 : 2.4	980	15
$Cs_2Cu_5Se_4$	99.99%	99.999%	99.999%	0.6 : 1 : 2.4	950	10

B. Resistivity

Resistivity measurements were made using usual dc four probe method. All the measurements were carried out on single crystals (except for $Cs_2Cu_5Se_4$). An electrical current of about 0.1~ 1mA was passed. Before all the measurements, Ohmic I-V dependences were confirmed. In order to make good electric contacts, gold wires were sometimes bound to the crystal, then fixed with gold paste.

C. Thermoelectric power

Thermoelctric powers (TEPs) were measured using two methods. The first method is a conventional one. The both ends of sample were fixed on sapphire heat sinks, one of which was heated by manganin heater during the measurements. The temperature difference between the two heat sinks (ΔT) measured by using a thermocouple and the emf of the sample $E_{x,Au}(T)$ measured by using Au wire, whose TEP was already known[36] as $S_{Au}(T)$, were recorded. The TEP of the sample ($S_x(T)$) was obtained using the following relation:

$$S_x(T)=S_{Au}(T)-E_{x,Au}(T)/\Delta T$$

The second method is as follows: two Au+0.07%Fe vs. chromel thermocouples were fixed to the both ends of a sample directly[37,38] with Au paste(Fig. 2-2). The temperature

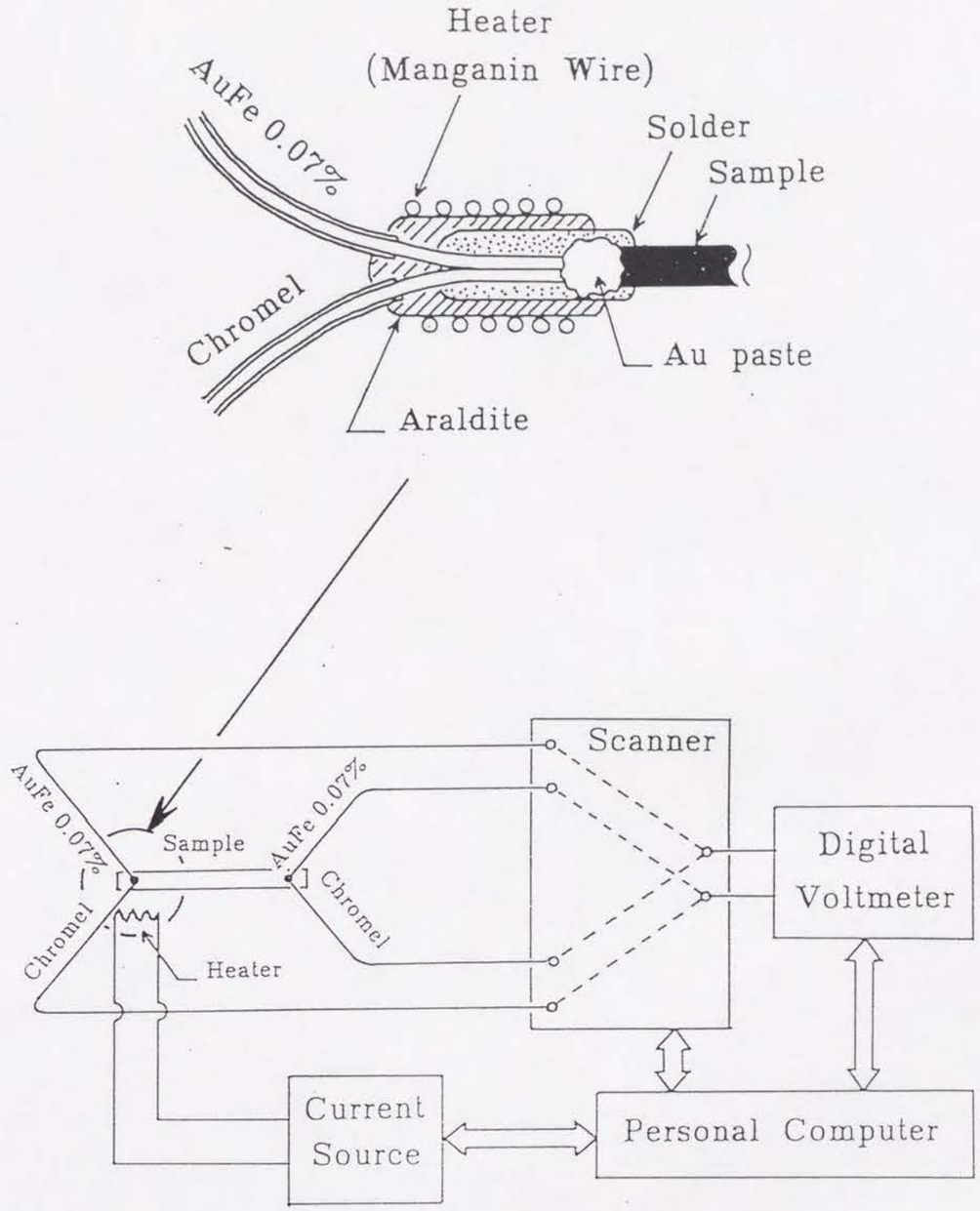

Fig. 2-2 The apparatus for measurements of thermoelectric power.

difference within 1K between the ends of a sample was generated by manganin heater. The emf of sample measured by using chromel wire ($E_{x,ch}(T)$) and measured by using Au+0.07%Fe wire ($E_{x,AF}(T)$) were independently recorded. The TEP of a sample ($S_x(T)$) was obtained using the following relation:

$$S_x(T)=S_{ch}(T)-S_{AF,ch}(T)\cdot E_{x,ch}(T)/(E_{x,ch}(T)-E_{x,AF}(T)),$$

where $S_{AF,ch}(T)$ and $S_{ch}(T)$ are the TEP of the thermocouple and the absolute TEP of chromel, respectively. $S_{ch}(T)$ was obtained by the TEP measurement of Pb wire whose absolute thermoelectric power has been already measured.[39] The second method has an advantage in measuring precise temperature difference of a sample because of the direct contact between a sample and thermocouples.

§ 2-3 Results and Discussion

A. KCu_4S_3 and $RbCu_4S_3$

(a) Resistivity

KCu_4S_3 and $RbCu_4S_3$ are blue-black square platelets with metallic luster. The typical size of the crystals is about $3\times 3\times 0.05$ (mm^3). As shown in Fig. 2-3, ACu_4S_3 has double-

layered crystal structure composed of only edge-shared CuS_4 tetrahedrons (see also Fig. 1-3(b)).

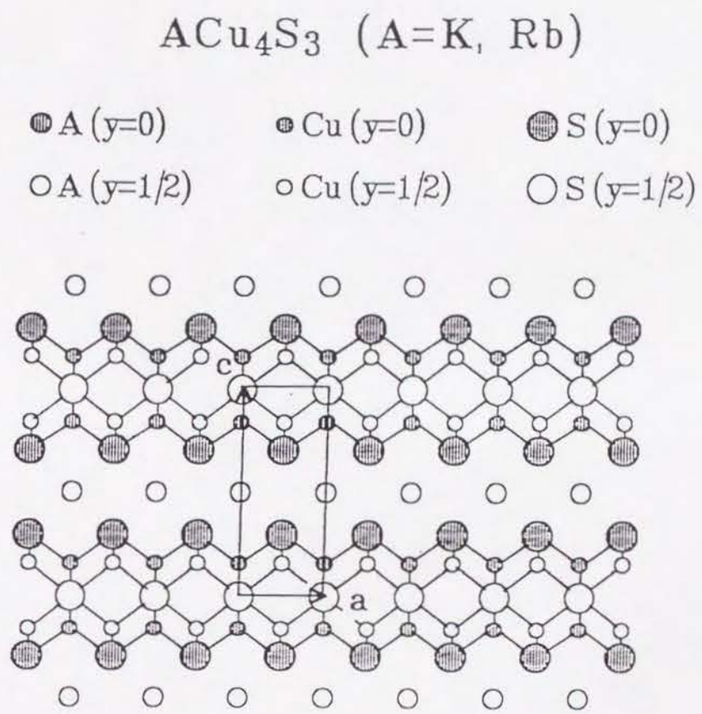

Fig. 2-3 The crystal structure of KCu_4S_3 and $RbCu_4S_3$.

The resistivities of ACu_4S_3[27,28,40] (A=K, Rb, Cs) have been already reported. All the reported data show that these compounds are normal metals down to the measuring lowest temperatures. (about 4.2K for KCu_4S_3[28], and 150K for $RbCu_4S_3$ and $CsCu_4S_3$[40]) In order to investigate the

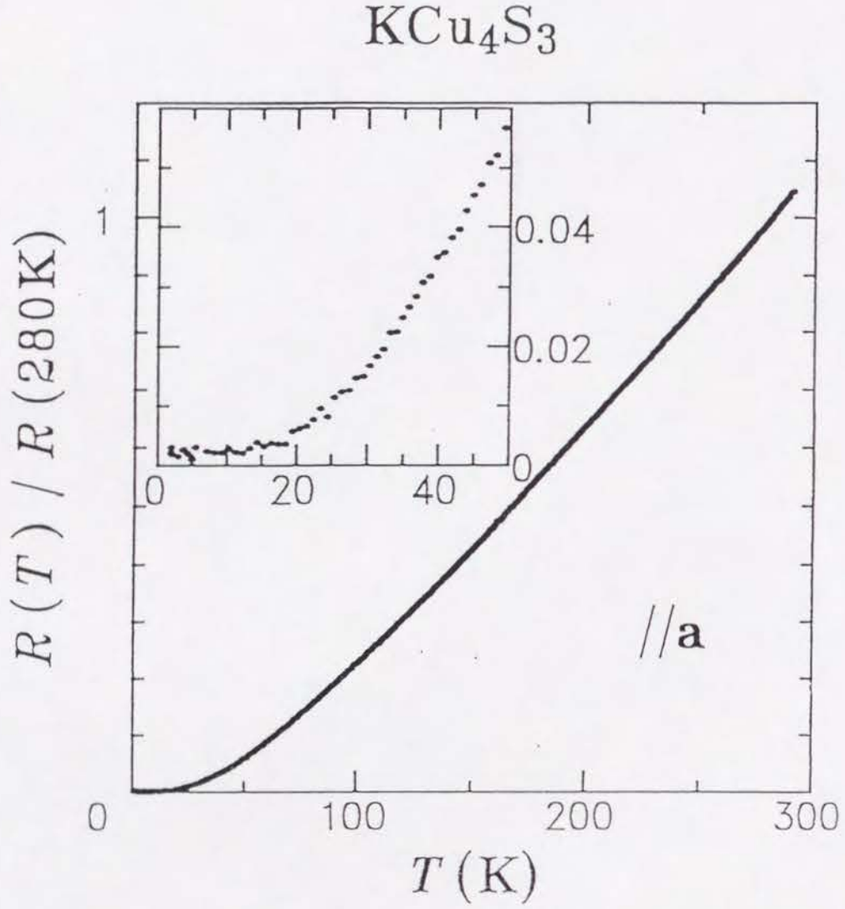

Fig. 2-4 The resistivity of KCu_4S_3 along the a-axis normalized by the room temperature value, $1.2\times 10^{-4}\ \Omega$ cm.

electronic state at low temperature below 4.2K, we measured the resistivity of KCu_4S_3 down to 1.4K.

Figure 2-4 shows the in-plane resistivity of KCu_4S_3 normalized by the value at room temperature, which is $1.2\times 10^{-4}\ \Omega$ cm. It shows metallic temperature dependence down to 1.4K. As shown in the inset of Fig. 2-4, the resistivity becomes almost temperature independent below 10K. No superconducting transition was observed. The residual resistance ratio (R.R.R.) in the present measurement is very large, about 400, indicating the good quality of the sample.

(b) Thermoelectric powers

Folmer et al. revealed[28] that the Hall coefficient and the TEP are positive as expected from the p-type metal scheme, $K^{+}Cu^{+}{}_4S^{(2-x)-}{}_3$, where x=1/3. However, their TEP measurement was made only above 80K and the behavior is not of usual diffusion TEP of a simple metal. In order to obtain information about the TEP at low temperature, we measured the TEPs of KCu_4S_3 and $RbCu_4S_3$ down to 4.2K.

Figure 2-5 shows the in-plane TEPs of KCu_4S_3 and $RbCu_4S_3$. The present result on KCu_4S_3 is almost in agreement with the result down to 80K by Folmer et al.[28] The temperature dependence of the TEP of KCu_4S_3 ($RbCu_4S_3$) is as follows. With decreasing temperature, it slightly decreases around room temperature, increases between 210K (170K) and 25K (30K). After reaching maximum of 8 μV/K (10 μV/K), it

decreases again below 25K (30K) and then approaches zero.

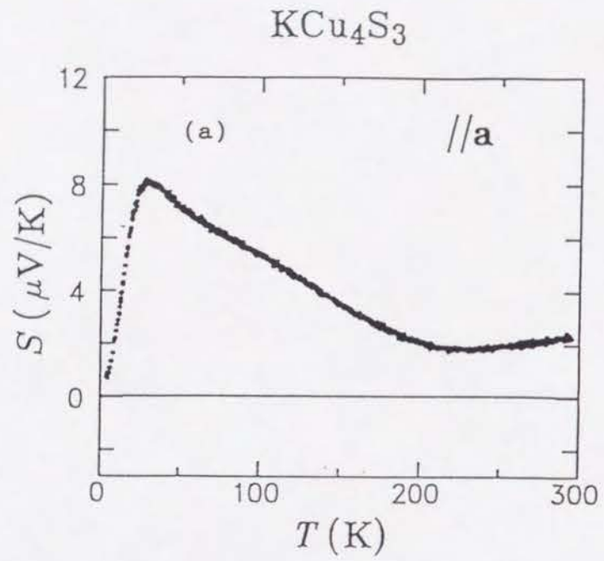

Fig. 2-5 The thermoelectric powers, along the a-axis, of (a) KCu_4S_3 and (b) $RbCu_4S_3$.

Generally, there are mainly two contributions to TEP of metals as follows[37]:

$$S = S_D + S_g , \tag{1}$$

where S_D and S_g denote diffusion TEP and phonon-drag TEP, respectively.

Furthermore, in the case of metals, S_D is expressed as follows:

$$S_D = -\frac{\pi^2 k^2 T}{3|e|} \left[\frac{\partial}{\partial E} \ln\sigma(E) \right]_{E=E_F} , \tag{2}$$

where k and e express Boltzmann's constant and electronic charge; $\sigma(E)$ and E_F express conductivity due to the electrons having energy E, and Fermi energy, respectively.

Within the three-dimensional free electron model, S_D is proportional to temperature as follows:

$$S_D = -\frac{\pi^2 k^2 T}{3|e|E_F} (3/2+p), \tag{3}$$

where it is assumed that the relaxation time τ is dependent on energy as $\tau(E) \propto E^p$.

On the other hand, S_g is proportional to T^3 at low temperature and to T^{-1} at high temperature showing a maximum

in the region $\theta_D/10<T<\theta_D/5$, where θ_D is Debye temperature. For examples, the TEPs of noble metals[41,42], Au, Ag and Cu, have maxima at 30K, 30K and 50K, respectively. These maxima are explained by phonon drag effect.

The temperature dependence of the TEPs of KCu_4S_3 and $RbCu_4S_3$ qualitatively resembles those of noble metals. Therefore, the behaviors having a maximum around 30K can be attributed to phonon drag effect.

In order to calculate S_D using (2), it is necessary to know the band structure and τ (E). However, the both are unknown at present. We can only estimated the order of S_D in free carrier model. Assuming that the the carriers are free electrons with the mass m and that τ (E) is independent of energy, eq. (3) is calculated as follows:

$$S(\mu V/K) = -\frac{3.665\times 10^{-2}}{E_F(eV)}\ T(K) \qquad (4)$$

$$E_F = \frac{1}{2m}\left(\frac{h}{2\pi}\right)^2 (3\pi^2 n)^{2/3}, \qquad (5)$$

where h and n are Planck's constant and carrier density, respectively. For hole carriers, we can use eq. (4) if only reverse the sign of S. In the case of the hole carriers whose mass is identical to that of free electron, S is

dependent only on n and expressed as follows:

$$S(\mu V/K) = 1.005\times 10^{13}\ [n(cm^{-3})]^{-2/3}\ T(K). \qquad (6)$$

The valence state of KCu_4S_3 is described formally as $K^+Cu^+_4S^{2-}_2S^-$. Since a S^- ion has a hole, we can estimate the hole concentration n from the concentration of S^- ions. Table 2-4 shows the hole concentrations, the TEPs calculated using eq. (6), and the observed TEPs of the alkali copper chalcogenides studied.

The calculated TEPs of KCu_4S_3 and $RbCu_4S_3$ are roughly in agreement with the observed values. Therefore, the metallic conduction can be explained by only p-type carriers. The discrepancy between calculated values and observed ones is not so large, taking account of the above assumption that the mass of holes are identical to that of free electrons.

B. $Na_3Cu_4S_4$

(a) Resistivity

The crystals of $Na_3Cu_4S_4$ are blue needles with metallic luster elongated along the c-axis. The typical size of the single crystal is $2\times 0.07\times 0.07$ (mm^3).

Normal metallic behavior of $Na_3Cu_4S_4$ has been already reported down to 15K by Peplinski et al.[43] However, the

Table 2-4 : Hole concentrations and thermoelectric powers (TEPs) of alkali copper chalcogenides studied. The hole concentration n is determined from the compositional ratios. S_{cal} is the TEP calculated from n using eq. (6), S_{obs} is observed TEP.

	n (cm^{-3})	S_{cal}(270K) (μV/K)	S_{obs}(270K) (μV/K)
KCu_4S_3	7.102×10^{21}	7.34	2.16
$RbCu_4S_3$	6.916×10^{21}	7.48	5.31
$Na_3Cu_4S_4$	5.063×10^{21}	9.20	3.84
$K_3Cu_8S_6$	3.142×10^{21}	12.65	0.71
$Rb_3Cu_8S_6$	2.998×10^{21}	13.05	0.89
$Rb_3Cu_8Se_6$	2.732×10^{21}	13.88	2.67
KCu_3S_2	0	---	13.87

electronic state below 15K has been unknown. A metal-insulator phase transition is expected because of the apparently one-dimensional crystal structure of $Na_3Cu_4S_4$: the Cu_4S_4 chains are separated by sodium ions (Fig. 2-6, see also Fig. 1-5).

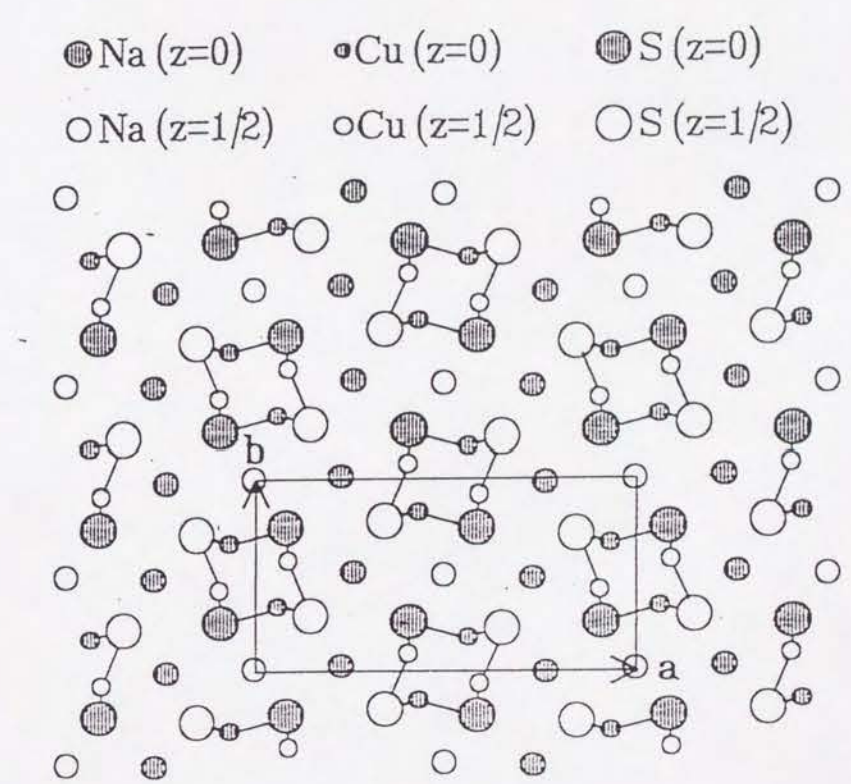

Fig. 2-6 The crystal structure of $Na_3Cu_4S_4$.

In order to investigate the electronic state at very low temperature, we carried out the resistivity measurement down to 0.5K. The measurement down to 1.5K was made using usual ^{4}He cryostat at Kyoto University. The measurement between 1.5K and 0.5K was made using the ^{3}He cryostat at Institute for Molecular Science.

Figure 2-7 shows the normalized resistivity of $Na_3Cu_4S_4$ along the c-axis. The resistivity at room temperature is $5\times 10^{-5}\,\Omega$ cm, in good agreement with the result by Peplinski et al. The resistivity shows metallic temperature dependence down to 1.5K. Moreover, the measurement using ^{3}He revealed that the resistivity is almost independent of temperature between 1.5K and 0.5K. The large R.R.R. of about 280 indicates that the quality of the crystal is good. No metal-insulator transition was observed down to 0.5K.

Oshiyama et al.[44] reported that the resistivity of a metal having quasi one-dimensional Fermi surface shows T^n dependence, where $2 \leqq n \leqq 3$, due to the electron-electron Umklapp scattering. In fact, quasi one-dimensional $TaSe_3$, $NbSe_3$ and Nb_3S_4 have the resistivities dependent on T^3, $T^{2.2}$ and T^3, respectively.[45] However, in the case of $Na_3Cu_4S_4$, the resistivity is proportional to about $T^{3.5}$ in the low temperature region.

Therefore, there is no evidence to prove that the electronic state of $Na_3Cu_4S_4$ is really one-dimensional. The

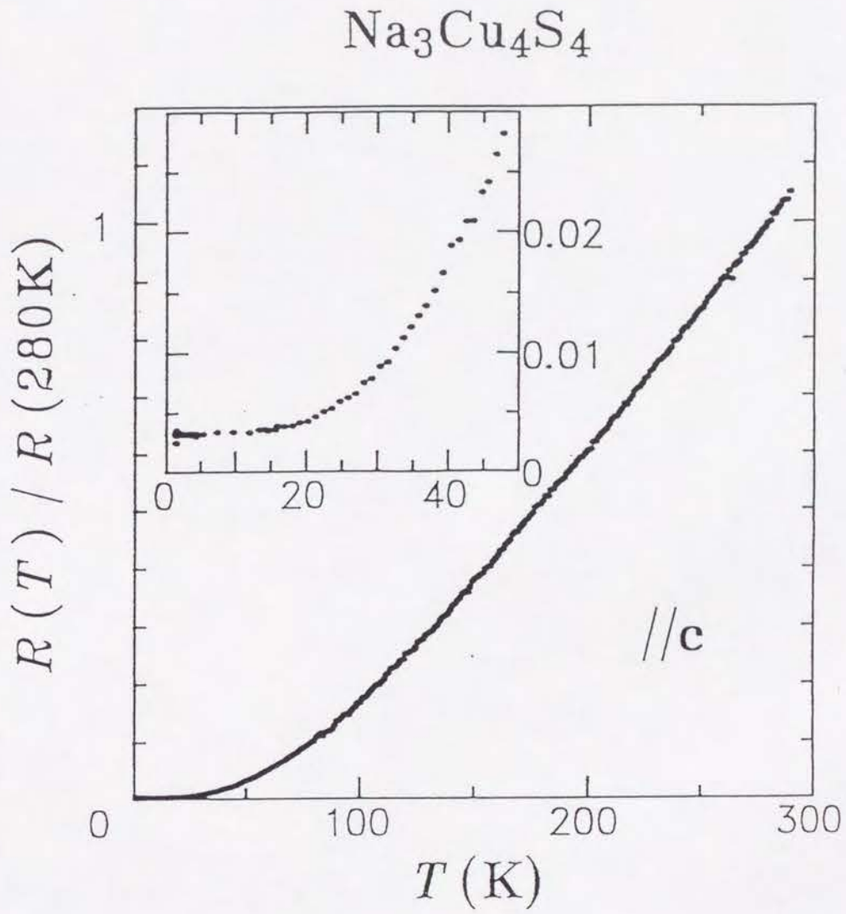

Fig. 2-7 The resistivity of $Na_3Cu_4S_4$ along the c-axis normalized by the room temperature value, $5\times 10^{-5}\,\Omega$ cm.

measurements on the anisotropy of the resistivity will give us helpful information about the dimensionality of the electronic state. However, the resistivity measurements along the other direction are unsuccessful at present because of the needle-like shape of the crystals.

On the other hand, Whangbo and Canadell[46] explained the reason why $Na_3Cu_4S_4$ has no CDW transition by considering the symmetry of the wave functions of the conduction band. Their conclusion is that the electronic state of $Na_3Cu_4S_4$ is one-dimensional but that the conduction electrons cannot be coupled with the symmetric deformation of the Cu_4S_4 chain.

(b) Thermoelectric power

The compositional ratio of $Na_3Cu_4S_4$ suggests the mixed valence electron state as $Na^+{}_3Cu^+{}_4S^{(2-x)-}{}_4$, where x=1/4. Therefore, it is expected that $Na_3Cu_4S_4$ is p-type metal like KCu_4S_3. In order to confirm this, we have measured the TEPs of $Na_3Cu_4S_4$.

The TEP of $Na_3Cu_4S_4$ is shown in Fig. 2-8. The room temperature value is about 4 μV/K. With decreasing temperature, the TEP slightly decreases between room temperature and 210K, slightly increases between 210K and 40K, and then decreases below 40K, approaching zero. The TEP is positive in the whole measuring temperature region. In order to conclude that the carriers are only p-type ones,

the measurement of Hall coefficient is necessary. However, the value of TEP at room temperature can be explained only p-type carriers because the discrepancy between the calculated value and observed value is not so serious (table 2-4).

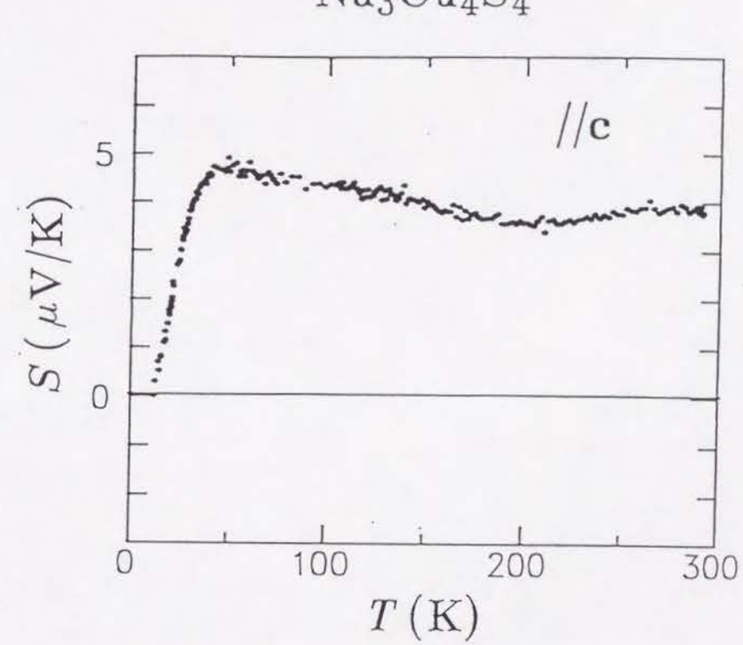

Fig. 2-8 The thermoelectric power of $Na_3Cu_4S_4$.

The behavior of showing a maximum around 40K resembles that in KCu_4S_3 and $RbCu_4S_3$ and can be attributed to phonon

drag effect. The TEP around room temperature is not proportional to temperature, unlike the diffusion TEP of usual metals. However, as Mori and Inokuchi reported[47], the calculation of the diffusion TEP, taking account of real anisotropic band structure, can reproduce the behaviors not proportional to temperature.

C. $K_3Cu_8S_6$, $Rb_3Cu_8S_6$ and $Rb_3Cu_8Se_6$

(a) introduction to charge-density wave transitions in $K_3Cu_8S_6$

The existence of the $K_3Cu_8S_6$ phase was first reported by Rüdorff et al. about forty years ago.[48] They also reported its high electrical conductivity at room temperature. Twenty-seven years later, Burschka analyzed the crystal structure of $K_3Cu_8S_6$ (Fig. 2-9). It has a layered structure; the Cu_8S_6 sheet structures are separated by potassium ions.[13] As already shown in Fig. 1-7(b), the Cu_8S_6 sheet is composed of the Cu_4S_4 chains bound each other by the columns of the edge-shared CuS_4 tetrahedrons.

Recently, ter Haar et al.[32] and Fleming et al.[33] have found CDW transitions in $K_3Cu_8S_6$. After their discovery, several studies on $K_3Cu_8S_6$ have been so far reported; such as pressure effects[49], magnetic field effect[50], XPS[51] and band calculations[52].

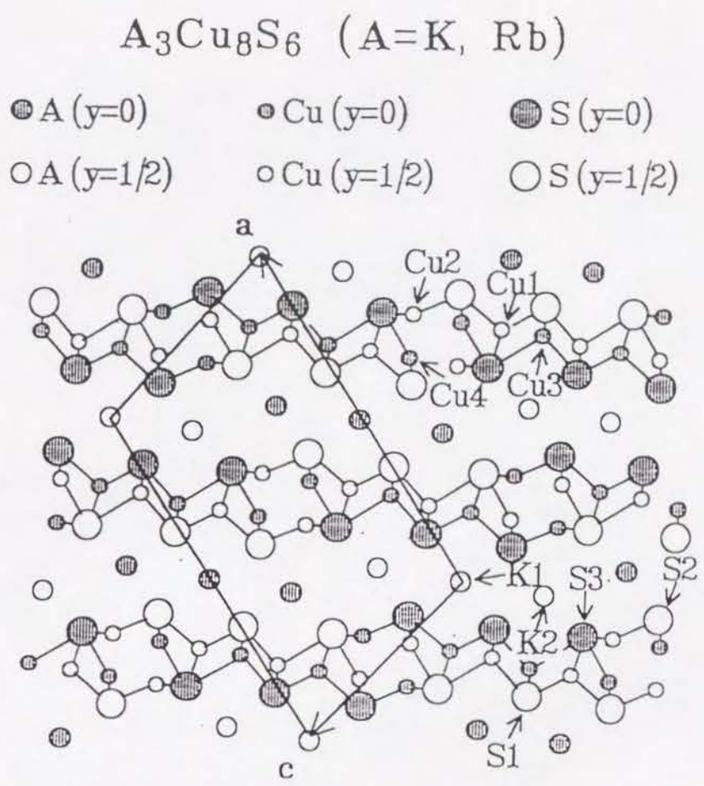

Fig. 2-9 The crystal structure of the $A_3Cu_8S_6$ (A=K or Rb) projected along the b-axis. The value y is the positional parameter along the b-axis.

Two phase transitions are observed at T_1 (153K) and at T_2 (55K) in $K_3Cu_8S_6$.[32,33] As shown in Fig. 2-10, the resistivity is metallic above T_1, but non-metallic between T_1 and T_2. An incommensurate superstructure (0 (1-δ)/2 0)

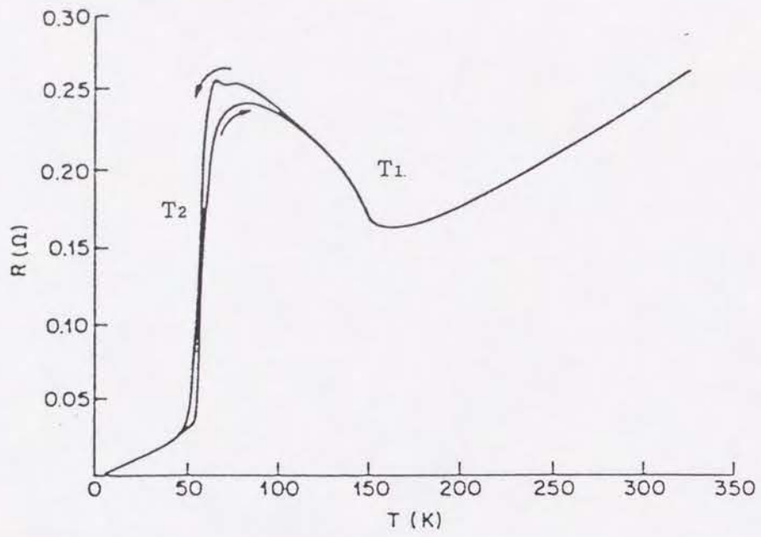

Fig. 2-10 The temperature dependence of the electrical resistance of $K_3Cu_8S_6$.[32]

appears between T_1 and T_2. The T_1 transition is interpreted as a CDW transitions. However, there are some anomalous behaviors such as a resistivity hump just above T_2, etc.

On further cooling, the resistivity decreases drastically at T_2. A thermal hysteresis is observed around T_2. Below T_2, the resistivity becomes metallic again, and the incommensurate superstructure disappears but another commensurate superstructure (1/2 1/2 0) instead appears. The

origin of the T_2 transition is not clear at present. A possible explanation is a lock-in transition of the CDW. However, the commensurate superstructure below T_2 is abnormally strong for considering an ordinary CDW.

(b) Resistivities

$Rb_3Cu_8S_6$, $Rb_3Cu_8Se_6$[14], and $Cs_3Cu_8Se_6$[14] also have the $K_3Cu_8S_6$-type crystal structures. However, their electrical properties have been unknown. In order to know whether the phase transitions of $K_3Cu_8S_6$ are observed universally in the $K_3Cu_8S_6$-type structure or not, we carried out the resistivity measurements on $Rb_3Cu_8S_6$ and $Rb_3Cu_8Se_6$. (The measurements on $Cs_3Cu_8Se_6$ is unsuccessful at present because of the poor quality of the crystals we synthesized.)

The crystals of $K_3Cu_8S_6$, $Rb_3Cu_8S_6$ and $Rb_3Cu_8Se_6$ are blue-black needles with metallic luster elongated along the b-axis.

With decreasing temperature, as shown in Fig. 2-11, the resistivity of $Rb_3Cu_8S_6$ decreases down to 120K, increases between 120K and 50K, and decreases again below 50K with decreasing temperature. Clearly, also in $Rb_3Cu_8S_6$, there is a transition which corresponds to the T_1 transition of $K_3Cu_8S_6$ around 110K. However, there is no abrupt drop in the resistivity corresponding to the T_2 transition of $K_3Cu_8S_6$. Further, unlike in $K_3Cu_8S_6$, there is no thermal hysteresis in the whole temperature region. Below 50K, the metallic

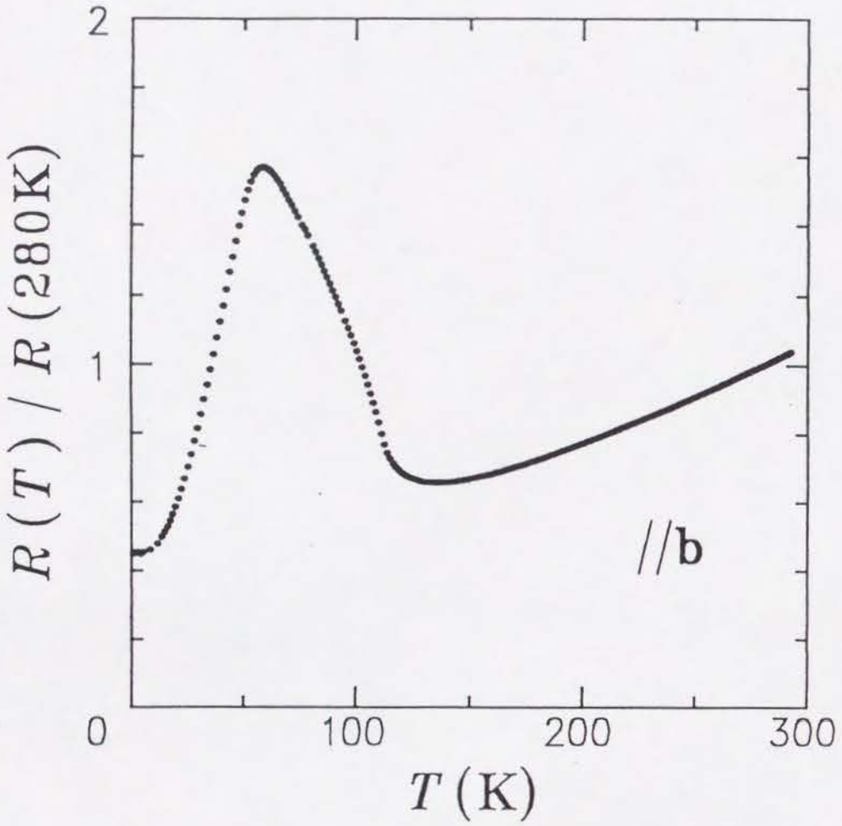

Fig. 2-11 The resistivities of $Rb_3Cu_8S_6$ along the b-axis normalized by the room temperature value 2×10^{-4} Ω cm.

behavior is recovered. However, as discussed in the following chapters, this is not due to a phase transition.

The present result on $Rb_3Cu_8S_6$ qualitatively agrees

with the result on a pellet down to 30K reported by Ro and Hatfield[51], but there are some differences in the absolute value and in the sharpness of the T_1 transition. This is probably because our result is of a single crystal while their result is of a pellet of $Rb_3Cu_8S_6$.

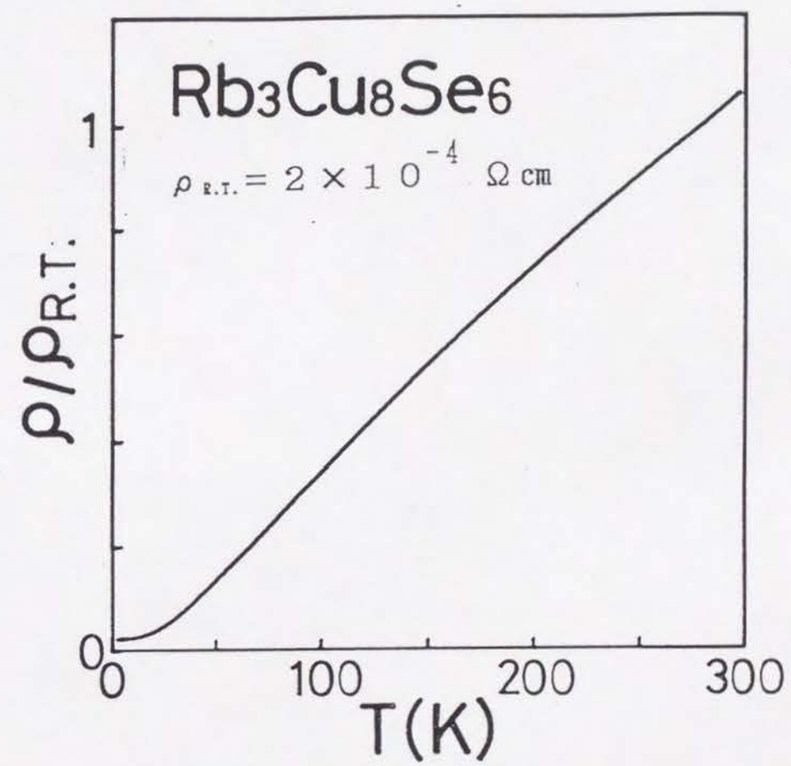

Fig. 2-12 The resistivities of $Rb_3Cu_8Se_6$ along the b-axis normalized by the room temperature value 2×10^{-4} Ω cm.

Figure 2-12 shows the resistivity of $Rb_3Cu_8Se_6$.

It exhibits metallic behavior, and there are no longer any CDW transitions. The absence of the CDW transition in $Rb_3Cu_8Se_6$ indicates that the shape of Fermi surface strongly depends on the difference in the chalcogen atoms.

(c) Thermoelectric powers

There have been no reports about the TEP of $K_3Cu_8S_6$-type compounds. In order to investigate the carriers, we measured the TEPs of $K_3Cu_8S_6$, $Rb_3Cu_8S_6$ and $Rb_3Cu_8Se_6$.

Figure 2-13 shows the TEP of $K_3Cu_8S_6$. Unlike KCu_4S_3 and $Na_3Cu_4S_4$, the behavior is not of a simple p-type metal. The TEP is slightly positive at room temperature. On cooling, S decreases with decreasing temperature and reaches minimum $-2.5\ \mu$V/K at 144K, crossing zero line at 253K. This behavior cannot be explained by only p-type carriers and suggests the coexistence of both p-type and n-type carriers. Between 140K and 57K, S increases with decreasing temperature, becoming positive at 110K. In the cooling curve, there is a sharp decrease around 55K, resulting from the T_2 transition. Below 25K, S approaches zero linearly as T approaches 0K. A thermal hysteresis is observed between 34K and 150K.

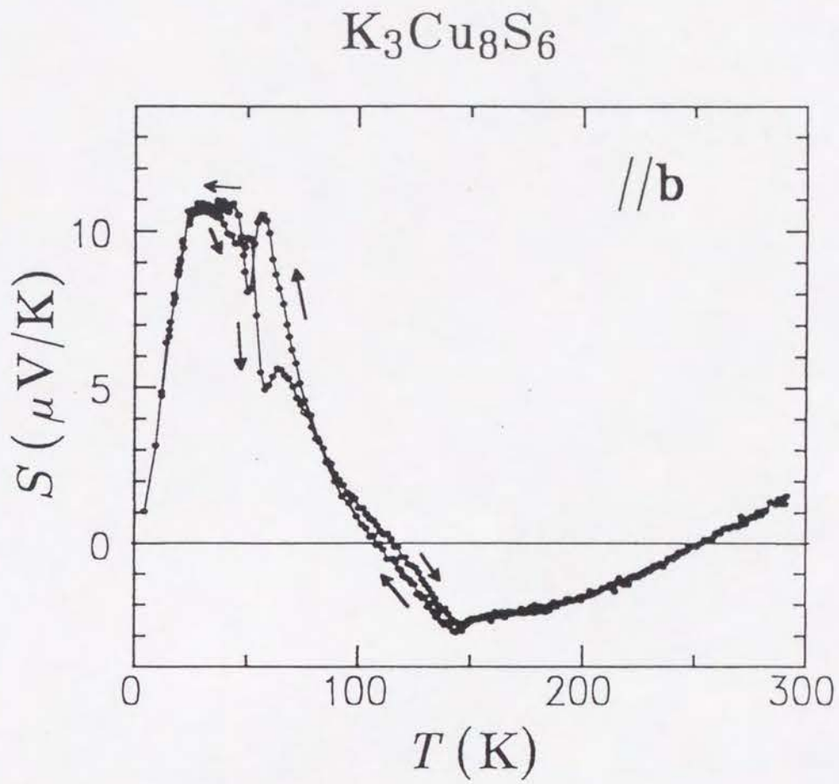

Fig. 2-13 Thermoelectric power of $K_3Cu_8S_6$ along the b-axis.

The TEP in a two carrier system of holes (p-type carriers) and electrons (n-type carriers) is calculated as follows[37]:

$$S = \frac{\sigma_h S_h + \sigma_e S_e}{\sigma_h + \sigma_e} \quad , \tag{7}$$

where S_h and S_e denote the TEPs of holes and electrons; σ_h and σ_e denote the conductivities of holes and electrons, respectively. The almost zero TEP around room temperature results from the compensation of hole TEP and electron TEP like eq. (7).

The resistivity of $K_3Cu_8S_6$ shows that a part of carriers disappears below T_1 due to the formation of the CDW. On the other hand, the TEP moves from negative to positive below T_1. According to eq. (7), it is most probable that the carriers extinguished by the CDW are n-type.

Figure 2-14 shows the TEP of $Rb_3Cu_8S_6$. The TEP is slightly positive at room temperature and becomes negative below 250K. After showing a dip around 110K, S begins to increases on further cooling, crossing the zero line at 135K. Around 50K, it reaches the maximum 8.6 μV/K, then moves to zero as T approaches 0K. Such a sharp decrease in TEP as seen in $K_3Cu_8S_6$ at T_2 is absent in $Rb_3Cu_8S_6$. In addition, no thermal hysteresis is observed. Therefore,

$Rb_3Cu_8S_6$ is unlikely to have the T_2 transition. This is in agreement with the resistivity result. The TEP of $Rb_3Cu_8S_6$ indicates the coexistence of p-type and n-type carriers around room temperature, and that the n-type ones disappear below T_1.

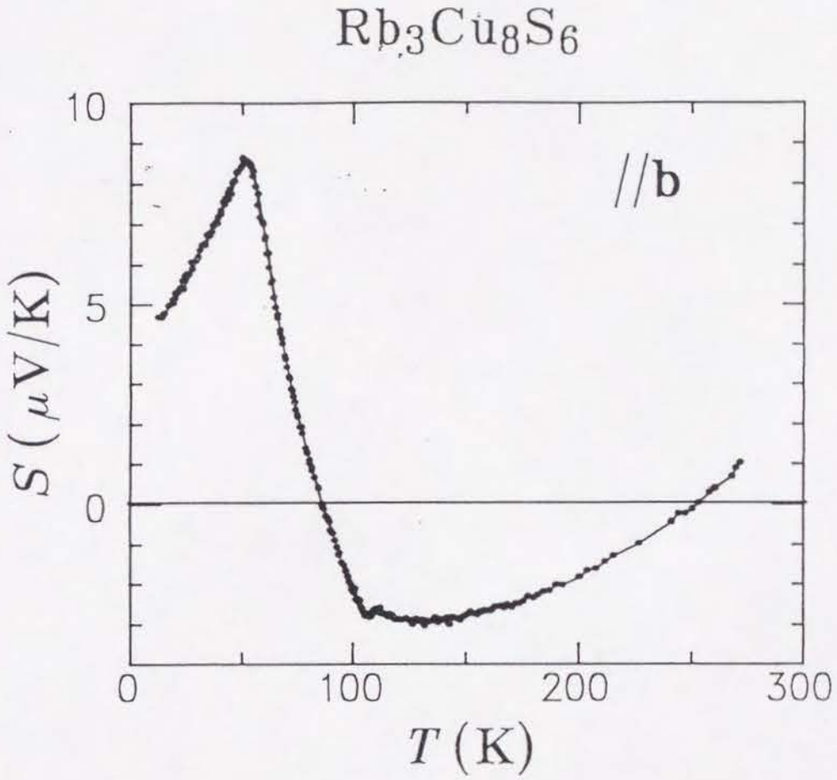

Fig. 2-14 Thermoelectric power of $Rb_3Cu_8S_6$ along the b-axis.

Figure 2-15 shows the TEP of $Rb_3Cu_8Se_6$. The TEP is about 3 μV/K at room temperature. With decreasing temperature, it decreases almost proportionally to T down to 230K. Between 230K and 30K, the TEP increases with decreasing temperature exhibiting a bend around 125K. On

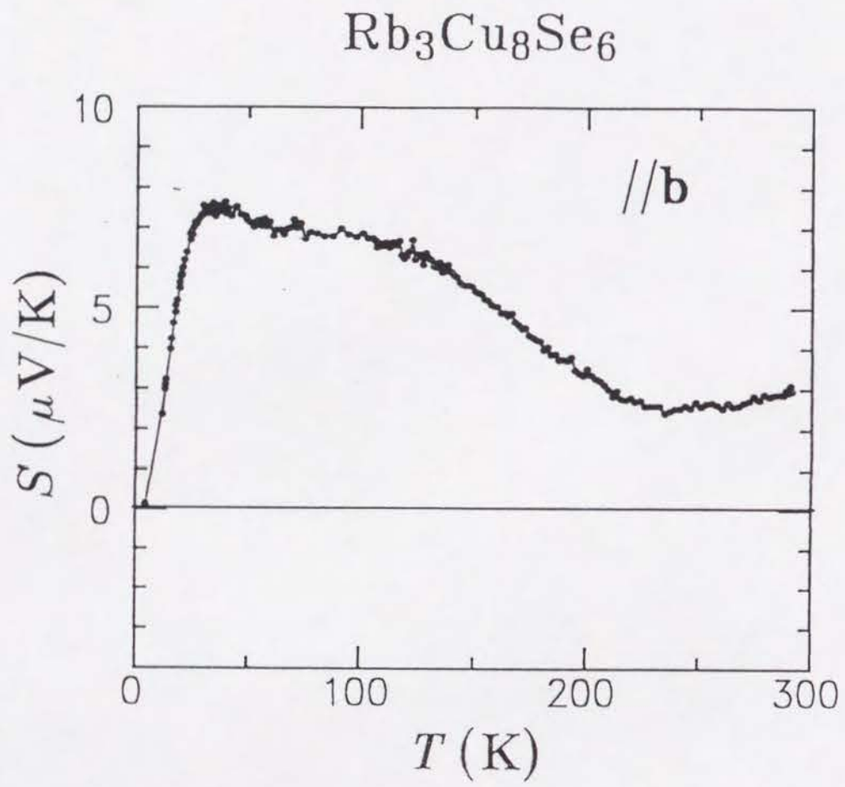

Fig. 2-15 Thermoelectric power of $Rb_3Cu_8Se_6$ along the b-axis.

further cooling, the TEP approaches zero as T→ 0K.

The maximum around 30K is common to KCu_4S_3, $RbCu_4S_3$ and $Na_3Cu_4S_4$, and can be attributed to phonon drag effect. However, the increase in the TEP below 230K cannot be explained by only phonon drag. In order to explain the complicated temperature dependence, information about the band structure is indispensable.

Unlike $K_3Cu_8S_6$ and $Rb_3Cu_8S_6$, the TEP of $Rb_3Cu_8Se_6$ is positive in the whole temperature region. As shown in table 2-4, the TEP at 270K is about 1/5 of the calculated value assuming only free carriers with the free-electron mass.

D. KCu_3S_2

(a) resistivity

As shown in Fig. 1-7(a), KCu_3S_2 has a layered structure composed of the Cu_4S_4 chain and tetrahedral columns. The crystals of KCu_3S_2 are blue-black, metallic-lustrous needles elongated along the b-axis.

In spite of the resemblance in the structures, the electronic state of KCu_3S_2 is expected to be considerably different from that of $K_3Cu_8S_6$ because KCu_3S_2 is not a mixed valence compound; its valence state can be expressed using only closed-shell ions as $K^+Cu^+{}_3S^{2-}{}_2$. Therefore, semiconducting behavior is expected because the 3p band of sulfur is completely filled.

However, large conductivity of 5×10^{2} S cm^{-1} was observed at room temperature. Furthermore, as shown in Fig. 2-16, the resistivity does not show a semiconducting

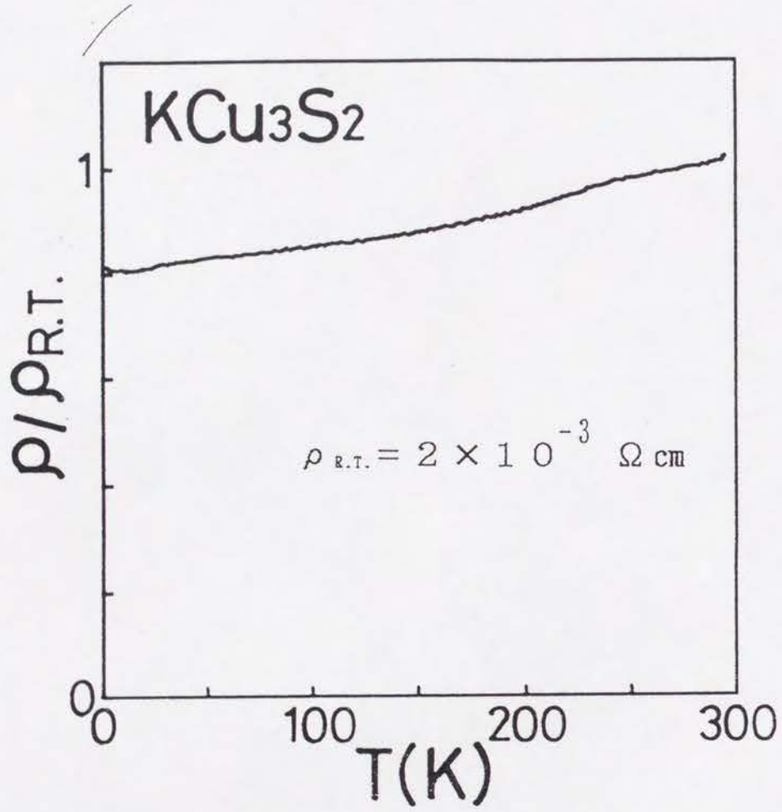

Fig. 2-16 The normalized resistivity of KCu_3S_2 along the b-axis.

behavior but is weakly dependent on temperature.

(b) thermoelectric power

As shown in Fig. 2-17, the TEP of KCu_3S_2 has a metallic temperature dependence. The TEP is positive in the whole temperature region.

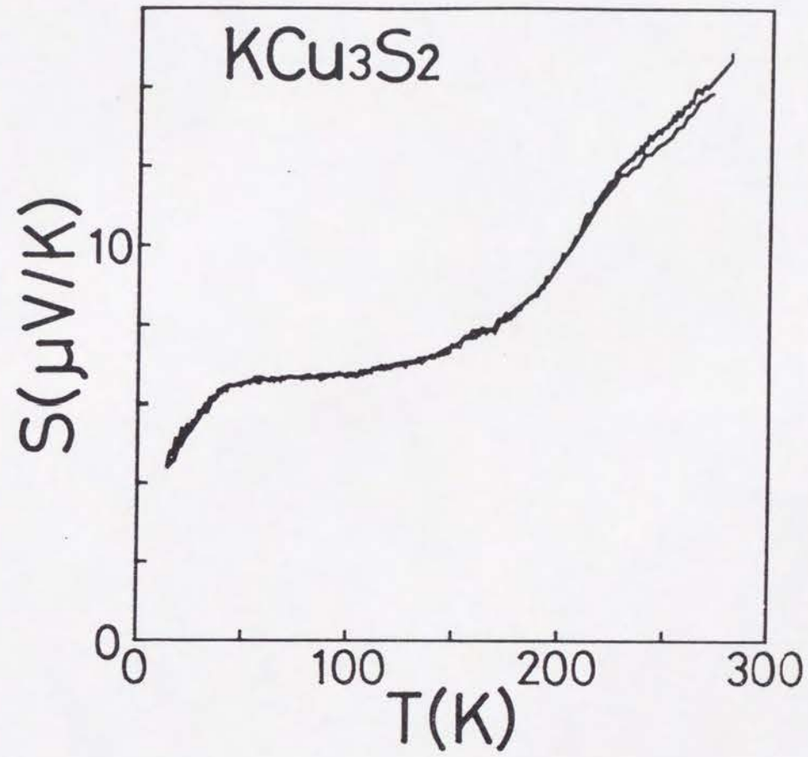

Fig. 2-17 The thermoelectric power of KCu_3S_2.

Non-stoichiometry possibly explains the fact that KCu_3S_2 is not a semiconductor.

It was reported that $TlCu_5Se_3$[16], $TlCu_7S_4$[20] and KCu_7S_4[20] show metallic behaviors with p-type carriers in spite of their compositional ratios indicating semiconducting electronic states. The refinements of the crystal structures of $TlCu_5Se_3$[16] and $TlCu_7Se_4$[17] suggest the existence of vacancies at the copper sites expressed as $TlCu_{4.8}Se_3$ and $TlCu_{6.8}Se_4$, respectively. Therefore, it is possible that there are vacancies at copper sites of KCu_3S_2.

Using eq. (6), the hole density is calculated as 0.28 per KCu_3S_2 formula.

E. $CsCu_3S_2$

As shown in Fig. 1-10(b), the crystal structure of $CsCu_3S_2$[23] is quite different from that of KCu_3S_2 in spite of their identical compositional ratios. It is interesting to compare the electronic properties between KCu_3S_2 and $CsCu_3S_2$.

The crystal of $CsCu_3S_2$ is a colorless transparent plate. As expected from its color, $CsCu_3S_2$ is an insulator. This is what is expected from its valence state, $Cs^+Cu^+{}_3S^{2-}{}_2$.

We found that its color easily changes into black by some chemical treatments. For example, by soaking in

ammonium solution, the color of a $CsCu_3S_2$ crystal becomes blue-black with metallic luster and the resistivity decreases drastically ($<10^{-2}$ Ω cm) without any change in the shape of the crystals. However, preliminary measurements of EPMA and x-ray powder patterns show that the decomposition into Cu_2S (chalcocite) probably occurs without any loss of the shape of the crystals.

G. $Cs_2Cu_5Se_4$

The crystal structure of $Cs_2Cu_5Se_4$ is shown in Fig. 1-9. From its mixed-valent compositional ratio, metallic conductivity is expected in $Cs_2Cu_5Se_4$.

The present resistivity results of $Cs_2Cu_5Se_4$ are preliminary ones because the measurements are made on the bundles of very narrow needle-like crystals. Figure 2-18 shows the resistivity of $Cs_2Cu_5Se_4$[21] measured on two samples (A and B). Although the detailed behavior of the resistivity is dependent on the sample, the resistivities at room temperature are in agreement, taking account the error in measuring the size of samples, 8×10^{-4} Ω cm for the sample A and 3×10^{-4} Ω cm for the sample B.

Their temperature dependences are metallic, but there are anomalies around 160K. The anomaly is more remarkable in sample B. However, the larger R.R.R. of the sample A (about 57) than that of the sample B (about 3.8) indicates that the

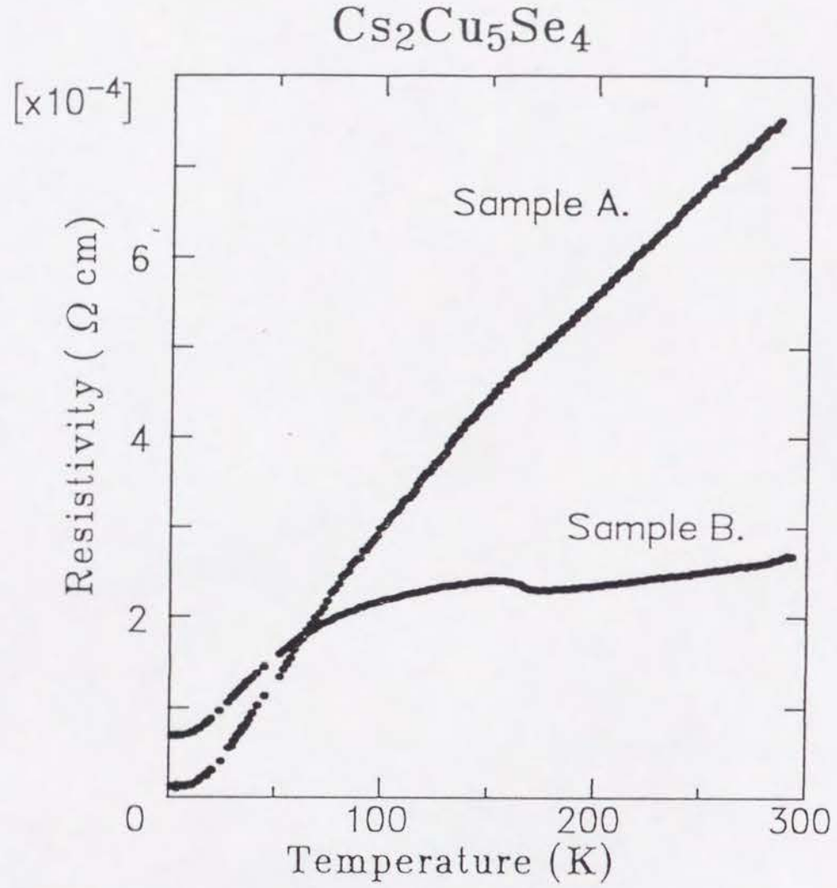

Fig. 2-18 Preliminary results on the resistivity of $Cs_2Cu_5Se_4$. Two types of the behaviors are observed.

quality of the sample A is better than that of the sample B. Therefore, it is possible that the anomaly at 160K is due to some extrinsic origin. The measurements on uniform single crystala are necessary to clarify the origin of the anomaly.

F. Na-Cu-S new phase

In the trials of synthesizing $Na_3Cu_4S_4$, we happened to obtain blue-black hexagonally-shaped platelets at the reaction temperature lower than that for $Na_3Cu_4S_4$. The synthetic condition is described in Table 2-3. The symmetry and the lattice constants determined by a four-circle x-ray diffractometer are as follows: hexagonal, a=3.876Å and c=30.31Å . The value a is close to that of CuS (a= 3.7938Å). This suggests that the present compound includes the trigonal layers of the CuS_4 tetrahedrons (Fig. 1-2(a)) or honeycomb Cu-S sheets (Fig. 1-2(b)).

The preliminary EPMA measurements, using $Na_3Cu_4S_4$ as standard, revealed that the composition of the hexagonal Na-Cu-S is close to $NaCu_8S_5$.

The resistivity at room temperature is 1×10^{-4} Ω cm. As shown in Fig. 2-19, the resistivity exhibits metallic temperature dependence with large R.R.R. (about 63).

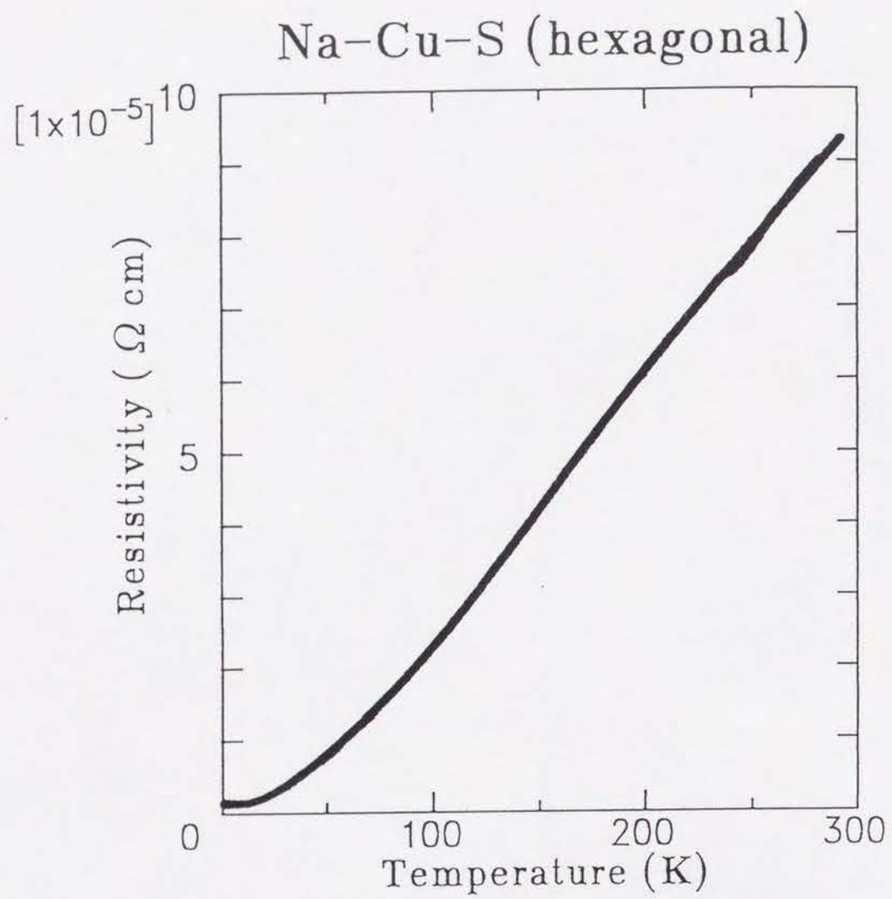

Fig. 2-19 The resistivity of the Na-Cu-S hexagonal phase.

§ 2-4 Summary

In order to investigate the electronic properties of alkali copper chalcogenides systematically, we carried out the measurements of the resistivities and the thermoelectric powers on KCu_4S_3, $RbCu_4S_3$, $Na_3Cu_4S_4$, $K_3Cu_8S_6$, $Rb_3Cu_8S_6$, $Rb_3Cu_8Se_6$, KCu_3S_2, $CsCu_3S_2$, $Cs_2Cu_5Se_4$ and Na-Cu-S hexagonal phase. The results are summarized as follows.

(1) It was found that $Na_3Cu_4S_4$ undergoes no metal-insulator transition such as a CDW transition down to 0.5K in spite of its apparently one-dimensional crystal structure.

(2) As already reported, $K_3Cu_8S_6$ undergoes two CDW transitions at T_1 (153K) and at T_2 (55K). In the present study it was revealed that the isostructural $Rb_3Cu_8S_6$ undergoes the T_1 transition only. Furthermore, the isostructural selenide $Rb_3Cu_8Se_6$ was found to be a normal metal without any phase transitions.

(3) The TEP results on KCu_4S_3, $RbCu_4S_3$ and $Na_3Cu_4S_4$ are consistent with the expectation that they are p-type metal due to the incomplete filling of the 3p band of sulfur like $A^+Cu^+_4S^{(2-x)-}_3$ and $Na^+_3Cu^+_4S^{(2-y)-}_4$, where x=1/3 and y=1/4, respectively.

(4) On the other hand, the TEP of $K_3Cu_8S_6$ and $Rb_3Cu_8S_6$ indicates the coexistence of p-type carriers and n-type

ones, while the TEP of $Rb_3Cu_8Se_6$ is positive in the whole temperature region. The temperature dependence of the TEP of $K_3Cu_8S_6$ and $Rb_3Cu_8S_6$ suggests that the n-type carriers are extinguished by the formation of the CDW.

(5) KCu_3S_2 shows semi-metallic behavior contrary to the insulating behavior expected from its valence state expressed by only closed-shell ions as $K^+Cu^+{}_3S^{2-}{}_2$. This suggests the non-stoichiometry. On the other hand, the $CsCu_3S_2$, whose structure is quite different from that of KCu_3S_2, is an insulator.

(6) Preliminary resistivity measurements on $Cs_2Cu_5Se_4$ shows that it is metallic as expected from its mixed-valent compositional ratio. We also reported the metallic behavior of a new hexagonal Na-Cu-S phase.

Among the compounds studied, only $K_3Cu_8S_6$ and $Rb_3Cu_8S_6$ undergo CDW transitions. It is strange that the isostructural $Rb_3Cu_8Se_6$ and also structurally one-dimensional $Na_3Cu_4S_4$ do not have such transitions. Therefore, it is doubtful to explain the phase transitions in $K_3Cu_8S_6$ and $Rb_3Cu_8S_6$ by only the low-dimensionality in the crystal structures.

On the other hand, the TEP measurements revealed that $K_3Cu_8S_6$ and $Rb_3Cu_8S_6$ are anomalous because they have n-type carriers. It is probable that their CDW transitions are

caused by these n-type carriers and not simply due to the apparently low-dimensional crystal structure.

In the following chapter, we report the further studies on the phase transitions of $K_3Cu_8S_6$-type compounds.

Chapter 3. Charge-Density Wave Transitions in $A_3Cu_8X_6$ (A=K, Rb; X=S, Se): Transport Properties.

§ 3-1 Introduction

As discussed in the previous chapter, several questions remain about the CDW transitions of $K_3Cu_8S_6$. Firstly, why do the isostructural $Rb_3Cu_8Se_6$ and more one-dimensional $Na_3Cu_4S_4$ have no CDW transitions? Secondly, is the existence of the n-type carriers essential for the CDW transitions? Finally, what is the origin of the T_2 transition of $K_3Cu_8S_6$, and why $Rb_3Cu_8S_6$ does not have such a transition?

In order to make further investigations on the phase transitions, the experiments on the mixed crystals are very helpful because they enable us to observe continuous change of physical properties from a compound to another compound. Therefore, we tried to prepare the mixed crystals of $K_3Cu_8S_6$, $Rb_3Cu_8S_6$, etc.

Application of pressure is also useful to modify the physical parameters continuously, so we also investigated the pressure effects on the phase transitions of the $K_3Cu_8S_6$-type compounds.

§ 3-2 Experimental

A. Resistivity under pressure

Resistivity measurements under hydrostatic pressures were made using a Be-Cu clamp cell (Fig. 3-1). A sample was

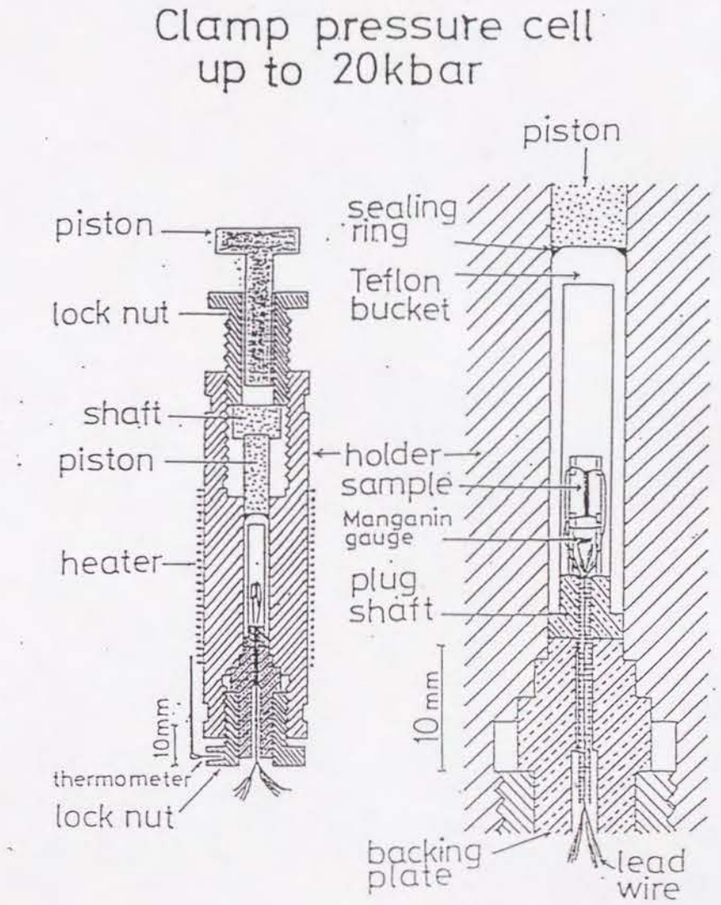

Fig. 3-1 The clump cell for resistivity measurements under hydrostatic pressures.

sealed up with pressure medium in a teflon bucket, then put in the clamp cell. As pressure medium, IDEMITSU Co. #7373 'DAPHNE' oil was mainly used. After a pressure was applied at room temperature by using an oil-pressure press, the pressure was kept by tightening a lock-nut. The pressures were determined from the change in the electrical resistance of manganin wire. In this method, a pressure drop of about 0.2GPa occurs by cooling down to liquid helium temperature because of the solidification of the pressure medium. The pressures denoted in this paper are the values measured at room temperature.

B. Magnetic susceptibility

Magnetic susceptibilities were measured by Faraday method. A number of single crystals which are almost randomly oriented were put in a quartz bucket with liquid paraffin, then it was hung in a magnetic balance. A magnetic field of 10 kG and a field gradient of about 1 kG/cm were applied by superconducting magnets. All the measurements were carried out only on warming. Blank contribution of the quartz bucket and liquid paraffin was independently measured and subtracted from the all susceptibility data.

§ 3-3 Results: alkali substitution effects.

A. $(K_{1-x}Rb_x)_3Cu_8S_6$

(a) Sample preparations

The mixed crystals $(K_{1-x}Rb_x)_3Cu_8S_6$ were prepared by the fusion reactions of the mixture of K_2CO_3, Rb_2CO_3, Cu and S.

Figure 3-2 shows the relation between the 'nominal' Rb

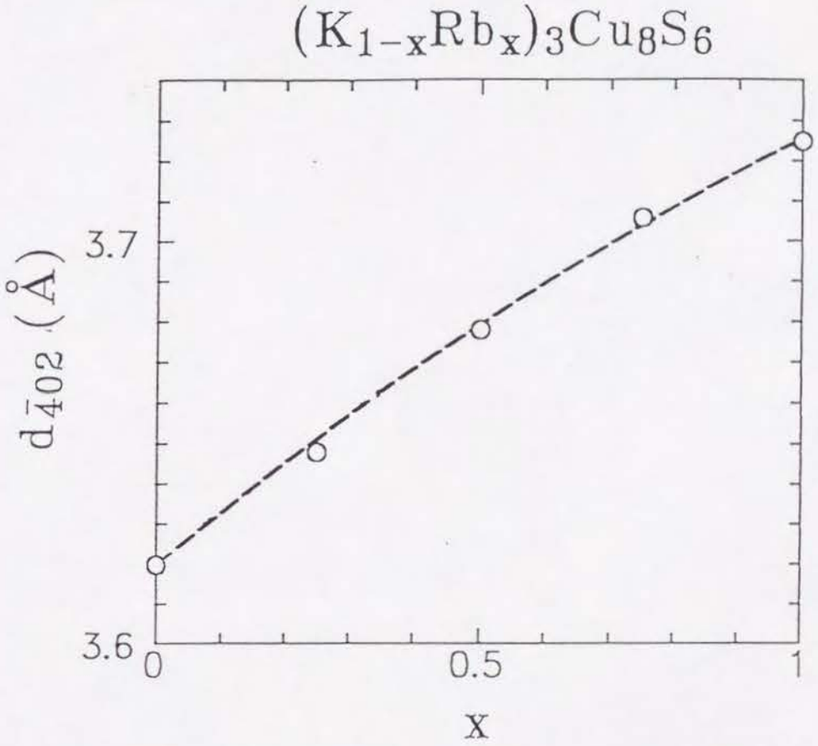

Fig. 3-2 Concentration dependence of the d-value of the (-4 0 2) reflection. The Rb concentrations x are calculated from the ratios of starting K_2CO_3 and Rb_2CO_3. The d-values were obtained by the powder x-ray diffraction measurements. The dashed line is the guide for the eyes.

concentration x, calculated from the K_2CO_3 : Rb_2CO_3 ratio in preparation, and the d value of the (-4 0 2) reflection of the x-ray powder patterns. As x increases, monotonical increase of the d-value is observed. Their powder patterns show neither significant broadening of peaks nor the superstructure suggesting the ordering of K and Rb is observed. This indicates that the alkali sites are randomly occupied by K and Rb.

In addition, the atomic absorption measurement on a nominal $(K_{0.50}Rb_{0.50})_3Cu_8S_6$ single crystal revealed that its observed compositional ratio is $(K_{0.48}Rb_{0.52})_3Cu_8S_6$.

Therefore, the discrepancy between nominal x and actual x is considered to be small. In the present paper, we use the nominal value as x.

(b) Resistivity

The resistivity of $K_3Cu_8S_6$ in the whole temperature region has been already reported by ter Haar et al.[32] (Fig. 2-10). We reported here the behavior of the thermal hysteresis in $K_3Cu_8S_6$. We repeated cooling and heating processes in the temperature region where the thermal hysteresis appears. After heating up to 70K, the sample was cooled again. As soon as it began to be cooled, the resistivity deviated from that of the heating curve and transferred to the first cooling curve at 63K (Fig. 3-3). Then the resistivity varied along the cooling curve.

Further, from 50K, the sample was heated again. The

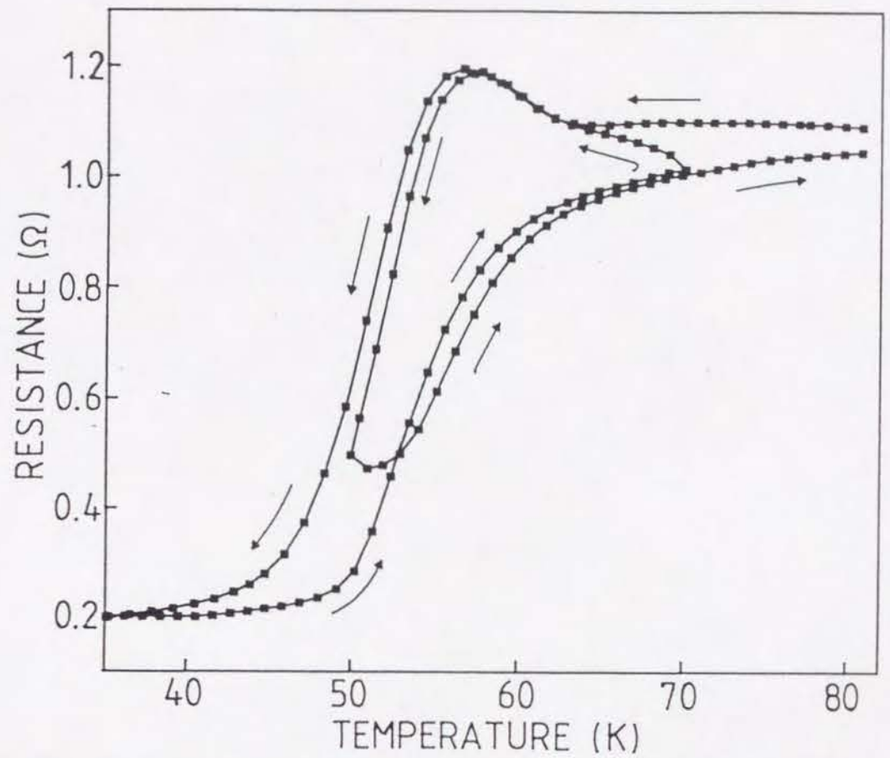

Fig. 3-3 The thermal hysteresis in the resistivity of $K_3Cu_8S_6$ along the b-axis. The sample is first cooled down to 2K and heated up to 70K, then cooled down to 50K and heated up to 300K.

resistivity immediately deviated from the cooling curve and reached the value of the heating curve. Thus it is concluded that the sample tends to have the resistivity of the cooling curve whenever on cooling and to have the value of heating curve whenever on heating.

The resistivities of $(K_{1-x}Rb_x)_3Cu_8S_6$ along the b-axis, are shown in Figs. 3-4～6. In all the mixed crystals, the resistivities at room temperature are of the order of 10^{-4} Ω cm. Since it is difficult to compare the absolute values because of the errors in measuring the size of samples, we show the resistivities normalized by the value at room temperature.

At x=0.02 (Fig. 3-4(b)), the behavior as a whole resembles that of pure $K_3Cu_8S_6$, except the enhancement in the hump around 53K.

At x=0.04 (Fig. 3-4(c)), the hump is absent and the slope of the cooling curve gradually increases with decreasing temperature between T_1 and T_2. The increase in the cooling curve below T_1 is more enhanced than that at x=0.02. The T_2 transition is observed between 51K and 38K, which is slightly broadened. Unlike at x=0.02, the resistivity at x=0.04 rises with decreasing temperature below T_2.

At x=0.06 (Fig. 3-4(d)), the increase in the cooling curve below T_1 becomes larger, while the amplitude of the resistivity drop at T_2 becomes smaller. The rise in the resistivity below T_2 is more enhanced. As shown in Fig. 3-6(b), there is a change in the slope around 15K.

At x=0.10, the increase in the resistivity below 50K becomes large. (Fig. 3-5) The increase is almost saturated

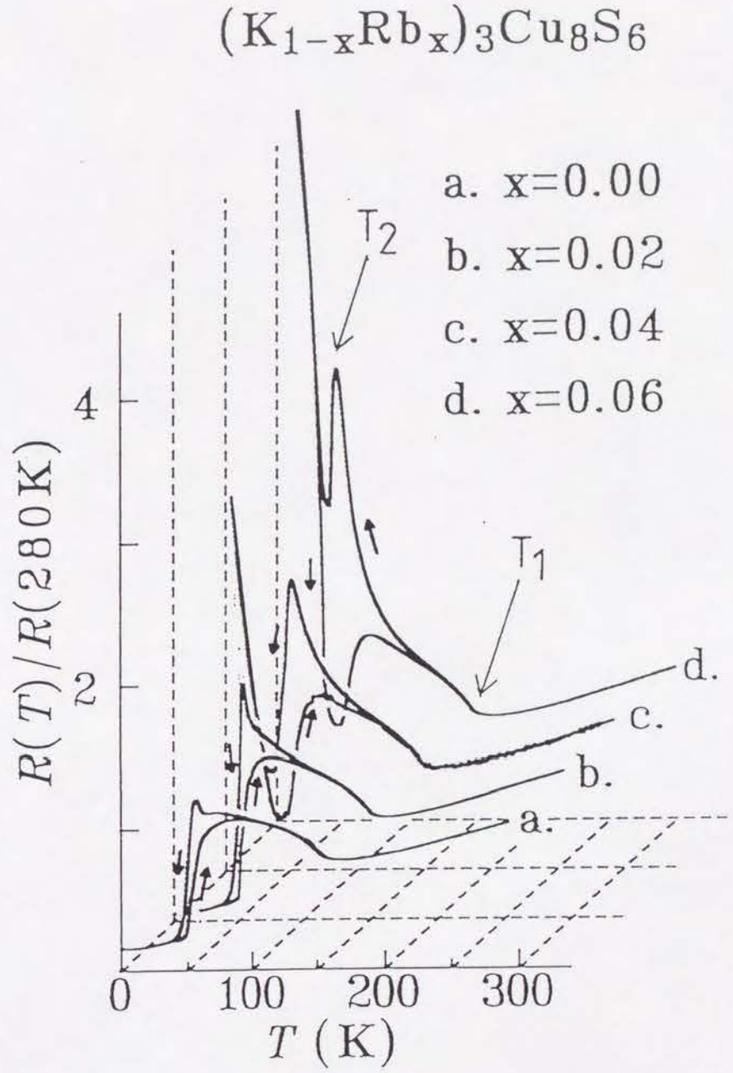

Fig. 3-4 Normalized resistivities, along the b-axis, of $(K_{1-x}Rb_x)_3Cu_8S_6$: (a) x=0.00, (b) x=0.02, (c) x=0.04 and (d) x=0.06.

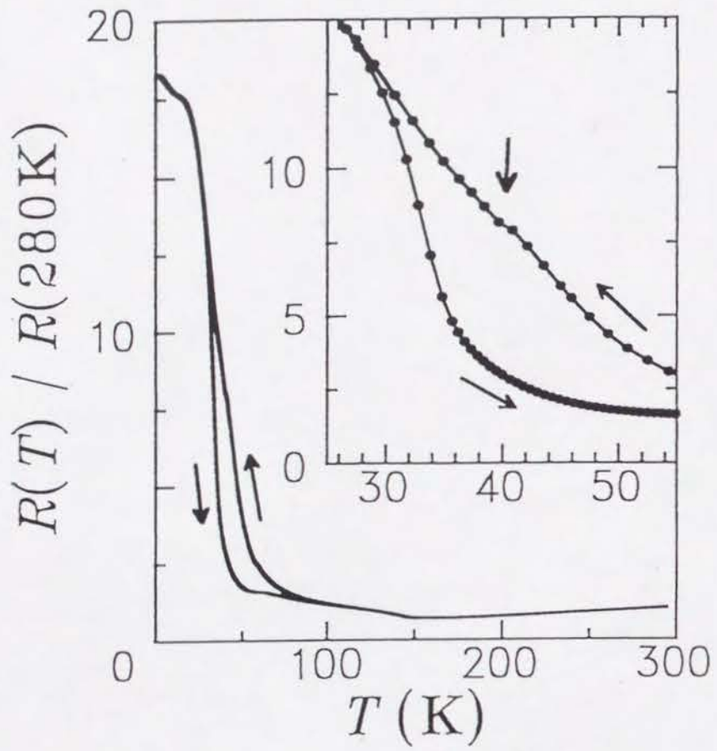

Fig. 3-5 Normalized resistivity of $(K_{0.90}Rb_{0.10})_3Cu_8S_6$. The inset shows the resistivity between 25K and 55K. There is a kink at 41K.

below 20K. There is no longer an abrupt drop of the resistivity indicating the T_2 transition, but a kink appears at 41K in the cooling curve (the inset of Fig. 3-5). So that we nominally define T_2 by this kink.

At x=0.25, the resistivity increases smoothly with decreasing temperature below T_1 without a kink and becomes metallic again below 40K (Fig. 3-6(c)). Unlike at x=0.10,

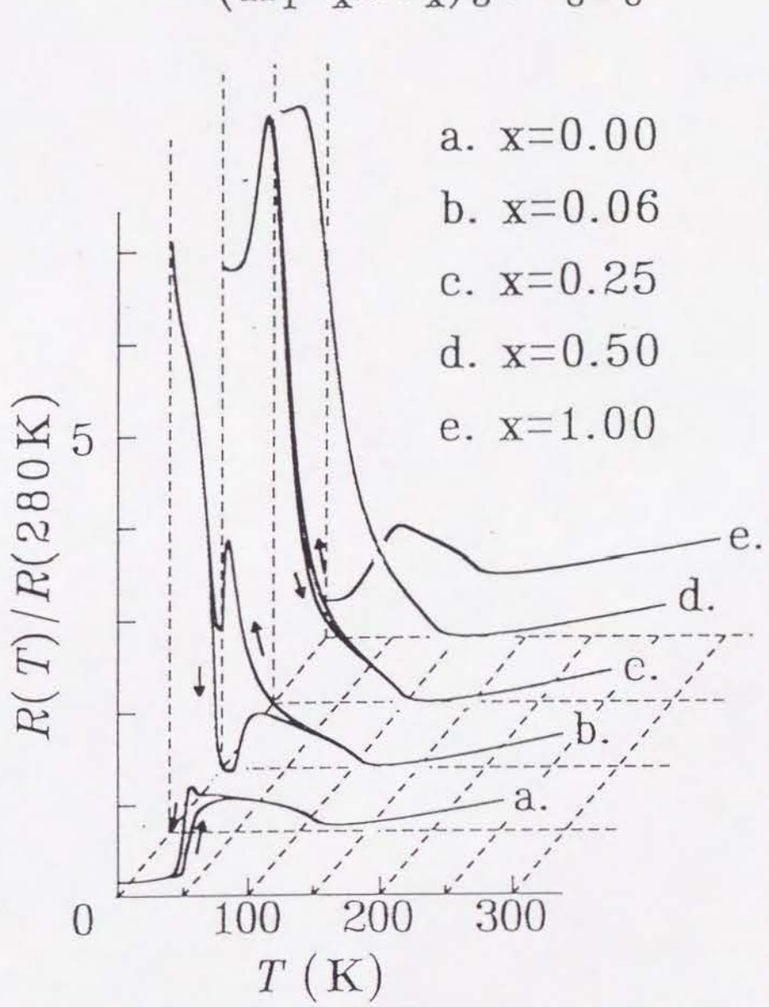

Fig. 3-6 Normalized resistivities of $(K_{1-x}Rb_x)_3Cu_8S_6$: (a) x=0.00, (b) x=0.06, (c) x=0.25, (d) x=0.50 and (e) x=1.00.

the resistivity does not rise in the lowest temperature region. There is a thermal hysteresis between 30K and 115K, but it is less clear than that at x=0.10.

At x=0.50 and at x=1.00, neither the abrupt drop of the resistivity nor the thermal hysteresis is observed (Fig. 3-6(d),(e)).

In all $(K_{1-x}Rb_x)_3Cu_8S_6$, T_1 is well defined by the cusp of dR/dT vs. T curve. As shown in Fig. 3-7, T_1 decreases

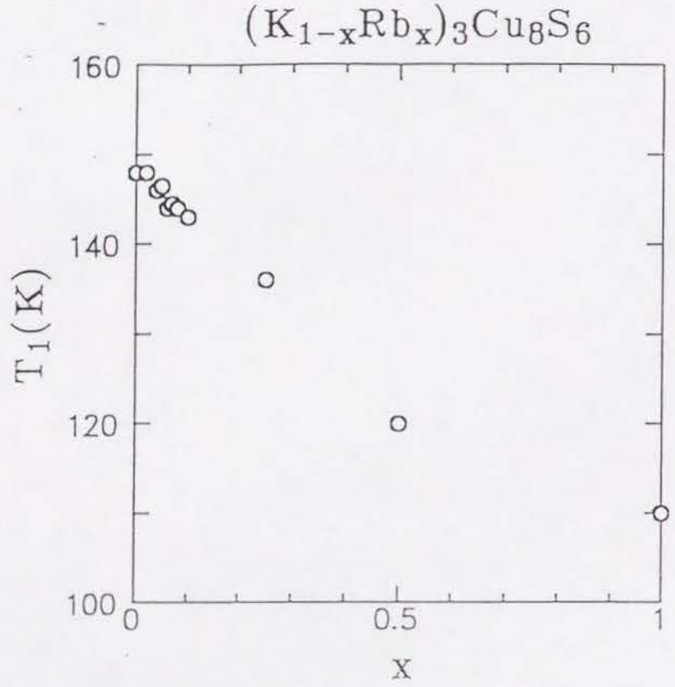

Fig. 3-7 Concentration dependence of the transition temperature T_1 of $(K_{1-x}Rb_x)_3Cu_8S_6$.

monotonically with increasing x.

In spite of the large difference in the behavior of the resistivity below T_1, all the curves above T_1 are similar. This suggests that there is no large difference among the electronic states of the normal metallic phase.

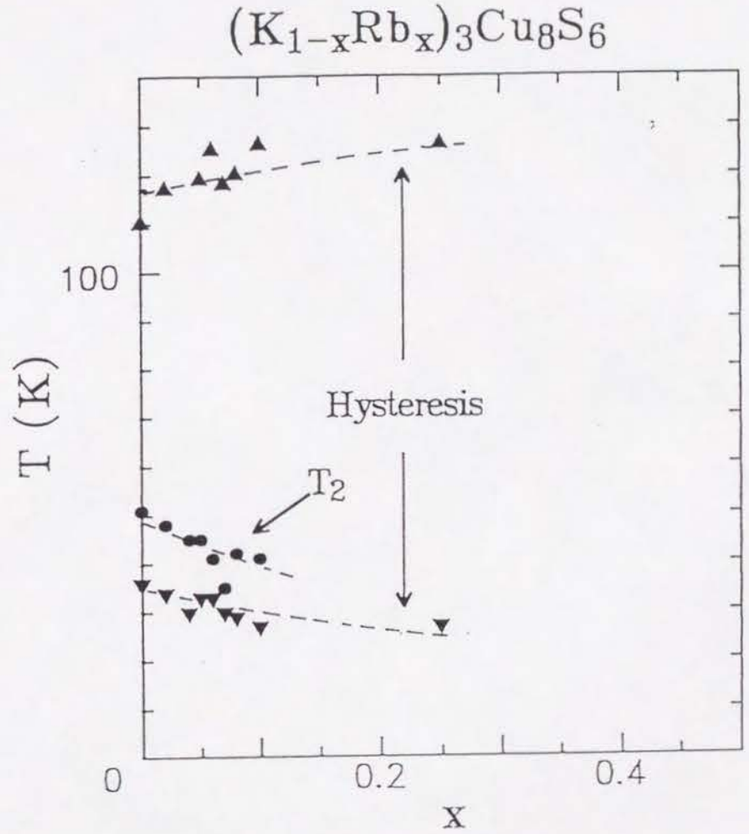

Fig. 3-8 Concentration dependence of T_2 (circle) and the temperature region in which hysteresis are observed in the resistivity curves (the region between upward triangles and downward triangles).

On the other hand, the T_2 transition is rapidly suppressed by the Rb doping as shown in Fig. 3-8. However, it is difficult to define T_2 exactly because the drop in the resistivity at T_2 becomes obscure with increasing x. Figure 3-8 also shows the temperature region in which the hysteresis appears in the resistivity curves. Unlike T_2, the region of the hysteresis is not lowered with increasing x.

(c) Thermoelectric powers

The TEP of $K_3Cu_8S_6$ and $Rb_3Cu_8S_6$ are also shown in Fig. 2-13 and Fig. 2-14 in the previous chapter, respectively.

At x=0.02, the peak around 55K, which corresponds to the hump of the resistivity, is enhanced (Fig. 3-9(b)).

At x=0.04 (Fig. 3-9(c)), in addition to the maximum around 50K, another local maximum is observed around 28K, but the resistivity has no anomaly at this temperature. It is to be emphasized that S approaches zero as T close to 0K, whereas the resistivity continues to increases. This suggests that metallic carriers survive in the temperature region where the resistivity rises.

As shown in Fig. 3-9(d), at x=0.10, there is only one maximum at 40K in the cooling curve. A small drop at 39K in the cooling curve, corresponding to the kink on the resistivity curve, suggests the existence of the T_2 transition (the inset of Fig. 3-9(d)).

At x=0.50, there is no longer a trace of the T_2

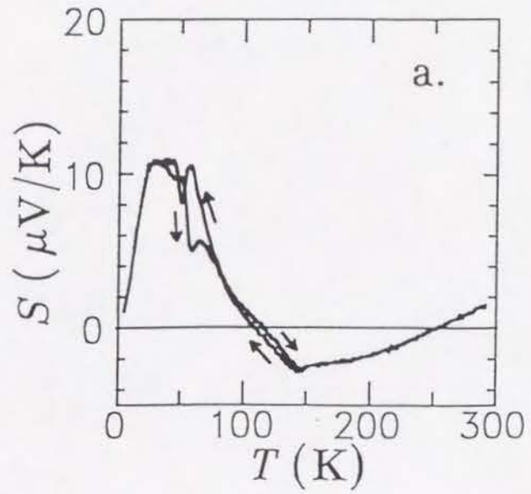

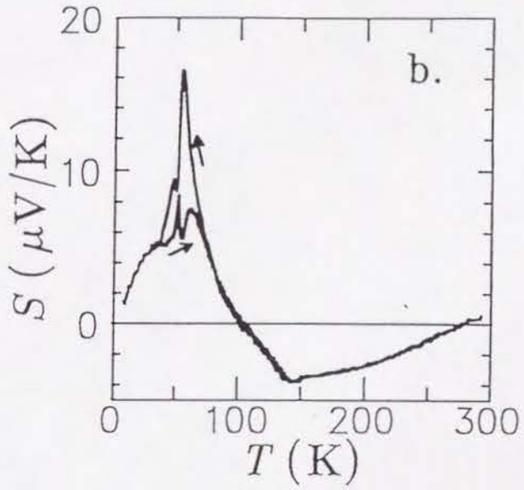

Fig. 3-9 Thermoelectric powers of $(K_{1-x}Rb_x)_3Cu_8S_6$: (a) x=0.00, (b) x=0.02, (c) x=0.04, (d) x=0.10, (e) x=0.50 and (f) x=1.00.

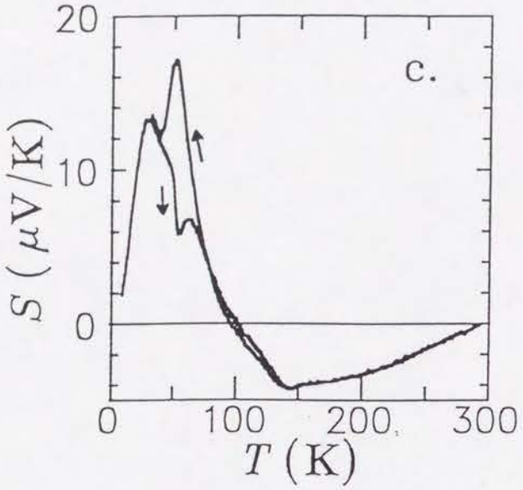
c.
20
10
0
S (μV/K)
0
100
200
300
T (K)

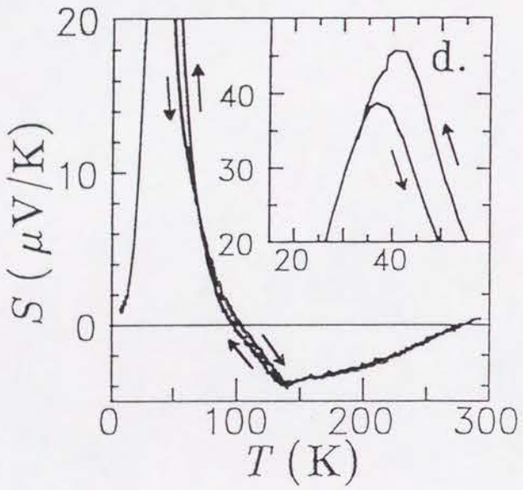
d.
20
10
0
S (μV/K)
40
30
20
20
40
0
100
200
300
T (K)

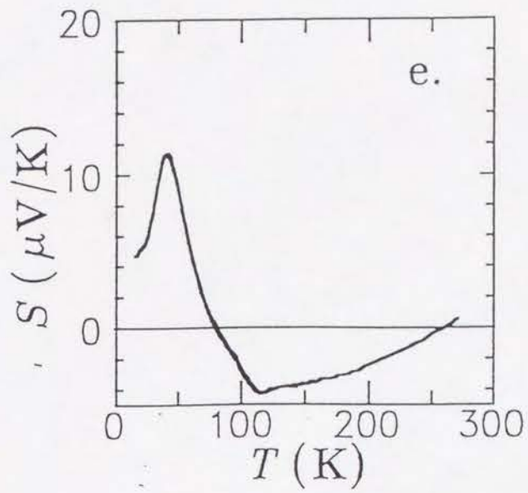
e.
20
10
0
S (μV/K)
0
100
200
300
T (K)

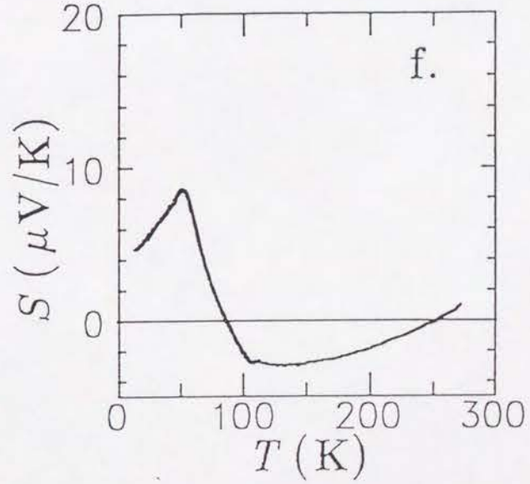
f.
20
10
0
S (μV/K)
0
100
200
300
T (K)

transition and a thermal hysteresis (Fig. 3-9(e)). This is consistent with the result of resistivity.

At all $(K_{1-x}Rb_x)_3Cu_8S_6$, TEPs are almost zero at room temperature and become negative on cooling. This behavior is far from that of a simple p-type metal and indicates the coexistence of both p-type carriers and n-type ones. At T_1, a kink appears in each TEP curve, and there is a minimum at the temperature about 10K lower than T_1. On further cooling, S begins to increase. This indicates that n-type carriers are extinguished by the formation of the CDW below T_1. Below about 25K, TEPs in all the compounds approach zero as T approaches 0K like a usual p-type metal. Like the resistivities, the TEPs above T_1 are almost independent of x, while the TEPs below T_1 are strongly dependent on x. The region of thermal hysteresis determined from the TEP data is wider than that from the resistivity data; the hysteresis begins to appear just below T_1.

(d) Magnetic susceptibilities

In order to estimate the decrease in the density of states at Fermi level by the formation of the CDW, the magnetic susceptibility measurements have been carried out. In the original data, Curie contributions, probably because of magnetic impurities such as 3d metals or divalent copper arising from the oxidation of the surface of sample, are observed in low temperature region.

In order to compare the decreases in Pauli paramagnetism caused by the CDW transition, the Curie contributions are subtracted from the original data. The Curie constants are 1.310×10^{-3}, 9.023×10^{-3}, 2.511×10^{-2}, 5.467×10^{-3} and 3.434×10^{-3} (in emu/mol) for x=0.04, 0.25, 0.50, 0.75 and 1.00, respectively. All the room temperature susceptibilities are diamagnetic due to the diamagnetism of core electrons. As the room temperature values vary between -1.14×10^{-4} and -1.52×10^{-3} (in emu/mol) from sample to sample because of the error in the estimation of the Curie contribution and the blank susceptibility, it is difficult to compare the absolute value of magnetic susceptibilities. However, the comparison of the temperature dependences is meaningful.

Figure 3-10 shows the temperature dependence of the magnetic susceptibilities. Above T_1, the susceptibilities are almost temperature independent. Below T_1, they decrease with decreasing temperature as seen in ordinary CDW systems. In all the mixed crystals, about 10^{-4} emu/mol of paramagnetism disappears below T_1. This value is almost the same as that of $K_3Cu_8S_6$ reported by ter Haar et al.[32] This shows that the amounts of Fermi surface destroyed by the CDW formation are almost the same in all the mixed crystals.

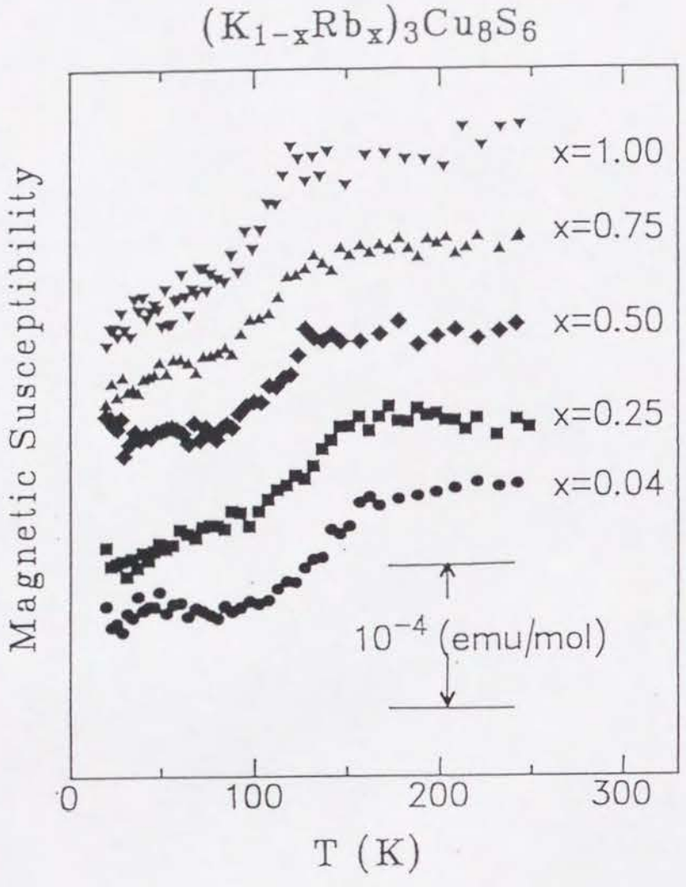

Fig. 3-10 Magnetic susceptibilities of $(K_{1-x}Rb_x)_3Cu_8S_6$. The Curie contributions were subtracted.

B. $(Rb_{1-x}Cs_x)_3Cu_8S_6$

(a) Sample preparation

The absence of the reports about the existence of the $Cs_3Cu_8S_6$ phase suggests that it is an unstable phase. In fact, our trial of synthesizing it has been unsuccessful.

However, we were able to obtain a mixed crystal from Rb_2CO_3, Cs_2CO_3, Cu and S. Since the molar ratio of Rb_2CO_3 and Cs_2CO_3 is 4:1, it is described as $(Rb_{0.80}Cs_{0.20})_3Cu_8S_6$ nominally. The x-ray powder pattern shows that the mixed crystal has larger inter-sheet distance than $Rb_3Cu_8S_6$.

(b) Resistivity

As shown in Fig. 3-11, the T_1 transition is seen in

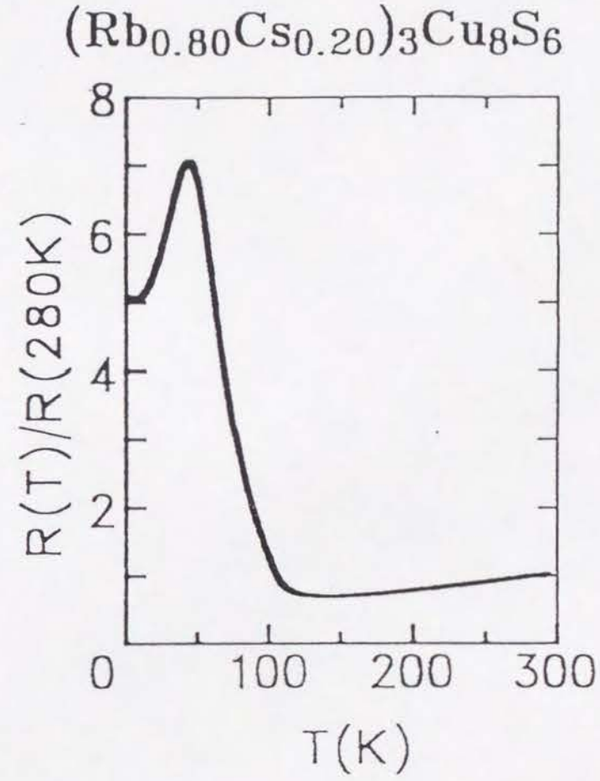

Fig. 3-11 Normalized resistivity of $(Rb_{0.80}Cs_{0.20})_3Cu_8S_6$.

$(Rb_{0.80}Cs_{0.20})_3Cu_8S_6$, although it is slightly dim. T_1 estimated using dR/dT vs. T curve is 103K, lower than that of $Rb_3Cu_8S_6$. The large residual resistivity is probably attributed to the disorder in the alkali sites as in $(K_{0.75}Rb_{0.25})_3Cu_8S_6$.

§ 3-4 Results: chalcogen substitution effects.

A. $K_3Cu_8(S_{1-x}Se_x)_6$

(a) Sample preparations

We have synthesized $K_3Cu_8(S_{1-x}Se_x)_6$ (where nominal x=0.01, 0.03, and 0.06) from K_2CO_3, Cu, S, and Se. It was confirmed by the x-ray powder pattern that the obtained crystals have the $K_3Cu_8S_6$ structure and by EPMA that they contain selenium.

(b) Resistivities

As shown in Fig. 3-12, the T_1 transition of $K_3Cu_8S_6$ is strongly suppressed by the Se doping. It should be noted that the Rb doping reduces only T_1 but that the Se doping reduces not only T_1 but also suppresses the increase in the resistivity below T_1. The T_2 transition is also strongly suppressed by the Se doping. The abrupt drop in the resistivity, clearly seen at T_2 in $K_3Cu_8S_6$, becomes dim with only 1% Se doping. The thermal hysteresis becomes less

remarkable with increasing x and disappears thoroughly for x=0.06.

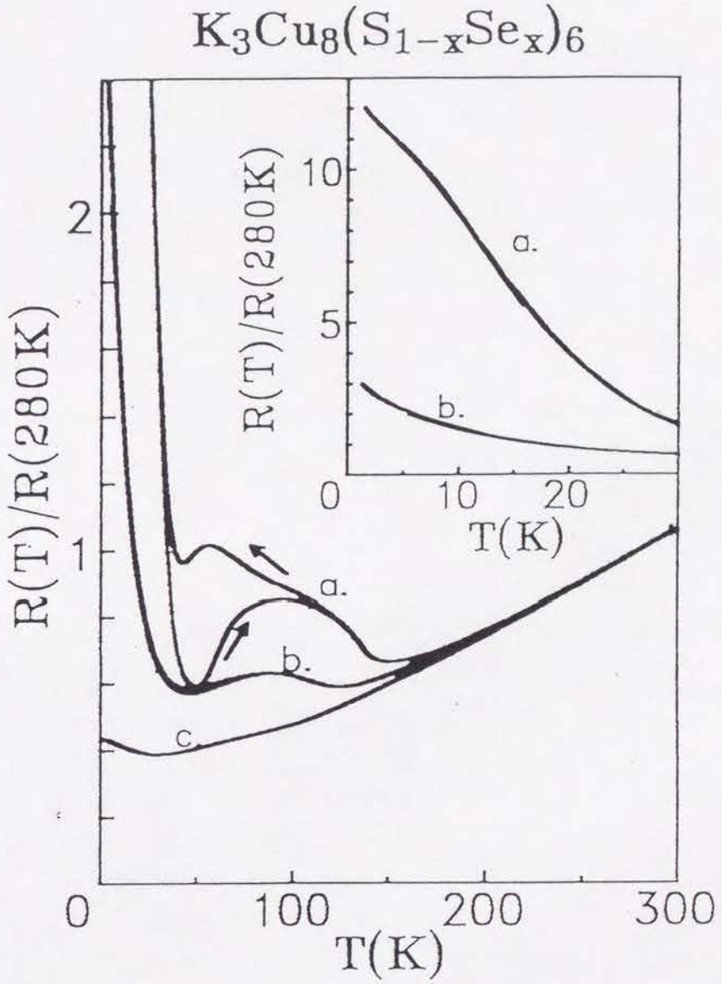

Fig. 3-12 Normalized resistivities of $K_3Cu_8(S_{1-x}Se_x)_6$; (a)x=0.01, (b)x=0.03, and (c)x=0.06.

Below 30K, the resistivity rises with decreasing temperature in all the mixed crystals. As shown in the inset of Fig. 3-13, the temperature dependence of the resistivity is apparently different from that of variable-range hopping and that of weak localization observed in the disordered electron systems. Furthermore, the rise is most remarkable for x=0.01 and becomes smaller with increasing x. Therefore, it is difficult to explain the rise only by the effect of the random potential in the chalcogen sites.

(c) Thermoelectric Powers

As shown in Fig. 3-13(b), the TEP of $K_3Cu_8(S_{0.94}Se_{0.06})_6$ is positive except between 120K and 220K. There is no longer a sharp bend in TEP because the T_1 transition is obscure. The TEP above T_1 is more positive than that of $K_3Cu_8S_6$. This suggests that the contribution of n-type carriers decreases with the Se doping. As already shown in the previous chapter, the TEP of $Rb_3Cu_8Se_6$ is thoroughly positive in the whole temperature region. The fact that the TEP becomes more positive as the CDW is suppressed suggests that the n-type carriers are essential for the CDW.

B. $Rb_3Cu_8(S_{1-x}Se_x)_6$

The T_1 transition of $Rb_3Cu_8S_6$ is considerably suppressed by only 1% Se doping (Fig. 3-14). Unlike

$K_3Cu_8(S_{1-x}Se_x)_6$, the resistivity of $Rb_3Cu_8(S_{0.99}Se_{0.01})_6$ does not rise in the low temperature region.

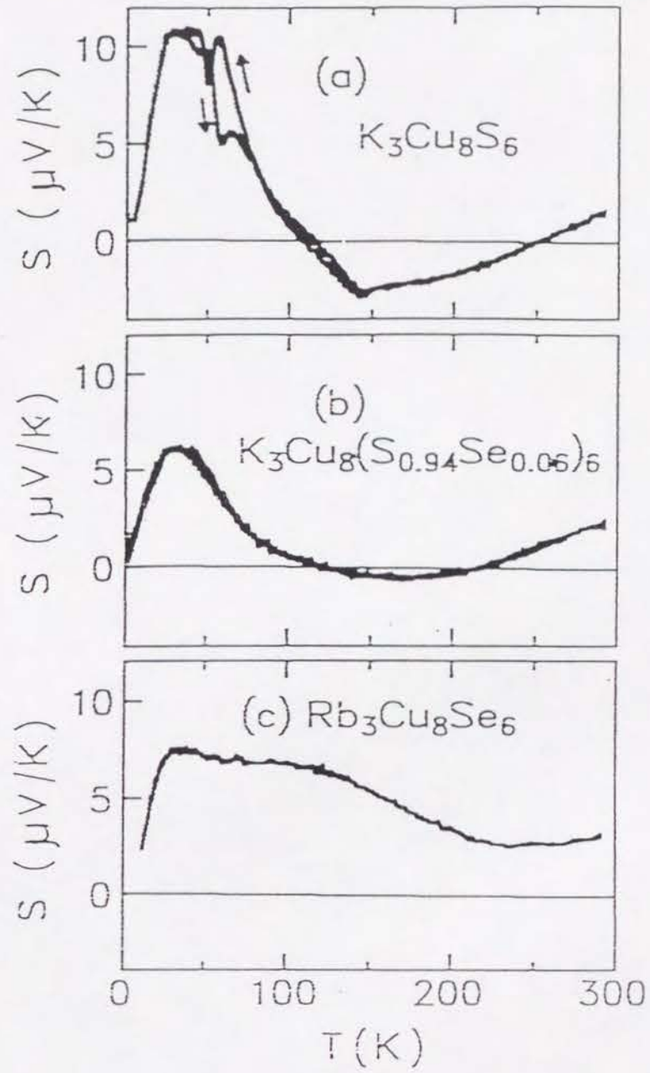

Fig. 3-13 Thermoelectric powers of (a) $K_3Cu_8S_6$, (b) $K_3Cu_8(S_{0.94}Se_{0.06})_6$, and (c) $Rb_3Cu_8Se_6$.

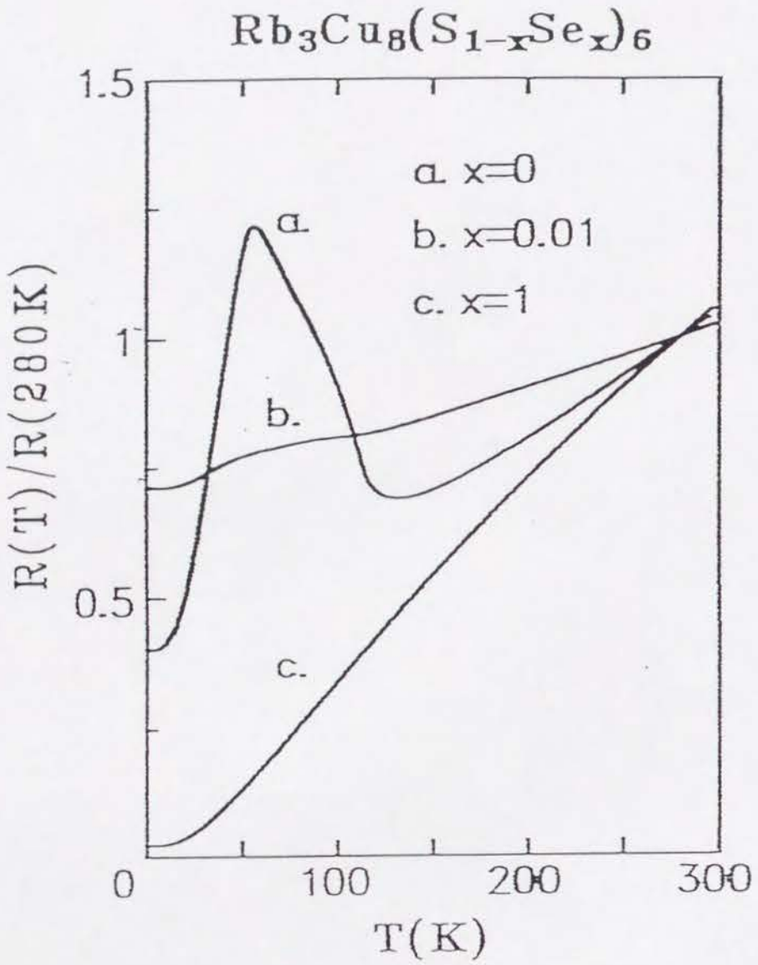

Fig. 3-14 Normalized resistivities of $Rb_3Cu_8(S_{1-x}Se_x)_6$.

§ 3-5. Results: hydrostatic pressure effects.

A. $K_3Cu_8S_6$

As pressure is applied, the resistivity of $K_3Cu_8S_6$ at room temperature gradually decreases without any transition. The resistivity at 1GPa is about 80% of that at ambient pressure. The temperature dependence of the resistivities at several hydrostatic pressures are shown in Fig. 3-15. Remarkable pressure effects are observed.

Firstly, as shown in Fig. 3-16, the transition temperature T_1 becomes lower and the increase in the resistivity below T_1 decreases with increasing pressure. Similar behavior can be seen in pseudo one-dimensional metals such as $NbSe_3$[53,54], which has CDW transitions.

Secondly, the hump observed at ambient pressure around 57K is completely extinguished by the pressure of at most 0.4GPa.

Finally, the T_2 transition under hydrostatic pressure is found to behave as follows: (1) the transition temperature rises with increasing pressure; (2) below T_2, the temperature dependence of the resistivity is metal-like; (3) the resistivity in this metallic region is insensitive to pressure.

The resistivity indicates that there are two metallic regions, above T_1 and below T_2. The non-metallic region

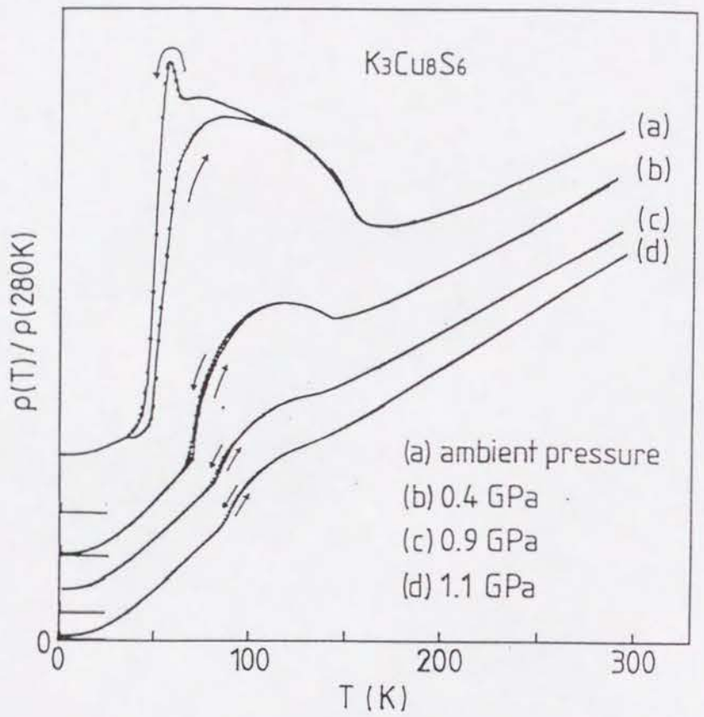

Fig. 3-15 Temperature dependence of the resistivity of $K_3Cu_8S_6$ at ambient pressure, 0.4 GPa, 0.9 GPa and 1.1 GPa. The difference in the residual resistances is attributed to the difference in samples used for the measurement. The resistivity at 280K under ambient pressure is 3×10^{-4} Ω cm.

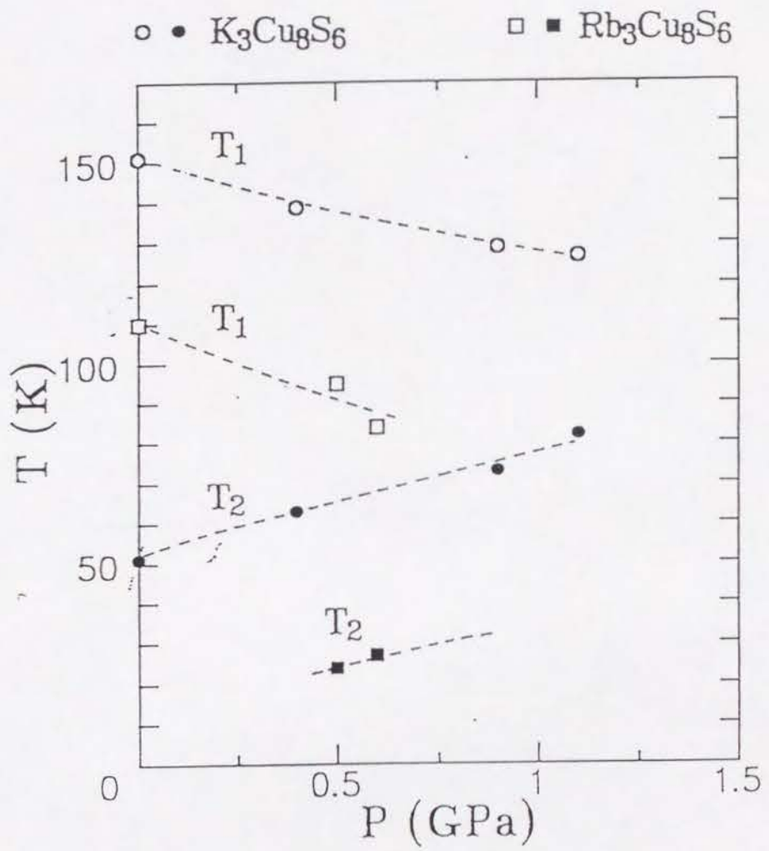

Fig. 3-16 Pressure dependences of the transition temperature, T_1 and T_2 of $K_3Cu_8S_6$ (circles) and $Rb_3Cu_8S_6$ (squares). The dashed lines are the guide for the eyes.

between T_1 and T_2 becomes narrower with increasing pressure as shown in Fig. 3-16. Therefore, under high pressure, it is expected that the non-metallic region disappears.

Contrary to this expectation, Raghu et al. have reported[49] the appearance of a pressure-induced metal-insulator transition due to a commensurate CDW at 2.2GPa from the resistivity measurements. However, there is no evidence to prove the formation of the commensurate CDW directly in thier report. In addition, there is a considerable discrepancy between our result at 0.9GPa (or 1.1GPa) and theirs at 1.0GPa; the resistance of theirs seems to be independent of temperature in the region between 77K and 140K, where temperature dependent resistance and the first-order transition have been observed in our data. We think that a more careful investigation about the "pressure-induced transition" is necessary.

B. $(K_{0.94}Rb_{0.06})_3Cu_8S_6$

Figure 3-17 shows the resistivity of $(K_{0.94}Rb_{0.06})_3Cu_8S_6$ at ambient pressure and at 0.9GPa. The sample used for the measurement of pressure effect is different from that used for Figs. 3-4 and 3-6. A slight sample dependence is observed especially in the sharpness of the T_2 transition and in the residual resistivity. As seen

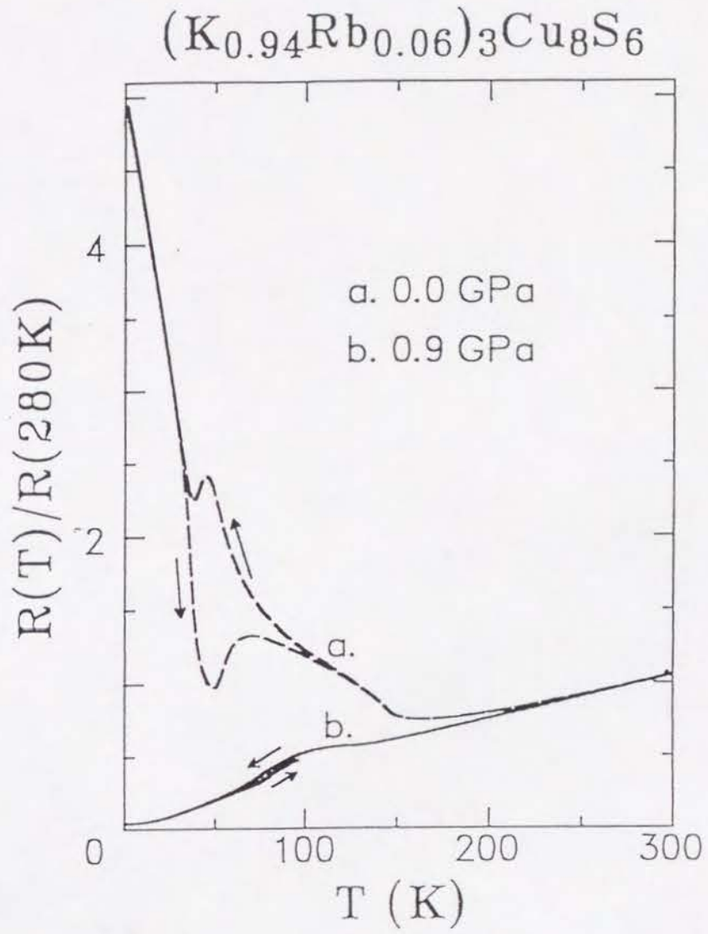

Fig. 3-17 Normalized resistivity of $(K_{0.94}Rb_{0.06})_3Cu_8S_6$ under pressures: (a) at ambient pressure, (b) at 0.9 GPa.

in $K_3Cu_8S_6$, the non-metallic behavior below T_1 is suppressed by pressure of 0.9GPa. Furthermore, the rise in the resistivity below T_2 is completely suppressed. The behavior at 0.9 GPa resembles that of $K_3Cu_8S_6$ at 0.9 GPa.

C. $Rb_3Cu_8S_6$

Figure 3-18 shows the resistivity of $Rb_3Cu_8S_6$ under several pressures. Both the transition temperature and the increase in the resistivity below T_1 are reduced by pressure. The most striking result of the pressure effect is the appearance of the T_2 transition. At 0.5GPa, besides thermal hysteresis, a steep decrease in the resistivity appears around 30K. This behavior resembles the T_2 transition of $K_3Cu_8S_6$. At 0.6GPa, the non-metallic behavior between T_1 and T_2 becomes less remarkable. At 0.9GPa, the T_2 transition becomes obscure and the resistivity is metallic in the whole temperature region. The pressure dependences of T_1 and T_2 of $Rb_3Cu_8S_6$ are shown in Fig. 3-16. With increasing pressure, T_1 decreases while T_2 increases. It was found that both pressure and the Rb doping lower T_1. However, it should be noted that pressure suppresses the magnitude of the resistivity change by the T_1 transition, while the Rb doping does not.

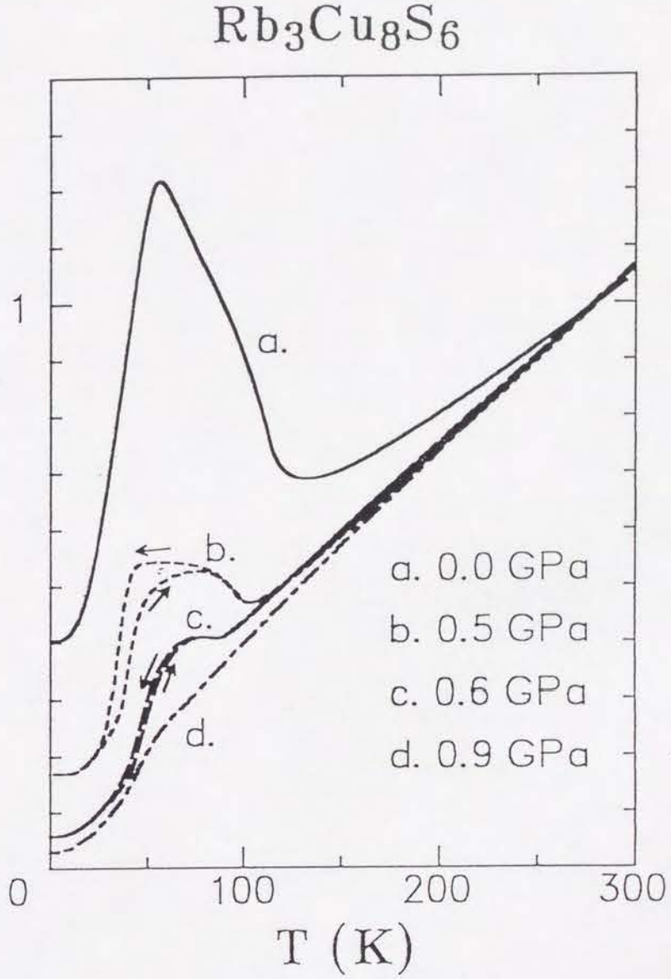

Fig. 3-18 Normalized resistivity of $Rb_3Cu_8S_6$ under pressures: (a) at ambient pressure, (b) at 0.5 GPa, (c) at 0.6 GPa and (d) at 0.9 GPa.

§ 3-6. Discussion

A. Substitution effect on the phase transitions

$K_3Cu_8S_6$ is an analogue of $K_{0.3}MoO_3$ (blue bronze), because the metallic Cu_8S_6 layers are separated by potassium ions which are not expected to contribute to the electronic conduction. However, the alkali substitution has a significant effect on T_1. The CDW transition temperature T_1 of $Rb_3Cu_8S_6$ is by about 40K lower than that of $K_3Cu_8S_6$. This is in contrast with the CDW transition of blue bronzes $A_{0.3}MoO_3$ (A=K, Rb ,Tl),[55] whose transition temperatures are independent of A.

Between $Rb_3Cu_8S_6$ and $K_3Cu_8S_6$, there is a difference in the Cu_8S_6 inter-sheet distance, reflecting the ionic radius of K and Rb. The nearest inter-sheet S-S distances are 3.78 Å and 4.00Å in $K_3Cu_8S_6$ and $Rb_3Cu_8S_6$, respectively. However, the change in T_1 is difficult to be explained by the difference in the inter-sheet transfer interaction because of the following two reasons. First, if the inter-sheet interaction were large enough to have a considerable effect on the shape of Fermi surface, $K_3Cu_8S_6$ should have lower CDW transition temperature than $Rb_3Cu_8S_6$ because of the less low-dimensionality. However, this contradicts with the fact. Second, if the inter-sheet interaction had the predominant effect on T_1, broadening of T_1 should be

observed in the mixed crystal $(K_{1-x}Rb_x)_3Cu_8S_6$ because of the distribution of inter-sheet S-S distance. However, unlike $(K_{1-x}Rb_x)_{0.3}MoO_3$,[56] there is little disorder effect; the T_1 transition is sharp in $(K_{1-x}Rb_x)_3Cu_8S_6$ and T_1 is simply reduced as x increases. It is also found that T_1 of $(Rb_{0.80}Cs_{0.20})_3Cu_8S_6$ is 7K lower than that of $Rb_3Cu_8S_6$. Therefore, we can conclude that T_1 becomes lower as the average size of the alkali ions.

On the other hand, the T_2 transition of $K_3Cu_8S_6$ is rapidly suppressed by the Rb doping. In 1T-TaS_2,[57] the lock-in transition is suppressed by a slight cation doping because the random potentials lower the gain of lock-in energy. However, the suppression of the T_2 transition cannot be explained only by the disorder in alkali sites because $Rb_3Cu_8S_6$ does not undergo the T_2 transition in spite of the absence of the disorder. Moreover, it is doubtful that the T_2 transition is a lock-in transition because the substitution of Rb for K is unlikely to change the CDW wave vector or the lock-in energy.

Therefore, the T_2 transition is probably some structural phase transition independent of the CDW. It is possible that the main effect of doping on the T_2 transition is not generating disorder but changing the average size of the alkali ions. The absence of the T_2 transition in $Rb_3Cu_8S_6$ suggests the existence of a critical ion size

beyond which the T_2 transition does not occur.

As thermal hystereses are observed when there are the T_2 transitions which are defined by the drop in the resistivity curve, it is natural to consider that there is a relationship between them. However, it is questionable that the hysteresis is caused by the first-order property of the T_2 transition. The behavior of thermal hysteresis (Fig. 3-3) is clearly different from that of an ordinary first-order transition such as the nearly-commensurate to commensurate transition of 1T-TaS_2[58] and rather resembles the magnetization curve of a ferromagnet. Such behaviors of hysteresis are commonly seen in many CDW systems.[59-62] In these systems, thermal hysteresis is explained by the existence of a number of metastable states resulting from the interaction between CDWs and pinning centers. Note that the thermal hysteresis is observed in the TEP of $K_3Cu_8S_6$ just below T_1 rather than around T_2. This indicates that the CDW causes many metastable states.

The resistivities of $K_3Cu_8(S_{1-x}Se_x)_6$ and $Rb_3Cu_8(S_{1-x}Se_x)_6$ show that the chalcogen substitution has larger and destructive effect on the CDW. Ultimately, in $Rb_3Cu_8Se_6$, there are no longer any phase transitions. This indicates that the shape of the Fermi surface, especially the part relating the CDW, strongly depends on the difference in the chalcogen atoms.

B. Pressure effect on the phase transitions

The pressure effects on the resistivities of $K_3Cu_8S_6$, $(K_{0.94}Rb_{0.06})_3Cu_8S_6$ and $Rb_3Cu_8S_6$ show that both the transition temperature and the resistivity anomaly of the T_1 transition are reduced by pressure of about 1 GPa. The x-ray diffraction studies on $K_3Cu_8S_6$ under high pressures using synchrotron orbital radiation[63] have revealed that the pressure of 1GPa reduces the lattice constants a, b and c by 0.60%, 0.26% and 0.70%, respectively. These are smaller than the differences in the lattice constants between $K_3Cu_8S_6$ and $Rb_3Cu_8S_6$, which are 2.9%, 0.91% and 1.2%, respectively. Therefore, it is unlikely that the nesting condition of the Fermi surface of $K_3Cu_8S_6$ is drastically modified by the applied pressure of less than 1GPa. Other explanations of the suppression of the T_1 transition are increase in the strain energy of the lattice[53], and the decrease in the electron-lattice interaction[54].

On the other hand, with increasing pressure, T_2 of $K_3Cu_8S_6$ becomes higher. Apparently, the resistivity drop at T_2 becomes less remarkable under high pressure. This is probably because the non-metallic behavior between T_1 and T_2 is suppressed. In $Rb_3Cu_8S_6$, the T_2 transition is induced by the applied pressure of 0.5GPa, and T_2 becomes higher with increasing pressure. These results indicate that the metallic phase below T_2 is stabilized by pressure in both

$K_3Cu_8S_6$ and $Rb_3Cu_8S_6$. The stabilization of the metallic phase below T_2 is commonly observed in also $(K_{0.94}Rb_{0.06})_3Cu_8S_6$.

At ambient pressure, the metallic phase of $K_3Cu_8S_6$ below T_2 is clearly different from the metallic phase above T_1, because the former is accompanied by a commensurate superstructure but the latter is not. However, judging from the resistivities, the difference between the two phases becomes smaller as pressure increases.

C. The rise in resistivity at low temperature

In all the mixed crystals $(K_{1-x}Rb_x)_3Cu_8S_6$, the increases in the resistivity below T_1 are clearly enhanced compared with pure $K_3Cu_8S_6$ and $Rb_3Cu_8S_6$. This is explained by the excess scattering by the disorder in alkali sites. However, when $0.04 \leqq x \leqq 0.10$, another rise in the resistivity appears below T_2. Since there is a disorder in the alkali site, Anderson localization may be one of the possible explanations. However, the trial of fitting the resistivities to the formula of variable-range-hopping:

$$\sigma(T) \propto \exp[-(T_0/T)^{1/(d+1)}],$$

where d is the dimensionality of the system, is unsuccessful.

Another possible mechanism which raises the resistivity is the impurity scattering enhanced by CDW clouds as seen in irradiated $NbSe_3$,[84] where the rise in the resistivity at low temperature is similar to that of $(K_{1-x}Rb_x)_3Cu_8S_6$. This mechanism can explain why pressure suppresses the rise in the resistivity, because the CDW clouds are reduced by pressure. However, some questions still remain. Is the disorder in the alkali sites strong enough to affect the CDW in the Cu_8S_6 sheet? Why is the rise in the resistivity most pronounced at $0.04 \leqq x \leqq 0.10$?

The explanation which can answer these questions is that the coexistence of the incommensurate CDW and the T_2 transition is essential for the rise in the resistivity. This can also explain why the steep rise in the resistivity at low temperature is seen in $K_3Cu_8(S_{0.99}Se_{0.01})_6$ but absent in $Rb_3Cu_8(S_{0.99}Se_{0.01})$. In the next chapter, we discuss the resistivity rises again on the basis of the x-ray diffuse scattering results.

D. Possible mechanism of the phase transitions

Another interpretation of the T_1 transition has been recently made by Whangbo and Canadell[52]. They considered that the T_1 transition is not a CDW transition because the nesting vector of the Fermi surface calculated by their extended Hückel tight-binding (EHTB) method is far from the

experimental value of the wave vector of the superstructure. Instead of a CDW transition, they proposed another mechanism: an order-disorder phase transition of the Cu3 atoms in the tetrahedral columns (see Fig. 2-8), because the Cu3 atoms of $K_3Cu_8S_6$ and $Rb_3Cu_8S_6$ have anomalously large anisotropic temperature factors at room temperature.[13)]

EHTB method[65)] is often useful for complexes and molecular crystals. However, it is not clear whether EHTB method is appropriate for the present metallic copper-sulfides, because the parameters, the energies and the extentions of atomic orbitals, used in the calculation are those of isolated atoms.

The analysis of the crystal structure of $K_3Cu_8S_6$ at low temperature is indispensable to verify the model by Whangbo and Canadell.

On the other hand, the T_2 transition is probably not a phase transition of electronic origin because it is unlikely that the Fermi surface of $Rb_3Cu_8S_6$ is very different from that of $K_3Cu_8S_6$. From a structural point of view, a following explanation for the T_2 transition is possible. The absence of such phases as $Na_3Cu_8S_6$ and $Cs_3Cu_8S_6$ indicates that the Cu_8S_6 sheet structure is stable only for the counter cations K and Rb which have suitable ionic radius for the Cu_8S_6 sheet structure. Furthermore, Rb is likely more suitable for the Cu_8S_6 sheet than K because $Rb_3Cu_8S_6$ is

a high temperature stable phase while $K_3Cu_8S_6$ is a "kinetic" phase[32)] located narrow region between high temperature KCu_3S_2 phase and low temperature KCu_4S_3 phase. It is possible that the T_2 transition of $K_3Cu_8S_6$ relates to such an instability of the Cu_8S_6 sheet structure.

§ 3-7. Summary

In order to investigate the two phase transitions of $K_3Cu_8S_6$ at T_1 and at T_2, the mixed crystals $(K_{1-x}Rb_x)_3Cu_8S_6$, $(Rb_{1-x}Cs_x)_3Cu_8S_6$, $K_3Cu_8(S_{1-x}Se_x)_6$ and $Rb_3Cu_8(S_{1-x}Se_x)_6$ were synthesized and their transport properties, including hydrostatic pressure effects, were studied. The results are summarized as follows.

(1) As x increases, T_1 of $(K_{1-x}Rb_x)_3Cu_8S_6$ is reduced. In addition, $(Rb_{0.80}Cs_{0.20})_3Cu_8S_6$ has lower T_1 than that of $Rb_3Cu_8S_6$. Thus, T_1 simply decreases as average size of alkali ions increases. The fact that the T_1 transition is sharp in the mixed crystal indicates that the disorder in alkali sites has little effect on the T_1 transition.

(2) The dopings of a few percent Se on $K_3Cu_8S_6$ and $Rb_3Cu_8S_6$ drastically suppress the CDW transitions.

(3) The T_2 transition becomes obscure as x increases and

thoroughly disappears when $x \geqq 0.50$. The absence of the T_2 transition in pure $Rb_3Cu_8S_6$ suggests that the suppression of the T_2 transition is not due to the disorder but due to the change in the average size of the alkali atoms.

(4) In both $K_3Cu_8S_6$ and $Rb_3Cu_8S_6$, pressure suppresses the T_1 transition.

(5) The T_2 transition is induced in $Rb_3Cu_8S_6$ by the pressure of at most 0.5GPa. Both in $K_3Cu_8S_6$ and $Rb_3Cu_8S_6$, pressure stabilizes the metallic state below T_2.

(6) In $(K_{1-x}Rb_x)_3Cu_8S_6$, where x is around 0.06, the resistivity sharply rises at low temperature below T_2. This rises are present in also $K_3Cu_8(S_{1-x}Se_x)_6$ but absent in $Rb_3Cu_8(S_{1-x}Se_x)_6$.

Chapter 4. Charge-Density Wave Transitions in $A_3Cu_8X_6$ (A=K, Rb; X=S, Se): Structural Studies

§ 4-1 Introduction

As already mentioned in the previous chapters, $K_3Cu_8S_6$ undergoes two phase transitions at T_1 (153K) and at T_2

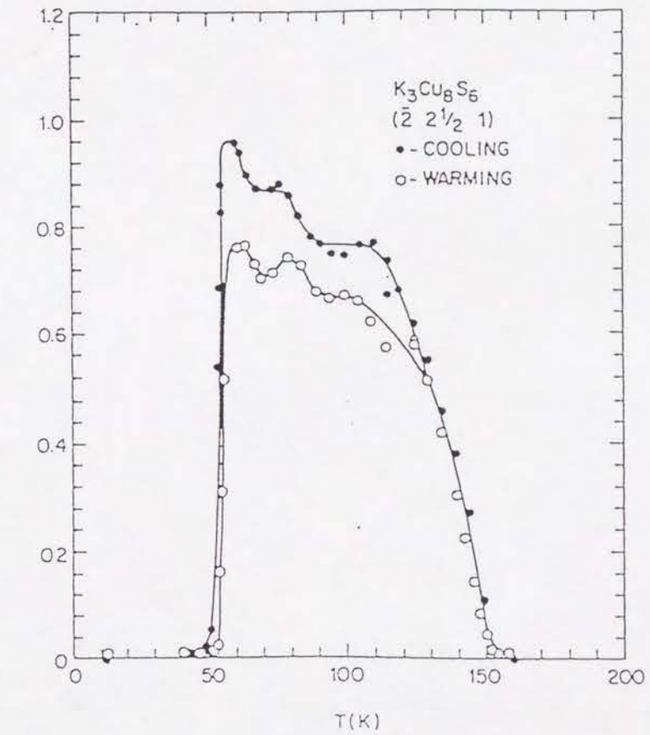

Fig. 4-1 The temperature dependence of the $(\overline{2}\ 2+\eta\ 1)$ satellite diffraction.[33]

(55K).[32,33] It was reported that an incommensurate superstructure (0 η 0), where η is about 0.44 at T_1, appears between T_1 and T_2 (Fig. 4-1). Below T_2, the incommensurate superstructure almost disappears and another strong commensurate superstructure (1/2 1/2 0) appears (Fig. 4-2). In addition to the non-metallic behavior of the

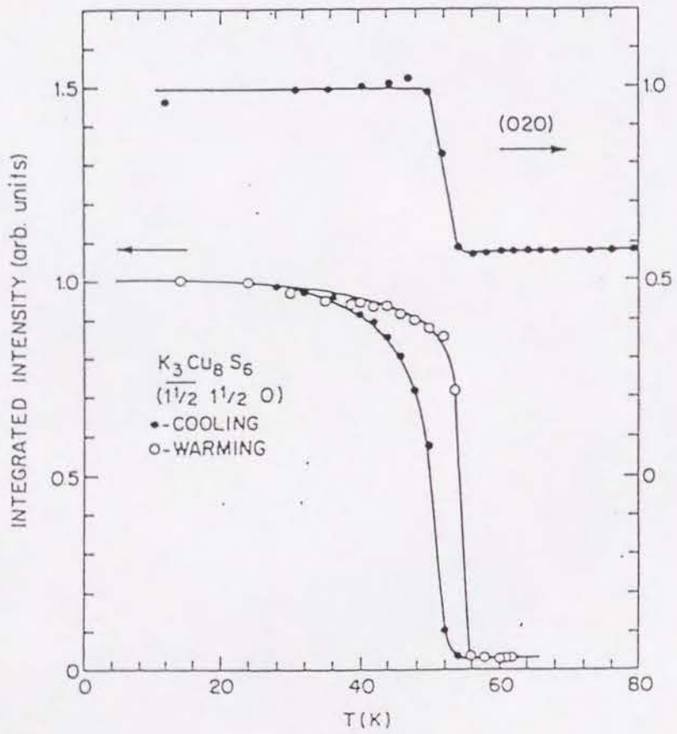

Fig. 4-2 The temperature dependence of the ($\overline{3/2}$ 3/2 0) satellite diffraction.[33]

resistivity, the appearance of the incommensurate superstructure below T_1 suggests that T_1 is the onset

temperature of an incommensurate CDW related to the instability of the Fermi surface of electrons.

On the other hand, the origin of the T_2 transition is not clear. The T_2 transition is difficult to be ascribed to a usual lock-in transition of the CDW, because the high conductivity is recovered below T_2 and the amplitude of the commensurate superstructure is anomalously large compared with that of a usual CDW.

Furthermore, about the interpretation of the T_1 transition, some questions still remain. First, the intensity of the incommensurate superstructure exhibits oscillation as a function of temperature.[33] This behavior is anomalous for a usual CDW. Second, the nesting vector of the Fermi surface calculated by Whangbo and Canadell[52] is inconsistent with the observed wave vector of the superstructure. Therefore, they proposed another interpretation of the T_1 transition: the order-disorder phase transition of a part of the copper atoms which have large amplitude of thermal vibration.

As discussed in Chapter 2, the resistivity measurements have revealed that $Rb_3Cu_8S_6$, which is isostructural with $K_3Cu_8S_6$, also undergoes the T_1 transition, but does not have an abrupt resistivity drop corresponding to the T_2 transition of $K_3Cu_8S_6$ (Fig. 2-11).

Furthermore, as shown in Chapter 3, the resistivities

of the mixed crystal $(K_{1-x}Rb_x)_3Cu_8S_6$ show the followings: as x increases, the resistivity drop at T_2 becomes smaller and duller, and at last disappears completely when x exceeds 0.50. On the other hand, the T_1 transition is still sharp in the mixed crystals and T_1 simply decreases as x increases. It was also found that, as shown in Fig. 3-4, a remarkable rise in the resistivity appears below T_2 in the mixed crystal $(K_{1-x}Rb_x)_3Cu_8S_6$, where $x \fallingdotseq 0.06$.

Certainly, the structural data are indispensable in order to make a further investigation on these phase transitions. Therefore, we carried out x-ray scattering measurements on $(K_{1-x}Rb_x)_3Cu_8S_6$, including $K_3Cu_8S_6$ and $Rb_3Cu_8S_6$. We have predominantly two aims in the present study. The first is to make clear whether $Rb_3Cu_8S_6$ undergoes the T_2 transition or not. The second is to obtain information about the superstructure of the mixed crystal $(K_{1-x}Rb_x)_3Cu_8S_6$.

§ 4-2 Experimental

A. X-ray diffuse scattering

The samples were synthesized by the fusion reaction of K_2CO_3, Rb_2CO_3, Cu and S. The obtained single crystals have the shape of needle-like prisms with the typical size of 3×

0.06× 0.04 mm^3 elongated along the b-axis (identical to the b^*-axis), which is parallel to the Cu_4S_4 chain axis. The largest face is the $(\bar{2}\ 0\ 1)$ plane.

X-rays were generated by a rotating-anode type generator. The CuKα characteristic x-rays with the electrical power of 8.1kW were collimated to the sample position by a bent graphite monochrometer.

The photographic measurements were made by the monochromatic Laue method.[66,67] An edge of the long sample was fixed on a copper plate with gold paste. The sample was cooled in vacuum by heat conduction through the copper plate attached to the cold finger of a closed-cycle helium refrigerator. The configuration of the apparatus is as follows; the incident x-ray beam and the b-axis of the crystal are in the horizontal plane making the angle of about 70° with each other. The scattering x-rays were recorded on a film wound on the cylindrically curved beryllium window of the cryostat. In the photographic measurements, we fixed the samples without paying attention to the direction of the a-axis and the c-axis. Judging from the shape of the crystals, however, it is most likely that the $(\bar{2}\ 0\ 1)$ plane is parallel to the vertical axis.

Measurements by counter method were made using a three-axis diffractometer with a position sensitive proportional counter (PSPC). The sample was cooled in He gas atmosphere

using a continuous-flow type cryostat. Since the size of the sample is larger than that of the beam and the absorption coefficient is not negligible, the comparison of the scattering intensity between different diffraction spots is difficult. Therefore, we discuss only the temperature dependence of the each spot.

§ 4-3 Results

A. Monochromatic Laue photographs

Figures 4-3~ 6 show the monochromatic Laue photographs of $(K_{1-x}Rb_x)_3Cu_8S_6$. In all the photographs, the b^*-axis is parallel to the horizontal line. The Bragg spots are located on the curved lines crossing perpendicularly with the b^*-axis. Those Bragg spots (h k l) which have the same k index are on the same line. The corresponding k numbers are indicated in the figures. The blank region in the photographs is the shadow of the beam stopper. Circles around the shadow are the Debye ring due to the diffraction by the sample holder.

Figure 4-3(a) shows the monochromatic Laue photograph of $K_3Cu_8S_6$ at room temperature. It should be noted that, even at room temperature, there are crescent-shaped areas in

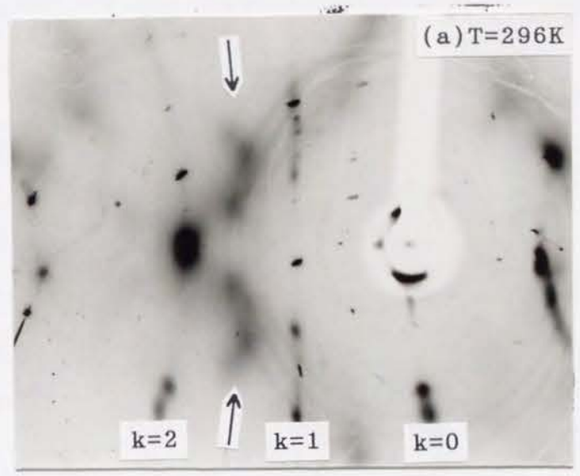

Fig. 4-3 Monochromatic Laue photographs of $K_3Cu_8S_6$; (a) at room temperature, (b) at 80K, and (c) at 15K. The arrows show the satellite reflections due to the incommensurate (in (a) and (b)), and due to the commensurate (in (c)) superstructures. At 15K, many spots appear on the "integer-l" lines. (See the text.)

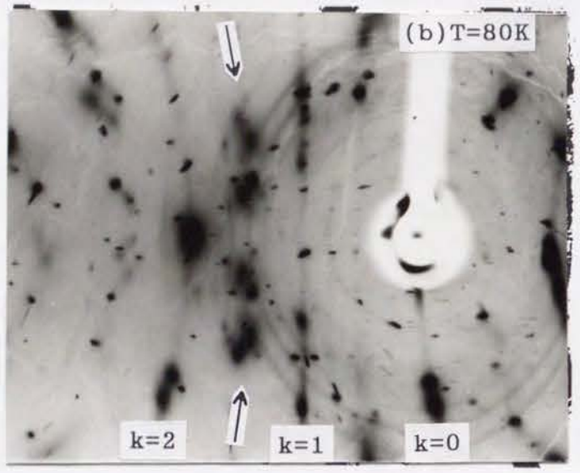

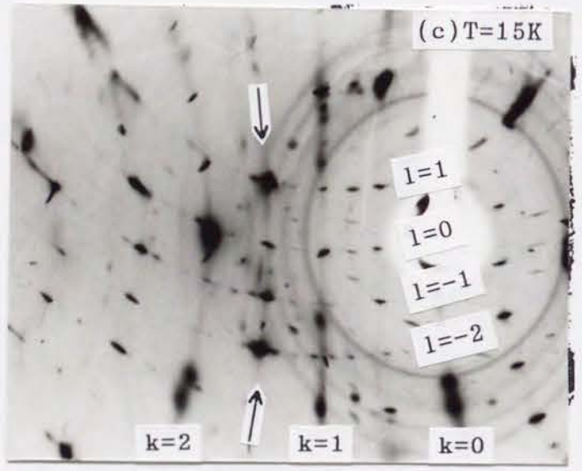

the region between the "integer-k" lines. In the crescents, there are somewhat strong points at the position corresponding to $k=n\pm\eta$ (n: integer, η : about 0.45). As shown in Fig. 4-3(b), at 80K ($T_2<T<T_1$), these points become intense and sharp satellite spots. This indicates that a long-range incommensurate superstructure with the wave vector $k\fallingdotseq\eta\,b^*$ develops. As shown in Fig 4-3(c), the incommensurate satellites almost disappear and strong spots appear at the positions of k=n+0.5 at T=15K ($T<T_2$). In addition, many spots appear forming a series of U-shaped lines. If we assume that the $(\bar{2}\ 0\ 1)$ plane is almost perpendicular to the incident beam, the curvatures and the intervals of these lines can be well explained by the scatterings having the scattering vector $S=ha^*+kb^*+lc^*$ with integer l and arbitrary h and k. Therefore, we call these lines "integer-l" lines. The corresponding l numbers are shown in Fig. 4-3(c).

Figures 4-4 show the monochromatic Laue photographs of $Rb_3Cu_8S_6$. As shown in Fig. 4-4(a), the diffuse spots resulting from the incommensurate superstructure are already observable at 125K ($T>T_1$). At 75K ($T<T_1$), the satellite spots become rather strong and sharp, as shown in Fig. 4-4(b). In the photographs, the intensity of satellite spots at 125K does not seem to be so different from that at 75K. However, as shown later, the satellite spots are not

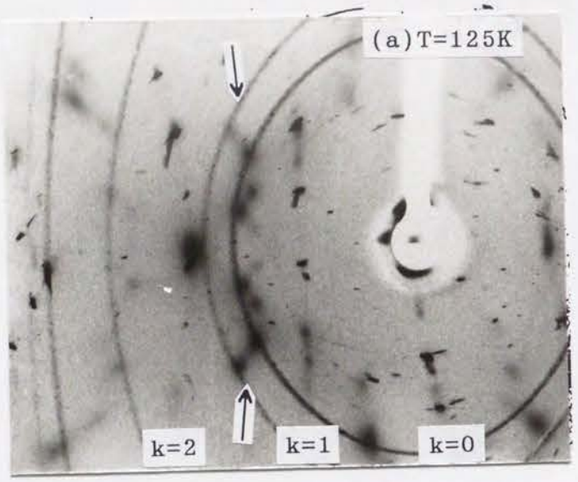

Fig. 4-4 Monochromatic Laue photographs of $Rb_3Cu_8S_6$; (a) at 125K, (b) at 75K, (c) at 15K. The arrows show the satellite reflections due to the incommensurate superstructure.

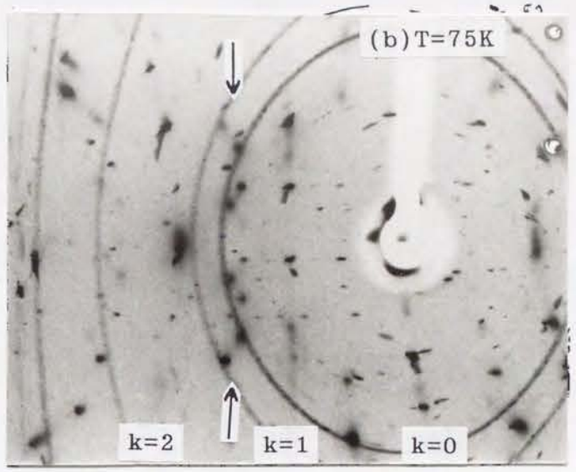

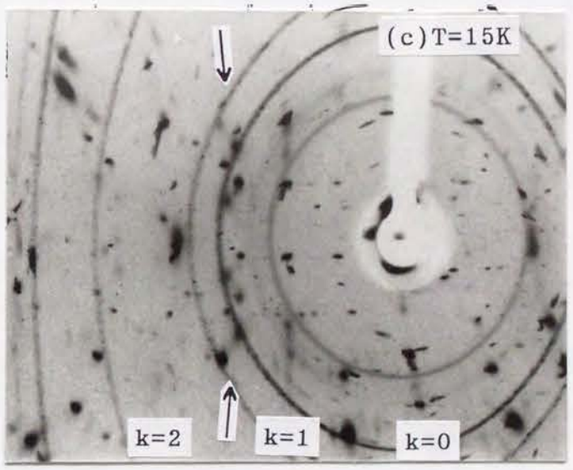

detectable by the counter method above 120K, while they are strong enough to be detected at 75K. As shown in Fig. 4-4(c), the photograph at 15K is almost the same as that at 75K. Therefore, unlike $K_3Cu_8S_6$, $Rb_3Cu_8S_6$ does not seem to undergo the T_2 transition. This was confirmed by the counter method as shown in the following section.

The mixed crystals $(K_{1-x}Rb_x)_3Cu_8S_6$, with x=0.33 and x=0.06 were also studied. In the both mixed crystals, the incommensurate diffuse spots are observed even at room temperature. Figures 4-5(a) and 4-5(b) show the monochromatic Laue photographs of $(K_{0.67}Rb_{0.33})_3Cu_8S_6$ at 100K and 15K, respectively. There is no qualitative difference between them; both of them have the identical incommensurate satellites. Therefore, it is probable that, in addition to $Rb_3Cu_8S_6$, $(K_{0.67}Rb_{0.33})_3Cu_8S_6$ also does not have the T_2 transition. On the other hand, the results of $(K_{0.94}Rb_{0.06})_3Cu_8S_6$ are rather complicated. As shown in Fig. 4-6(a), the photograph of $(K_{0.94}Rb_{0.06})_3Cu_8S_6$ at 100K ($T_2<T<T_1$) has incommensurate satellite spots. At 15K ($T<T_2$), many new spots appear forming series of curves (Fig. 4-6(b)). These curves are essentially the same* as the "integer-l" curves which appear in the photograph of $K_3Cu_8S_6$ at 15K. The corresponding l numbers are expressed in the figure. It should be noted that the incommensurate satellites still remain at 15K unlike in $K_3Cu_8S_6$. We show

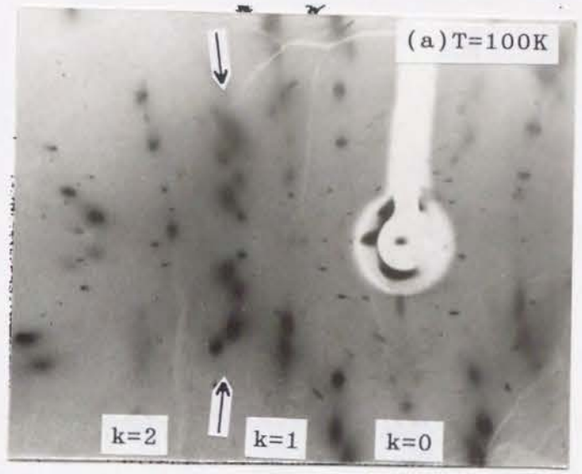

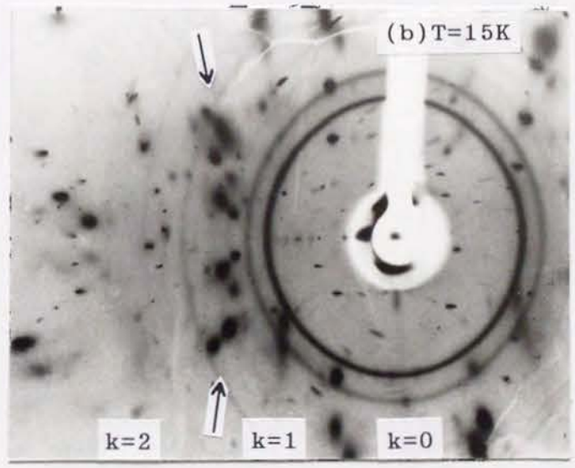

Fig. 4-5 Monochromatic Laue photographs of $(K_{0.67}Rb_{0.33})_3Cu_8S_6$; (a) at 100K, (b) at 15K. The arrows show the satellite reflections due to the incommensurate superstructure.

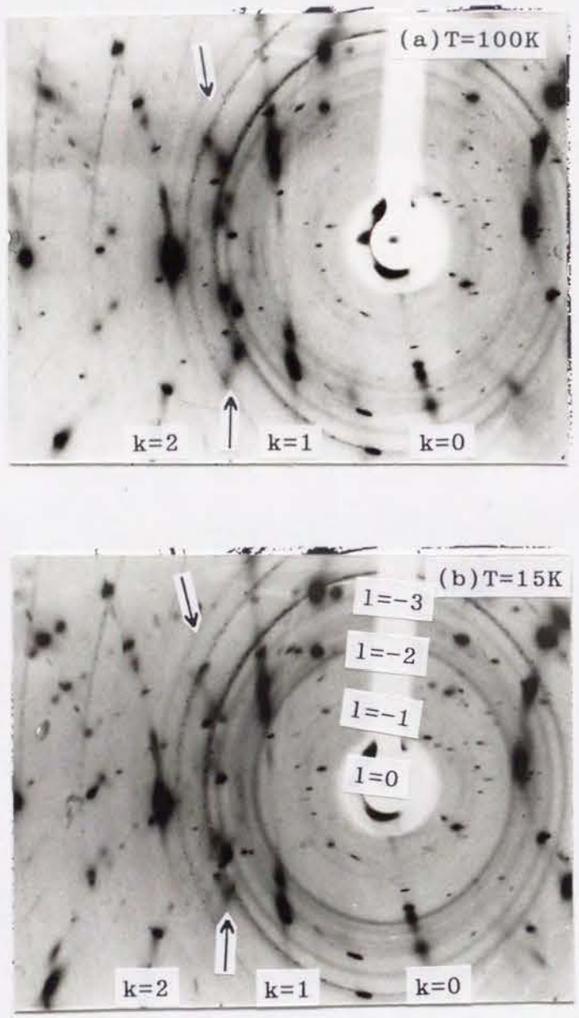

Fig. 4-6 Monochromatic Laue photographs of $(K_{0.94}Rb_{0.06})_3Cu_8S_6$; (a) at 100K, (b) at 15K. The arrows show the satellite reflections due to the incommensurate superstructure. At 15K, many spots appear on the "integer-l" lines. (See the text.)

later the detailed results on this mixed crystal using the counter method.

B. Counter results on $Rb_3Cu_8S_6$

In counter measurements on $Rb_3Cu_8S_6$, we investigated mainly the (h k l) zones, where h=-4~ 1, k=1~ 3 and l=0~ 2. At room temperature, the Bragg reflections were found at the (h k l) point (h+k=2n, n=integer), obeying the extinction rule.[13] No diffuse scatterings from the incommensurate superstructure were detectable by the counter method at room temperature, although they appear in the photographs.

The satellite spots appear below 115K, which is almost in agreement with the transition temperature estimated by the resistivity data. In the presence of the satellite structures, the extinction rule of the Bragg peaks is

---

* Of course, there is a difference; the curves observed in $(K_{0.94}Rb_{0.06})_3Cu_8S_6$ are convex upward, while the streaks in the photograph of $K_3Cu_8S_6$ are convex downward (U-shaped). However, this difference is due to the difference in the direction of the sample. Even though the direction of the b-axis and that of the $(\bar{2}\ 0\ 1)$ plane are fixed, there are two possible directions of the crystal because of the monoclinic symmetry.

conserved. The satellites are located at the point apart by $\pm \eta$ b* from the nearby Bragg point, where η is about 0.45. Especially the satellites (0 $2-\eta$ 1), ($\bar{2}$ $2-\eta$ 2) and ($\bar{2}$ $2-\eta$ 0) have large intensities comparable to those of the Bragg reflections. However, the satellite ($\bar{2}$ $2+\eta$ 1) which has been investigated in the study of $K_3Cu_8S_6$[33] is far weaker than them. Therefore, we chose the ($\bar{2}$ $2-\eta$ 0) satellite as a probe for the incommensurate superstructure.

Figure 4-7 shows the temperature dependence of the integrated intensity of the ($\bar{2}$ $2-\eta$ 0) satellite in $Rb_3Cu_8S_6$. The intensity increases with decreasing temperature from 115K to about 50K, below which it becomes almost temperature independent. The value η is about 0.45 and almost independent of temperature. Therefore, the superstructure remains incommensurate down to 20K as expected from the photographic results. The temperature dependence of the intensity is that of a usual CDW. Unlike in $K_3Cu_8S_6$, neither the anomalous oscillation of the intensity nor abrupt disappearance of the superstructure was observed in $Rb_3Cu_8S_6$. Therefore, we conclude that $Rb_3Cu_8S_6$ does not undergo the phase transition corresponding to the T_2 transition of $K_3Cu_8S_6$. It is to be noted that no satellite diffractions were observed at the (0 k 0) zones. As we show in the following chapter, this is a useful result in considering the mode of the lattice distortion.

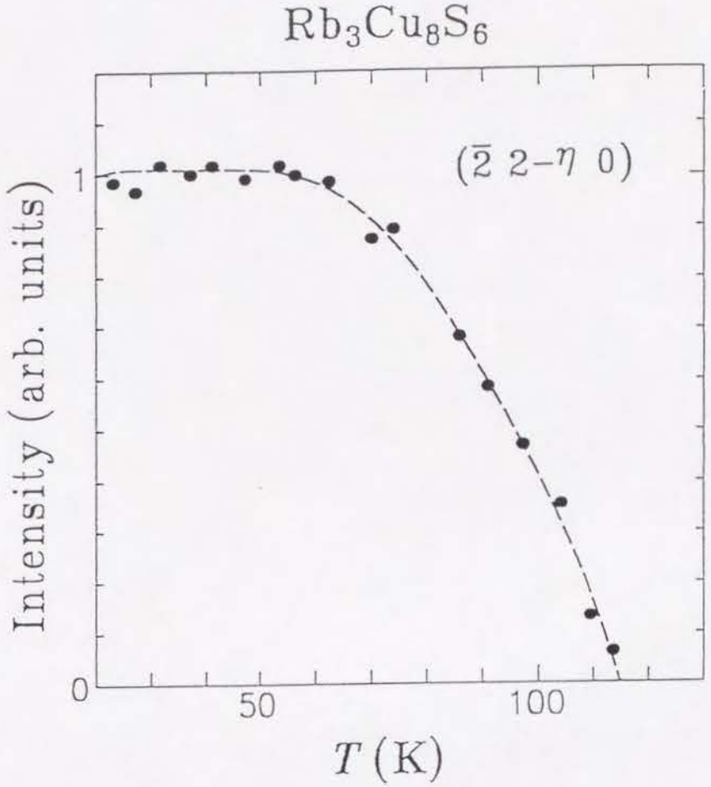

Fig. 4-7 Temperature dependence of the intensity of the incommensurate satellite reflection ($\bar{2}$ $2-\eta$ 0) of $Rb_3Cu_8S_6$. The value η is about 0.45.

C. Counter results on $(K_{0.94}Rb_{0.06})_3Cu_8S_6$

Now we know that the superstructure of $Rb_3Cu_8S_6$ at the lowest temperature is incommensurate (0 η 0), while that of $K_3Cu_8S_6$ is commensurate (1/2 1/2 0). On the other hand, the

photographic result of $(K_{0.94}Rb_{0.06})_3Cu_8S_6$ at 15K shows that the superstructure is still incommensurate, although there are "integer-1" curves which are also observed in the photograph of $K_3Cu_8S_6$ at 15K. In order to obtain further information about the superstructure of $(K_{0.94}Rb_{0.06})_3Cu_8S_6$, we made a measurement by the counter method. The investigated zones are (h k l): h=-4~ 0, k=1~ 3 and l=0~ 2. The extinction rule of the Bragg spots is the same as that of $Rb_3Cu_8S_6$. The satellites are detectable below 150K at (h p± η 1); where h+p=2n (p, n : integer) and η =0.45 at 150K. The satellites (0 2-η 1), ($\bar{2}$ 2-η 2) and ($\bar{2}$ 2-η 0) have large intensities comparable to that of the Bragg reflections. There are no satellite diffractions at the (0 k 0) zones. It was also found that the satellites ($\bar{2}$ 2-η 1) and ($\bar{4}$ 2-η 2) were not detected, while ($\bar{2}$ 2+η 1) and ($\bar{4}$ 2+η 2) are strong enough to be detected.

Figure 4-8 shows the temperature dependence of the integrated intensity of the ($\bar{2}$ 2-η 0) satellite spot. In $(K_{0.94}Rb_{0.06})_3Cu_8S_6$, the temperature dependence above 80K is not anomalous. On further cooling, after exhibiting an anomalous kink at 80K, the intensity increases steeply between 80K and 75K. This anomalous behavior is reminiscent of the oscillation of the intensity in $K_3Cu_8S_6$[33]. The intensity reaches the maximum around 60K and then decreases with decreasing temperature. The decrease of the intensity

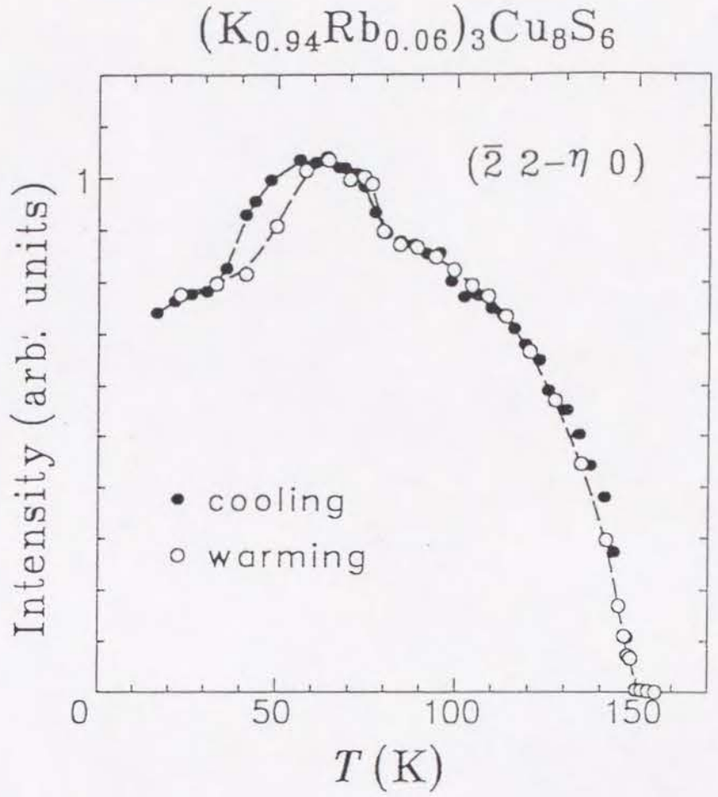

Fig. 4-8 Temperature dependence of the intensity of the incommensurate satellite reflection ($\bar{2}$ 2-η 0) of $(K_{0.94}Rb_{0.06})_3Cu_8S_6$.

is most pronounced around 45K. Below 35K, where the cooling curve has a kink, the intensity is less temperature dependent. A thermal hysteresis is observed between 35K and 60K. The temperature dependence of the wave vector is shown in Fig. 4-9. With decreasing temperature, the value η

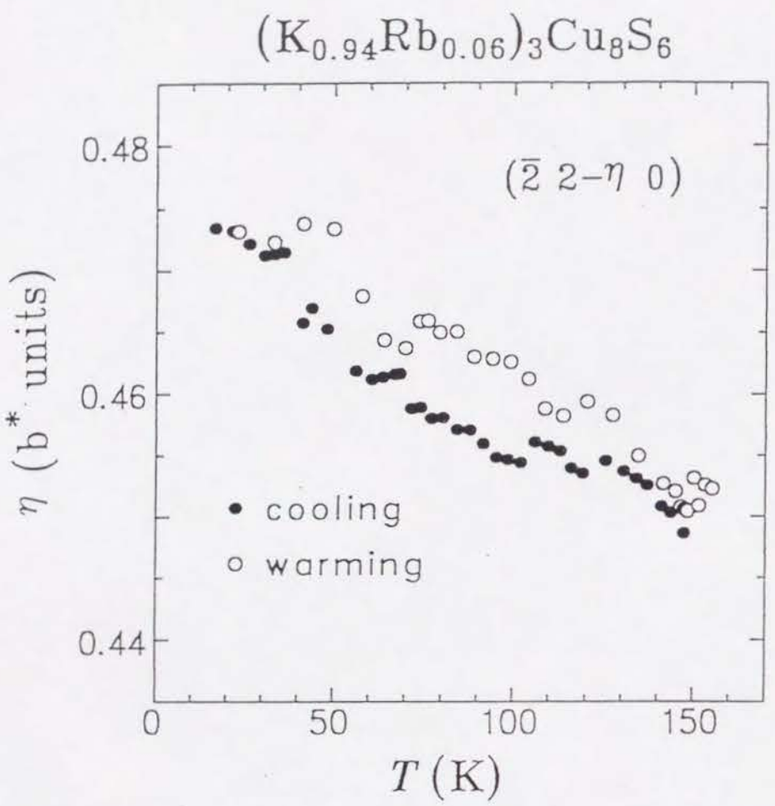

Fig. 4-9 Temperature dependence of the magnitude of the wave vector of the incommensurate superstructure of $(K_{0.94}Rb_{0.06})_3Cu_8S_6$ calculated by using the the incommensurate satellite reflection ($\bar{2}$ 2-η 0).

increases from 0.45 at 150K to 0.47 at 20K. The value and the temperature dependence of η are almost the same as those of $K_3Cu_8S_6$[33].

Figure 4-10 shows the full width at half maximum (FWHM)

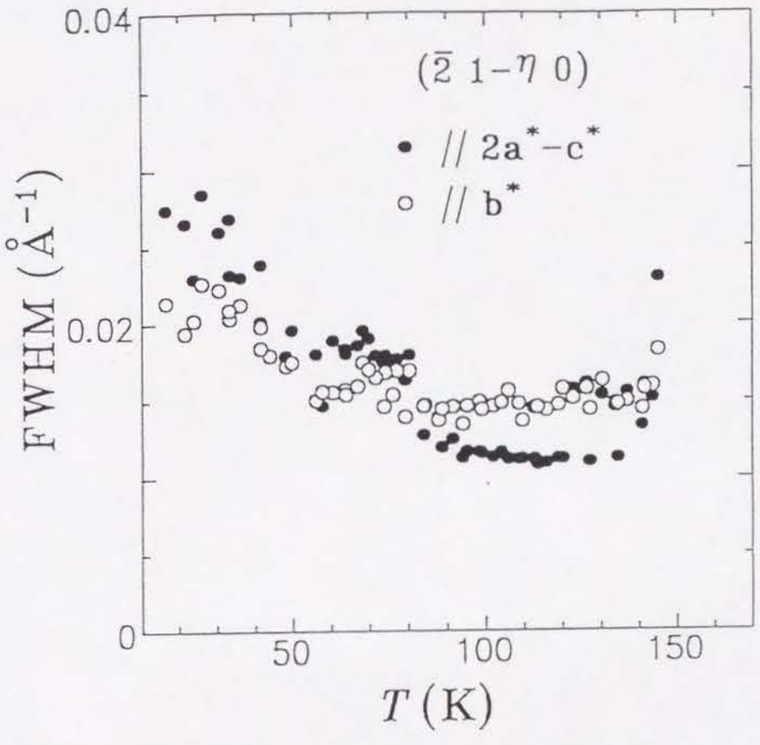

Fig. 4-10 Temperature dependence of the linewidth of the incommensurate satellite reflection ($\bar{2}$ 2-η 0) of $(K_{0.94}Rb_{0.06})_3Cu_8S_6$.

of the ($\bar{2}$ 2-η 0) satellite spot. The FWHM exhibits anomalous increase below 80K. In particular, the increase is remarkable around 45K, where the intensity of the satellite also shows anomalous decrease.

In the case of $K_3Cu_8S_6$, the incommensurate (0 η 0) superstructure disappears almost completely and another commensurate (1/2 1/2 0) superstructure appears below 50K. However, the (1/2 1/2 0) superstructure was not detectable in $(K_{0.94}Rb_{0.06})_3Cu_8S_6$ even at 20K.

Fleming et al. reported[33] that the satellite reflections due to the incommensurate (0 η 0) superstructure of $K_3Cu_8S_6$ have intensities about 10^{-3} times the intensity of ordinary Bragg peaks. However, in the present measurements on $(K_{0.94}Rb_{0.06})_3Cu_8S_6$, the satellites such as (0 $2-\eta$ 1), ($\bar{2}$ $2-\eta$ 2) and ($\bar{2}$ $2-\eta$ 0) have the intensities comparable to those of the Bragg reflections. Furthermore, it was found that some Bragg peaks change their intensities below T_1. As shown in Fig. 4-11, the intensity of the ($\bar{1}$ 1 0) Bragg peak decreases by 40% as the superstructure develops below 150K.

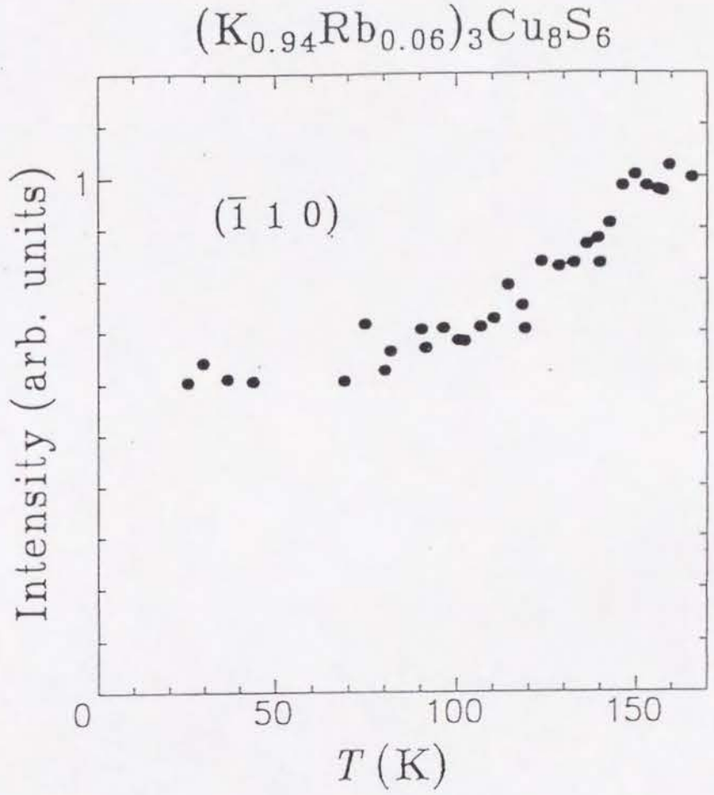

Fig. 4-11 Temperature dependnece of the intensity of the Bragg reflection ($\bar{1}$ 1 0) of $(K_{0.94}Rb_{0.06})_3Cu_8S_6$.

§ 4-4 Discussion

A. The T_1 transition and a possible mode of the incommensurate distortion

It is found that the diffuse spots appear in all the photographs of $(K_{1-x}Rb_x)_3Cu_8S_6$ even at room temperature. This suggests the existence of fluctuating CDW state above T_1. The existence of such a state is also expected from the fact that the resistivities of $(K_{1-x}Rb_x)_3Cu_8S_6$ slightly deviate from the linear temperature dependence a little above T_1.

Below T_1, a long-range order develops and clear satellite spots appear. The wave vector of the incommensurate superstructure is about $0.45b^*$ for $Rb_3Cu_8S_6$, which is almost the same as that of $K_3Cu_8S_6$, as expected from a rigid-band model. Since the number of the satellite spots observed in the present measurements is only 10~ 20, it is difficult to determine the displacement of each atom in the CDW state. However, the extinction rule of the satellites and the intensity distributions give us the information about the mode of lattice distortions. Although the superstructure below T_1 is incommensurate, we consider a commensurate distortion with the wave vector of $5/11b^*$ as a first approximation. Furthermore, we assume sinusoidal atomic displacement. It is a reasonable assumption because

the higher-order satellites are absent. Then, the structure factor is described as follows*;

$$F_{hkl}=(1/11)\sum_{n=0}^{11}\exp(2\pi\, ink)\sum_{j=1}^{36} f_j(hkl)\exp[2\pi\, i(hx_j+ky_j+lz_j)],$$

$$\begin{cases} x_j=x_{j0}+\{u_{xj}\exp[2\pi\, i(5/11)(y_{j0}+n)]+u_{xj}^*\exp[-2\pi\, i(5/11)(y_{j0}+n)]\}, \\ y_j=y_{j0}+\{u_{yj}\exp[2\pi\, i(5/11)(y_{j0}+n)]+u_{yj}^*\exp[-2\pi\, i(5/11)(y_{j0}+n)]\}, \\ z_j=z_{j0}+\{u_{zj}\exp[2\pi\, i(5/11)(y_{j0}+n)]+u_{zj}^*\exp[-2\pi\, i(5/11)(y_{j0}+n)]\}, \end{cases} \quad (1)$$

where x_{j0}, y_{j0}, and z_{j0} denote the equilibrium positional parameters of atoms and u_{xj}, u_{yj} and u_{zj} are complex amplitudes of the sinusoidal modulations. For small u_{xj}, u_{yj} and u_{zj}, eq. (1) is expressed as follows,

$$F_{hkl}=\begin{cases} F_{hkl}^0-4\pi^2\sum_{j=1}^{36}\{f_j(hkl)\exp[2\pi\, i(hx_{j0}+ky_{j0}+lz_{j0})] \\ \qquad\qquad \times |hu_{xj}+ku_{yj}+lu_{zj}|^2\} \qquad (k:\ \text{integer}) \\ 2\pi\, i\sum_{j=1}^{36}\{f_j(hkl)\exp[2\pi\, i(hx_{j0}+py_{j0}+lz_{j0})](hu_{xj}+ku_{yj}+lu_{zj})\} \\ \qquad\qquad (k=p-5/11) \\ 2\pi\, i\sum_{j=1}^{36}\{f_j(hkl)\exp[2\pi\, i(hx_{j0}+py_{j0}+lz_{j0})](hu^*_{xj}+ku^*_{yj}+lu^*_{zj})\} \\ \qquad\qquad (k=p+5/11), \end{cases} \quad (2)$$

---

* The unit cell includes 34 atoms, but we artificially duplicate the K1 sites, which are located at the positions of higher symmetry than the other sites, for the convenience of the later discussion. This will be allowed if we halve the atomic scattering factor of the K1 sites.

where $F_{hkl}{}^0$ is the structure factor of the Bragg spot when the lattice distortion is absent and p is an integer. Taking account of the symmetry of the crystal structure[13), we can choose index j so that the following relations are satisfied;

$$\begin{cases} f_{j+9}(hkl)=f_j(hkl) \\ x_{j+9,0}=-x_{j0} \\ y_{j+9,0}=-y_{j0}=0 \\ z_{j+9,0}=-z_{j0}, \end{cases} \qquad (1\leqq j\leqq 9)$$

and

$$\begin{cases} f_{j+18}(hkl)=f_j(hkl) \\ x_{j+18,0}=x_{j0}+1/2 \\ y_{j+18,0}=1/2 \\ z_{j+18,0}=z_{j0}. \end{cases} \qquad (1\leqq j\leqq 18) \qquad (3)$$

From the extinction rule of the satellite reflection, the relation,

$$\begin{cases} u_{x,j+18}=u_{xj} \\ u_{y,j+18}=u_{yj} \\ u_{z,j+18}=u_{zj}, \end{cases} \qquad (4)$$

must be satisfied. We can further halve the number of parameters because the mode of the distortion must be symmetric or anti-symmetric with respect to the C2 rotation around the b-axis. Then the structure factor for the symmetric distortion becomes as follows;

$$F_{hkl}=\begin{cases} 4\pi i\sum_{j=1}^{9}\{f_j(hkl) \\ \quad\times[2i(hu_{xj}+lu_{zj})\sin2\pi(hx_{j0}+lz_{j0})+2ku_{yj}\cos2\pi(hx_{j0}+lz_{j0})]\} \quad (\text{for } k=p-5/11) \\ 4\pi i\sum_{j=1}^{9}\{f_j(hkl) \\ \quad\times[2i(hu^*_{xj}+lu^*_{zj})\sin2\pi(hx_{j0}+lz_{j0})+2ku^*_{yj}\cos2\pi(hx_{j0}+lz_{j0})]\} \quad (\text{for } k=p+5/11). \end{cases} \qquad (5)$$

On the other hand, the structure factor for the anti-symmetric case is as follows;

$$F_{hkl}=\begin{cases} 4\pi i\sum_{j=1}^{9}\{f_j(hkl) \\ \quad\times[2(hu_{xj}+lu_{zj})\cos2\pi(hx_{j0}+lz_{j0})+2iku_{yj}\sin2\pi(hx_{j0}+lz_{j0})]\} \quad (\text{for } k=p-5/11) \\ 4\pi i\sum_{j=1}^{9}\{f_j(hkl) \\ \quad\times[2(hu^*_{xj}+lu^*_{zj})\cos2\pi(hx_{j0}+lz_{j0})+2iku^*_{yj}\sin2\pi(hx_{j0}+lz_{j0})]\} \quad (\text{for } k=p+5/11). \end{cases} \qquad (6)$$

Remember the absence of the (0 k 0) satellites here. For the symmetric distortion, this requires the following relation;

$$\sum_{j=1}^{9} f_j(hkl)u_{yj}=0. \qquad (7)$$

Then, in the case of the symmetric distortion, the scattering intensity of the satellite is proportional to

$$\left|\sum_{j=1}^{9} f_j(hkl)\{(hu_{xj}+lu_{zj})\sin2\pi(hx_{j0}+lz_{j0})\}\right|^2 \qquad (\text{for } k=p\pm 5/11). \qquad (8)$$

Therefore, the intensity depends on k only through the atomic scattering factor $f_j(hkl)$. In the practical calculation for $1.55 \leqq k \leqq 2.45$, it is not a bad approximation to extract the same hkl-dependence from $f_j(hkl)$ for K, Cu and S as follows;

$$f_j(hkl) \fallingdotseq g(hkl) f_j , \tag{9}$$

where f_j are functions depending only on the atomic number. Therefore, the intensity of the $(\bar{2}\ 2-\eta\ \ 1)$ reflection is expected to be about 1.5 times that of the $(\bar{2}\ 2+\eta\ \ 1)$ reflection. However, this contradicts with the experimental result that the satellite $(\bar{2}\ 2-\eta\ \ 1)$ is absent or very weak while the satellite $(\bar{2}\ 2+\eta\ \ 1)$ is strong. Therefore, we can exclude the possibility of the symmetric distortion.

On the other hand, in the case of the anti-symmetric distortion, the absence of the (0 k 0) satellites is a necessary consequence of the eq. (6). However, according to eq. (6), if the distortion is purely longitudinal or purely transverse, we come to the same conclusion as in the case of the symmetric distortion; the intensity of the $(\bar{2}\ 2-\eta\ \ 1)$ satellite must be about 1.5 times lager than that of the $(\bar{2}\ 2+\eta\ \ 1)$ satellite. Therefore, the most probable mode of the incommensurate $(0\ \eta\ \ 0)$ distortion is such a distortion

that is anti-symmetric under the C2 rotation around the b-axis and that includes both the longitudinal and the transverse components.

The change in the intensity of the Bragg reflection $(\bar{1}\ 1\ 0)$ comes from the second term of the eq. (2). If we collect the data about the change in the intensity of many Bragg peaks as well as about that of the satellites, we will be able to reproduce the displacement of each atom. More detailed studies using 4-circle diffractometer are in progress now.

Whangbo and Canadell[52] made another interpretation of the T_1 transition. They remarked that the Cu3 atoms, which is located at the center of the CuS_4 tetrahedron (Fig. 2-8), have anomalously large anisotropic temperature factors especially along the c*-axis. Therefore, it is possible that the copper atoms at the Cu3 sites are displaced randomly from the center of their thermal ellipses at room temperature. They considered the T_1 transition as the order-disorder transition of these displacement of the Cu3 atoms. However, the analysis of the present experimental data using their model was unsuccessful. We emphasize that not only the Cu3 atoms but also the Cu1 atoms have large temperature factors.[13]

Furthermore, in their model, the reason why the superstructure is incommensurate is explained by the

existence of 'kink' appearing between the commensurate distortions. If it is the case, the higher-order satellite structures should be observed in the x-ray scattering measurement. However, no higher-order satellites are observed.

B. The T_2 transition

The present x-ray structural study made clear that $Rb_3Cu_8S_6$ does not undergo a transition which corresponds to the T_2 transition of $K_3Cu_8S_6$. Therefore, we can attribute the recovery of the metallic behavior below 50K (Fig. 2-11) to the remaining part of the Fermi surface, as in the case of $NbSe_3$[88], etc.

The measurements on the mixed crystal $(K_{0.94}Rb_{0.06})_3Cu_8S_6$ revealed that the (1/2 1/2 0) phase of $K_3Cu_8S_6$ disappears and that the (0 η 0) phase remains down to the lowest temperature, when only 6% of K is replaced by Rb. This seems to be strange because the resistivity of $(K_{0.94}Rb_{0.06})_3Cu_8S_6$ has the anomaly corresponding to the T_2 transition of $K_3Cu_8S_6$ as shown in Fig. 3-4(d). As shown in Fig. 4-8 and Fig. 4-10, however, we found anomalies both in the intensity and the linewidth of the satellites of the (0 η 0) superstructure at about 45K, where the resistivity measurements suggest the presence of the T_2 transition. The

broadening of the satellite spots means that the correlation length of the (0 η 0) superstructure becomes very short below T_2.

As shown in Fig. 4-10, the FWHMs of the ($\bar{2}$ 1-η 0) satellite parallel to $2a^*-c^*$ and to b^* at 20K are by $0.015Å^{-1}$ and $0.007Å^{-1}$ larger than those at 100K, respectively. If we assume that long-range order of the incommensurate superstructure develops enough at 100K, we can roughly estimate the correlation length of the superstructure at 20K from the increase in the FWHM. The correlation lengths parallel to $2a^*-c^*$ and to b^* are estimated about 70Å and 140Å, respectively. This suggests that the incommensurate superstructure is divided into a number of domains below T_2.

As discussed in the previous chapter, we can interpret the T_2 transition as a structural phase transition caused by such a structural instability because of the mismatch between the Cu_8S_6 sheet and the potassium ions. At present, the exact crystal structure of $K_3Cu_8S_6$ is unclear below T_2 except the formation of the superlattice (2a, 2b, c). In $K_3Cu_8S_6$, we consider that the structural change at T_2 is large enough to change the shape of the Fermi surface, resulting in the absence of the (0 η 0) CDW below T_2. The drastic decrease in the resistivity at T_2 (Fig. 2-10) can be explained by such an abrupt disappearance of the CDW.

The structural instability of $K_3Cu_8S_6$, which causes the T_2 transition, is suppressed by replacing K by Rb. In $(K_{0.94}Rb_{0.06})_3Cu_8S_6$, consequently, the structural change at T_2 which prefers the (1/2 1/2 0) periodicity is insufficient to overcome the (0 η 0) CDW. Therefore, the (0 η 0) superstructure remains below T_2, but the correlation length of the (0 η 0) superstructure becomes very short below T_2. The long-range (0 η 0) periodicity is considered to be disturbed by the weak (1/2 1/2 0) distortion below T_2.

According to the above interpretation, the origin of the (1/2 1/2 0) superstructure is independent of that of the (0 η 0) superstructure. Therefore, these two superstructures are not necessarily exclusive with each other. If we assume that these two superstructures can coexist, the interpretation of the "integer-l" curves which appear at 15K in the photographs of $K_3Cu_8S_6$ (Fig. 4-3(c)) and of $(K_{0.94}Rb_{0.06})_3Cu_8S_6$ (Fig. 4-6(b)) is straightforward. The appearance of the "integer-l" curves mean that the periodicity is disturbed except for along the c-axis. This is what is expected when the (0 η 0) and the (1/2 1/2 0) superstructures coexist, because l is the only index that is common between these superstructures.

We have now the idea about the origin of the rise in resistivity of $(K_{0.94}Rb_{0.06})_3Cu_8S_6$, etc. As already discussed, the T_2 transition is likely a structural phase

transition independent of the CDW. In $K_3Cu_8S_6$, the T_2 transition destroys the incommensurate (0 η 0) CDW, and another commensurate (1/2 1/2 0) superstructure appears. On the other hand, in $(K_{0.94}Rb_{0.06})_3Cu_8S_6$, the competition of these two superstructures may result in the occurrence of a number of microdomains, just like a discommensurate state. If the many domain walls contribute to the scattering of carriers, the rise in the resistivity will appear.

§ 4-5 Summary

In order to investigate the phase transitions of the low-dimensional metals $K_3Cu_8S_6$, $Rb_3Cu_8S_6$ and the mixed crystal $(K_{1-x}Rb_x)_3Cu_8S_6$, x-ray scattering studies were carried out. The results are summarized as follows.

(1) The monochromatic Laue photographs of $K_3Cu_8S_6$ are consistent with the counter results[32] reported by Fleming et al.; the incommensurate (0 η 0) superstructure appears between T_1 (153K) and T_2 (55K) and the commensurate (1/2 1/2 0) superstructure below T_2.

(2) In $Rb_3Cu_8S_6$, only the incommensurate (0 η 0) superstructure appears below 115K down to 15K, the lowest temperature in the present study. This shows that $Rb_3Cu_8S_6$

has no phase transition which corresponds to the T_2 transition of $K_3Cu_8S_6$.

(3) The mixed crystal $(K_{0.94}Rb_{0.06})_3Cu_8S_6$ undergoes the phase transition into the (0 η 0) phase at T_1 (150K). Unlike in $K_3Cu_8S_6$, the (0 η 0) structure remains down to 15K and the (1/2 1/2 0) structure is not observed. However, there is a transition around 45K, below which the correlation length of the (0 η 0) superstructure drastically decreases. This transition can be explained in terms of the interaction between the (0 η 0) and the (1/2 1/2 0) structures below 45K.

Chapter 5. General Conclusion

We have been interested in alkali copper chalcogenides (A-Cu-X) for a variety of their structures and their valence states. Because of their low-dimensional chalcogen-copper networks, A-Cu-X compounds are expected to be a new series for studying charge-density wave (CDW) which is characteristic of a low-dimensional electron system.

Among A-Cu-X compounds, however, only $K_3Cu_8S_6$ has been reported to undergo CDW transitions. It has been unknown whether these transitions are universally observed in the low-dimensional A-Cu-X compounds. Therefore, we investigated the electronic properties at low temperature of several A-Cu-X compounds.

The results of the present studies are summarized as follows:

a) The layered compounds KCu_4S_3 and $RbCu_4S_3$ are normal metals down to 1.4K. The carriers are p-type.

b) In spite of its apparently one-dimensional structure, $Na_3Cu_4S_4$ is normal metal down to 0.5K. The carriers are p-type.

c) $K_3Cu_8S_6$ undergoes a CDW transition at T_1 and another structural phase transition at T_2. The origin of the T_2 transition is probably independent of the CDW.

d) $Rb_3Cu_8S_6$ undergoes the T_1 transition but does not have the T_2 transition.

e) In $K_3Cu_8S_6$ and $Rb_3Cu_8S_6$, p-type carriers and n-type carriers coexist. The n-type carriers are extinguished by the CDW transitions.

f) $Rb_3Cu_8Se_6$ is a normal metal without any phase transitions. The carriers are p-type.

These results give rise to new problems.

The first problem is that: why only $K_3Cu_8S_6$ and $Rb_3Cu_8S_6$ undergo CDW transitions?

Since CDW transitions are absent in $Na_3Cu_4S_4$ and $Rb_3Cu_8Se_6$, it is too hasty to attribute the CDW transitions of $K_3Cu_8S_6$ to its apparently low-dimensional crystal structure. The present results indicate that the existence of the n-type carriers relates the CDW transition.

A natural explanation is that $K_3Cu_8S_6$ and $Rb_3Cu_8S_6$ have n-type parts of Fermi surface which are likely to nest. In order to verify this speculation, further knowledge about the transport properties, such as Hall coefficient and magnetoresistance, etc., is necessary. Also the band calculations will help us understand the CDW transition of $K_3Cu_8S_6$. Although there is a band calculation on $K_3Cu_8S_6$ by Whangbo and Canadell[52], their result does not reproduce the n-type carriers we observed by TEP. It must be verified

whether their calculation using the parameters of the isolated atoms is appropriate for the present compound.

The second problems is that: what is the origin of the T_2 transition of $K_3Cu_8S_6$?

A possible interpretation is that the T_2 transition is due to the mismatch between the Cu_8S_6 sheets and the counter cations. In order to make further discussion, structural analysis of $K_3Cu_8S_6$ below T_2 is indispensable. The measurement of the specific heat will also give us information about the mechanism of the T_2 transition.

There are a number of studies on charge-density waves of many compounds such as MX_2[69], MX_3[70], $(MX_4)_nI$[70], molybdenum bronzes and oxides[55], and organic conductors[70]. What is new of the CDW transition of $K_3Cu_8S_6$?

It is worth while to mention the similarity[32] between the CDW transitions of $K_3Cu_8S_6$ and those of thiospinel CuV_2S_4[71-74]. Since the electron state of CuV_2S_4 is three-dimensional, it is difficult to explain its transitions by conventional CDW mechanisms. The result of the electron diffraction[74] on CuV_2S_4 by Mahy et al. suggests that the dimerization-type displacements of copper atoms, which are tetrahedrally surrounded by sulfur atoms, occur.

In CuV_2S_4, Cu^+ ions can be move from the equilibrium position in the tetrahedral "cage" of sulfur atoms probably

because of the small ionic radius of Cu^{+}.

Such large displacements of the copper ions at the tetrahedral sites are expected in also $K_3Cu_8S_6$. As Fleming et al.[33] and Whangbo et al.[52] pointed out, the anisotropic temperature factors of copper atoms in the tetrahedral columns are extraordinary large in $K_3Cu_8S_6$ and $Rb_3Cu_8S_6$. Therefore, it is possible that the CDW transition of $K_3Cu_8S_6$ is not a conventional one but a phase transition caused by the coupling between the conduction electrons and the motion of those copper atoms which have large anisotropic temperature factors.

It has been recently reported by Ohtani et al.[20] that $TlCu_7S_4$ and KCu_7S_4 undergo phase transitions similar to those of $K_3Cu_8S_6$. It is possible that these transitions are also due to the motion of the copper atoms at the tetrahedral sites.

The large displacements of Cu^{+} ions in the tetrahedral sites are universally observed in several chalcogenides. The extreme example is $Cu_{2-x}Se$, in which the copper ions are mobile in the selenium sublattice and exhibit superionic conduction[75].

Therefore, it is expected that the further studies on the phase transitions of $K_3Cu_8S_6$, etc., discover new field between solid state physics and solid state ionics.

Acknowledgments

This work has been accomplished with support of a number of coworkers.

The author would like to thank Professor Gunzi Saito (Kyoto Univ.), Honorary Professor Ikuji Tsujikawa (Kyoto Univ.) and Professor Koji Kosuge (Kyoto Univ.) for thier continuous encouragements and stimulating discussions.

This work has been started since Professor Norimichi Kojima (Kyoto Univ.) initially brought alkali copper chalcogenides to the author's attention. The author thanks him for continuous encoragement and various discussion.

The author is grateful to Research Associate Toshiro Ban (Kyoto Univ.) for many experimental supports, Dr. Hideki Yamochi (Kyoto Univ.) and Dr. Akihiro Ohtsuka (Kyoto Univ.) for helpful advices and encouragements.

The author thanks Professor Toshiaki Enoki (Tokyo Institute of Tech.), Dr. Kazuya Suzuki (Tokyo Institute of Tech.) and Mr. Isao Tomomatsu (Tokyo Institute of Tech.) for kindly help and useful discussion in the TEP measurements at their laboratory.

The x-ray diffuse scattering experiments have been carried out at Kagoshima laboratory in University of Tokyo. The author wishes to acknowledge Professor Seiichi Kagoshima (Univ. of Tokyo) for willing consent to carry out the

experiments at his laboratry and invaluable discussion, and also thanks Dr. Yoshio Nogami (Kyoto Univ.) and Dr. H. Sawa (Univ. of Tokyo) for valuable discussion, Dr. Masahiko Hasumi (Univ. of Tokyo) for technical help in the x-ray scattering measurements.

The author is grateful to Professor Kazuko Motizuki (Osaka Univ.) and Dr. Masafumi Shirai (Osaka Univ.) for giving helpful advice from a theoretical point of view, Professor Tsukio Ohtani (Okayama Univ. of Science) for useful discussion and encoragement and Professor Hiroshi Nagasawa (Univ. of Tsukuba) for valuable discussion and preliminary NMR measurements.

The measurements of magnetic susceptibility and EPMA were carried out at the Instrument Center, Institute for Molecular Science with kind help of Professor Keisaku Kimura (Himeji Institue of Tech.), Dr. Shunji Bandow (Institute for Molecular Science) and Mr. Masahiro Sakai (IMS). The author thanks Mr. Kiyonori Kato (IMS) for the help in the resistivity measurements at liquid ^{3}He temperature, and Tamotsu Inabe (IMS) for the x-ray diffraction experiment.

The author wishes to thank Professor Kazuhiko Tsuji (Keio Univ.), Professor Tetsuo Nakajima (National Lab. for High Energy Physics), Dr. M. Imai (National Research Institute for Metals), Dr. K. Yaoita (National Institute for Research in Inorganic Materials) and Professor Ichimin

Shirotani (Muroran Institute of Tech.) for the x-ray powder diffraction measurements under high pressures.

A part of this work is a collaboration with Miss Emiko Igaki (Matsushita Techno-research). The author thanks her for discussion and encouragemnt.

The author thanks Mr. Fujitsugu Amita (Kyoto Univ.) for useful technical advice, Mr. Hirotsugu Nishishita (Kyoto Univ.) and Mr. Noboru Kasugai (Kyoto Univ.) for the assistance in the low-temperature experiments.

The author wishes to thank Dr. Naohiro Watanabe (Kyushu Institute of Tech.), Dr. Iwao Mogi (Tohoku Univ.), Dr. Hiroaki Okada (Kyoto Univ.), Dr. Nobuyuki Matsushita (Univ. of Tokyo), Dr. Shoich Kutsumizu (Univ. of Gifu), Dr. Hiroshi Kitagawa (IMS), Mr. Toshikazu Nakamura (Gakushuin Univ.), Mr. Taichi Terashima (Kyoto Univ.), Mr. Tokutaro Komatsu (Kyoto Univ.) and all the members of Saito laboratory for various useful discussion and encouragement.

The author thanks to Miss Noriko Hayashi for her hearty encouragement.

The author is very grateful to his parents for their continuous encouragement and invaluable support during his study at the graduate school.

References

1) For example, see Mechanism of Superconductivity, ed. Y. Muto, JJAP Series 7 (Publication Office, Japanese Journal of Applied Physics, Tokyo, 1992)

2) H.T. Evans, Jr. and J.A. Konnert: Am. Mineral. 61 (1976) 996

3) G. Burn, B. Gardes, J.C. Tedenac, A. Raymond and M. Maurin: Mat. Res. Bull. 14 (1979) 743

4) R. Berger: Chemica Scripta 28 (1988) 41

5) K. Klepp and H. Boller: Monatshefte fur Chemie 109 (1978) 1049

6) R. Berger: J. Less-Common metals 147 (1989) 141

7) M. Saeki, M. Onoda and H. Nozaki: Mat. Res. Bull. 23 (1988) 603

8) M. Onoda and M. Saeki: Mat. Res. Bull. 24 (1989) 1337

9) K. Klepp, H. Boller and H. Vollenkle: Monatshefte fur Chemie 111 (1980) 727

10) R. Berger and L. Eriksson: J. Less-Common Metals 161 (1990) 165

11) C. Burschka: Z. Naturforsch 34b (1979) 396

12) C. Burschka and W. Bronger: Z. Naturforsch 32b (1977) 11

13) C. Burschka: Z. Naturforsch, 34b, 675 (1979).

14) H. Schils and W. Bronger: Z. Anorg. Allg. Chem. 456 (1979) 187

15) R. Berger and A. Meerschaut: Eur. J. Solid State Inorg. Chem. 25 (1988) 279

16) R. Berger, L. Eriksson and A. Meerschaut: J. Solid State Chem. 87 (1990) 283

17) L. Eriksson, P.-E. Werner, R. Berger and A. Meerschaut: J. Solid State Chem. 90 (1991) 61

18) G. Gattow: Acta. Crystallogr. 10 (1957) 549

19) R.A. Berger and R.J. Sobott: Monatshefte fur Chemie 118 (1987) 967

20) T. Ohtani, J. Ogura, M. Sakai and Y. Sano: Solid State Commun. 78 (1991) 913

21) W. Bronger and H. Schils: J. Less-Common Metals 83 (1982) 279

22) G. Savelsberg and H. Schafer: Z. Naturforsch 33b (1978) 711

23) C. Burschka: Z. Anorg. Allg. Chem. 463 (1980) 65

24) W. Bronger: Angew. Chem. Int. Ed. Engl. 20 (1981) 52

25) C. F. van Bruggen: Ann. Chim. Fr. 7 (1982) 171

26) M.B. Robin and P. Day: Adv. Inorg. Chem. Radiochem. 10 (1967) 247

27) D.B. Brown, J.A. Zubieta, P.A. Vella, J.T. Wrobleski, T. Watt, W.E. Hatfield and P. Day: Inorg. Chem. 19 (1980) 1945

28) J.C.W. Folmer and F. Jellinek: J. Less-Commom Metals 76 (1980) 153

29) G. van der Laan, C. Westra, C. Haas and G.A. Sawatzky: Phys. Rev. B23 (1981) 4369

30) G.A. Sawatzky: Solid State Chemistry 1982, Proc. the 2nd European Conf., Veldhoven, The Netherlands, 7-9 June 1982, eds. R. Metselaar, H.J.M. Heijligers and J. Schoonman, Studies in Inorganic Chemistry, Vol.3, p.3

31) J. Ghijsen, L.H. Tjeng, J. van Elp, H. Eskes, J. Westerink, G.A. Sawatzky and M.T. Czyzyk: Phys. Rev. B38 (1988) 11322

32) L.W. ter Haar, F.J. Di Salvo, H.E. Bair, R.M. Fleming, J.V. Waszczak and W.E. Hatfield: Phys. Rev. B35 (1987) 1932

33) R.M. Fleming, L.W. ter Haar, and F.J. DiSalvo: Phys. Rev. B35 (1987) 5388

34) There are a number of reviews about charge-density wave. For example, see R.H. Friend and D. Jerome: J. Phys. C.: Solid State Phys. 12 (1979) 1441

35) W. Buckel and R. Hilsh: Z. Phys. 128 (1950) 324

36) R.P. Huebener: Phys. Rev. 135 (1964) A1281

37) R.D. Barnard: Thermoelectricity in Metals and Alloys (Taylor & Francis, London, 1972)

38) J. Chaussy, A. Guessous and J. Mazuer: Rev. Sci. Instrum. 52 (1981) 1721

39) R.B. Roberts: Phil. Mag. 36 (1977) 91

40) B.P. Ghosh, M. Chaudhury and K. Nag: J. Solid State Chem. 47 (1983) 307

41) D.K.C. Mac Donald: Principles of Thermoelectricity (John Wiley and Sons Inc., New York, 1964)

42) W.B. Pearson: Solid State Physics (U.S.S.R.) 3 (1961) 141

43) Z. Peplinski, D.B. Brown, T. Watt, W.E. Hatfield, and P. Day: Inorg. Chem. 21 (1982) 1752

44) A. Oshiyama, K. Nakao and H. Kamimura: J. Phys. Soc. Jpn. 45 (1978) 1136

45) M.H. Rashid and D.J. Sellmyer: Phys. Rev. B29 (1984) 2359

46) M.-H. Whangbo and E. Canadell: Inorg. Chem. 29 (1990) 1395

47) T. Mori and H. Inokuchi: J. Phys. Soc. Jpn. 57 (1988) 3674

48) W. Rudorff, H.G. Schwarz and M. Walter: Z. Anorg. Allg. Chem. 269 (1952) 141

49) M. Raghu, S.V. Subramanyam, and S. Chatterjee: Solid State Commun. 69 (1989) 949

50) M.F. Hundley, U. Walter and A. Zettl: Solid State Commun. 73 (1990) 477

51) H.K. Ro and W.E. Hatfield: Mixed Valency Systems: Applications in Chemistry, Physics and Biology, ed. K. Prassides (Kluwer Academic Publishers, Dordrecht, 1991) p. 407

52) M.-H. Whangbo and E. Canadell, Solid State Commum. 81 (1992) 895

53) A. Briggs, P. Monceau, M. Nunez-Regueiro, J. Peyrard, M. Ribault, and J. Richard: J. Phys. C: Solid State Phys. 13 (1980) 2117

54) M. Ido, Y. Okayama, T. Ijiri and Y. Okajima: J. Phys. Soc. Jpn. 59 (1990) 1341

55) M. Greenblatt: Low-Dimensional Electronic Properties of Molybdenum Bronzes and Oxides, ed. C. Schlenker (Kluwer Academic Publisher, Dordrecht, 1989) p. 1

56) L.F. Schneemeyer, F.J. DiSalvo, S.E. Spengler and J.V. Waszczak: Phys. Rev. B30 (1984) 4297

57) F.J. DiSalvo, J.A. Wilson, B.G. Bagley and J.V. Waszczak: Phys. Rev. B12 (1975) 2220

58) J.A. Wilson, F.J. DiSalvo and S. Mahajan: Adv. Phys. 24 (1975) 117

59) S. Gnanarajan and R.F. Frindt: Phys. Rev. B33 (1986) 1443

60) Z.Z. Wang and N.P. Ong: Phys. Rev. B34 (1986) 5967

61) M. Almeida, E.B. Lopes and J. Dumas: Synth. Met. 41-43 (1991) 3833

62) A. Smontara, K. Biljakovic, J. Mazuer, P. Monceau and F. Levy, J. Phys: Condens. Matter 4 (1992) 3273

63) H. Sato, N. Kojima, K. Tsuji, M. Imai, K. Yaoita and T. Nakajima: Photon Factory Activity Report 9 (1991) 100

64) W.W. Fuller, P.M. Chaikin and N.P. Ong: Solid State Commum. 39 (1981) 547

65) M.-H. Whangbo and R. Hoffmann: J. Am. Chem. Soc. 100 (1978) 6093

66) R. Comes, M. Lambert and A. Guinier: Acta Crystallogr. A26 (1970) 244

67) Y. Nogami, K. Kubo and S. Kagohima: Kotaibutsuri (Solid State Physics) 22 (1987) 187 (in Japanese)

68) P. Haen, P. Monceau, B. Tissier, G. Waysand, A. Meerschaut, P. Molinie and J. Rouxel: Low Temperature Physics -LT14, eds. M. Krusius and M. Vuorio (North-Holland, Amsterdam, 1975) p. 445

69) V. Grasso (ed.): Electronic Structure and Electronic Transitions in Layered Materials (D.Reidel Publishing Company, Dordrecht, 1986)

70) J. Rouxel (ed.): Crystal Chemistry and Properties of Materials with Quasi-One-Dimensional Structures (D.Reidel Publishing Company, Dordrecht, 1986)

71) N. Le Nagard, A. Katty, G. Collin, O. Gorochov and A. Willig: J. Solid State Chem. 27 (1979) 267

72) R.M. Fleming, F.J. DiSalvo, R.J. Cava and J.V. Waszczak: Phys. Rev. B24 (1981) 2850

73) T. Sekine, K. Uchinokura, H. Iimura, R. Yoshizaki, E. Matsuura: Solid State Commun. 51 (1984) 187

74) J. Mahy, D. Colaitis, D. Van Dyck and S. Amelinckx: J. Solid State Chem. 68 (1987) 320

75) There are a number of papers on $Cu_{1-x}Se$. For example, see H. Terauchi, Y. Nishihata, H. Maeda, M. Hida and N. Kamijo: J. Phys. Soc. Jpn. 53 (1984) 3286, and the references.